Asia-Pacific
Economic Cooperation

Advancing Free Trade
for Asia-Pacific Prosperity

Research on Cloud-based Sharing Platform of Multi-Energy Microgrids for APEC Economies

APEC Energy Working Group

July 2020

APEC Project: EWG 03 2018S0120

Produced by (in alphabetical order):

Xiaopeng Fu, Peng LI, Yixin LIU, Yunfei MU, Guanyu SONG, Chengshan WANG, Wei WEI, Tao XU

School of Electrical and Information Engineering, Tianjin University
Building 26E, 92 Weijin Road, Nankai District, Tianjin 300072, China

Corresponding Contact Email: cswang@tju.edu.cn; taoxu2011@tju.edu.cn

For
Asia-Pacific Economic Cooperation Secretariat
35 Heng Mui Keng Terrace
Singapore 119616
Tel: (65) 68919 600
Fax: (65) 68919 690
Email: info@apec.org
Website: www.apec.org

APEC#220-RE-01.8

Contents

Executive Summary

It has been noted recently that the world's energy systems are undertaking an evolutional transformation due to the depletion of fossil fuels, increasing conflicts between energy supply and demand, as well as rising environmental concerns. In order to maintain economic optimization goals and achieve carbon footprint minimization without compromising on the reliability, flexibility as well as resilience of the grid, multi-energy microgrids (MEMGs) that are featured with multiple terminal resources and multiple distributed components for energy production, conversion, and storage within clearly defined boundaries have been introduced and implemented.

Researchers and practitioners are eager to develop promising technologies, business models, standards and software supporting MEMGs' planning, operation and management that are economically viable worldwide. Consequently, a cloud-based sharing platform of MEMGs is established by Tianjin University to share the existing knowledge and techniques, to help fill the information gap and to inform how best to promote and accelerate MEMG adoption in APEC economics by learning about how successful projects have been developed worldwide. In addition, drawing experiences and data from existing projects connected on the cloud based sharing platform throughout Japan, UK, Sweden, Middle East, China *etc*. help build a broader understanding of MEMG solutions and guide the industry about best practices for economic viability.

This project was supported by the APEC Energy Working Group in 2018 (No. EWG03 2018S), it aims to grow the research community and enhance the capability in the planning, operation and management of MEMGs for APEC economies, which can facilitate the goal of doubling the share of renewables in the APEC energy mix from 2010 level by 2030.

With the support of the cloud based MEMG sharing platform, as well as the distributed generation and lab facilities in Tianjin University, research has been carried out to develop related techniques, management strategies, software, standards and policy recommendations. Insights gathered from this project will be considered to enhance technological progress of renewable energy in the APEC region, to grow the market for MEMGs through public and private sector actions, to meet APEC's future energy supply, resiliency, and climate change goals and to guide the public authorities' future electric pricing and incentive programs for MEMGs.

List of Abbreviations

AI	Artificial Intelligence
BAS	Building Automation System
BIPV/T	Building-Integrated PV with Thermal
CAC	Central Air Conditioning
CCHP	Combined Cold Heat and Power
CEC	California Energy Commission
CHP	Combined Heat and Power
CIES	Community Integrated Energy System
CMHC	Canada Mortgage and Housing Corporation
CPS	Cyber Physical System
CSC	Customer Service Center
DER	Distributed Energy Resource
DER-CAM	Distributed Energy Resources Customer Adoption Model
DFIG	Doubly Fed Induction Generator
DG	Distributed Generation
DHW	Domestic Hot Water
DOE	Department of Energy
DR	Demand Response
DUIT	Distributed Utility Integration Test
EMS	Energy Management System
ESS	Energy Storage System
FRT	Fault Ride Through
FYP	Five Year Plan
GA	Genetic Algorithm
GCVRF	Grid Converter Voltage Reference Frame
GE	General Electric
GEJE	Great East Japan Earthquake
GHG	Green House Gas
GHP	Gas Heat Pump
GSHP	Ground Source Heat Pump
HMI	Human Machine Interface
ICES	Integrated Community Energy Solutions

IEGS	Integrated Electricity and Gas community energy System
IPS	Integrated Power Supply
JSCA	Japan Smart Community Alliance
LA	Lead Acid
LBNL	Lawrence Berkeley National Laboratory
MANA	Modified Augmented Nodal Analysis
MCFC	Molten Carbonate Fuel Cell
M-CSP	Microgrid Cloud based Sharing Platform
MEMG	Multi-Energy Micro-Grid
METI	Ministry of Economy, Trade and Industry
MILP	Mixed-Integer Linear Programming
MG	Micro-Grid
MNA	Modified Nodal Approach
MPC	Model Predictive Control
MRI	Magnetic Resonance Imaging
NDRC	National Development and Reform Commission
NEA	National Energy Administration
NEDO	New Energy and Industrial Technology Development Organization
NREL	National Renewable Energy Laboratory
NTUA	National Technical University of Athens
NTT	Nippon Telegraph and Telephone
NZEH	Net-Zero Energy Houses
HS	Heat Storage
ICT	Information and Communications Technology
OE	Office of Electricity Delivery and Energy Reliability
PAFC	Phosphoric Acid Fuel Cells
PCC	Point of Common Coupling
PCS	Power Conversion System
PET	Power Electronic Transformer
PFC	Power Flow Controller
PMSG	Permanent Magnet Synchronous Generator
PV	Photovoltaic
RDSI	Renewable and Distributed Systems Integration
REIDS	Renewable Energy Integration Demonstration
RES	Renewable Energy System

RHCC	Revised Hard Cycle Charge
SDS	Static Disconnect Switch
SDO	Standards Development Organization
SIEM	Smart Integrated Energy Microgrid
SGCC	State Grid Corporation of China
SOC	State of Charge
SOFC	Solid Oxide Fuel Cell
SOP	Soft Open Point
SPIDERS	Smart Power Infrastructure Demonstration for Energy Reliability and Security
TOU	Time of Use
VPP	Virtual Power Plant
WECS	Wind Energy Conversion System
WTG	Wind Turbine Generator

Nomenclature

Indices

$C_{\text{total}}^{\text{ann}}$	Total annual cost	$C_{\text{f}}^{\text{ann}}$	Annual fixed cost
$C_{\text{TEI}}^{\text{ann}}$	Total annual equipment investment cost	$C_{\text{d}}^{\text{ann}}$	Annual demand cost
$C_{\text{C}}^{\text{ann}}$	Annual capital cost	$C_{\text{e}}^{\text{ann}}$	Annual energy cost
$C_{\text{OM}}^{\text{ann}}$	Annual operation and maintenance cost	$C_{\text{I},i}$	Initial investment cost of equipment i
$C_{\text{fuel}}^{\text{ann}}$	Annual fuel cost	C_{inv}	Annual investment cost
$C_{\text{elec}}^{\text{ann}}$	Total annual electricity charge	C_{ope}	Annual operation cost
C_{elec}	Total electricity charge	C_t^{P}	Purchase price of electricity
C_{fuel}	Total fuel cost	P_t^{TL}	Tie-line power
S_{ES}	SOC of the electrical ESS	F	Operation cost and the startup penalty of each cooling unit

Variables

P_{w}	Power captured from the wind	I_s	Dark saturation current
v	Wind velocity	N_{P}	Number of PV cells connected in parallel in the solar array
ω	Rotation speed of the rotor blade	P_{grid}	Electric power purchased from the grid
ω_{g}	Rotation speed of the generator	P_{load}	Electric load
u_{d}	Terminal voltage of the stator in the d-axis	$P_{\text{CS,C}}$	Charging electric power of cooling storage devices
u_{q}	Terminal voltage of the stator in the q-axis	$Q_{\text{AC,smoke}}^{\text{in}}$	Thermal power of smoke input of the absorption chiller
i_{d}	Stator current in the d-axis	$Q_{\text{load,h}}$	Heat load
i_{q}	Stator current in the q-axis	$Q_{\text{CS,D}}$	Discharging cooling power of cooling storage devices
T_{e}	Electromagnetic torque of the generator	$Q_{\text{load,c}}$	Cooling load
T_{m}	Mechanical torque of the generator	N_{S}	Number of PV cells connected in series in the solar array
P_{g}	Output active power of the generator	U_{FC}	Output voltage of the fuel cell
Q_{g}	Output reactive power of the generator	I_{FC}	Output current of the fuel cell

U_{dc}	Capacitor voltage of the Back-to-Back convertor	E_{enerst}	Reversible open circuit voltage of the battery
u_{acd}	D-axis component of the GSC grid-connected bus voltage	U_{ohm}	Ohmic overvoltage
u_{acq}	Q-axis component of the GSC grid-connected bus voltage	U_{act}	Voltage drop of the activation overvoltage equivalent resistance
Q_r	Residual capacities of the battery	U_{con}	Voltage drop of the concentration overvoltage equivalent resistance
U_{B}	Terminal voltage of the battery	$\boldsymbol{G}$	Conductance matrix
I_{B}	Discharge current of the battery	$\boldsymbol{u}_{\mathrm{n}}$	Nodal voltage vector
E_{m}	Open circuit voltage of the battery	$\boldsymbol{u}_{\mathrm{b}}$	Branch voltage vector
I_{h}	History current source of the Norton equivalent circuit	$\boldsymbol{I}_{\mathrm{IF}}$	History current vector of the interface
G_{eq}	Equivalent conductance of the Norton equivalent circuit	Q^{C}	Cooling power
U^{S}	Cooling-storage modes	Q^{S}	Cooling-storage power
I_{ph}	Light generated current	U^{C}	Cooling modes

Parameters

ρ	Air density	λ	Permanent magnet flux linkage
R	Length of rotor blades	q	Charge of an electron
ω_{ref}	Rated speed of the generator	k	Boltzmann's constant
α	Blade tip speed ratio	T	Absolute temperature of the PV cell
β	Blade pitch angle	R_{ohm}	Ohmic overvoltage equivalent resistance
J'_{w}	Inertia constant of the wind turbine	R_{act}	Activation overvoltage equivalent resistance
J_{g}	Inertia constant of the generator	R_{con}	Concentration overvoltage equivalent resistance
D_{tg}	Damping coefficient of the wind turbine	C	Equivalent capacitance reflecting the electric double layer effect of the fuel cell
k_{tg}	Stiffness coefficient of the wind turbine	R_{p}	Ohmic polarization resistance
L_{d}	Inductance of the stator in the d-axis	R_{o}	discharge overvoltage resistance
L_{q}	Inductance of the stator in the q-axis	C_{o}	Discharge overvoltage capacitor
R	Resistance of the stator winding	τ_{o}	Time constant of the electric double layer effect
p	Pole pair number	L'	Inductance per unit length of the Bergeron line model

R'	Resistance per unit length of the Bergeron line model	ΔT	Time-step of the slow subsystem
C'	Capacitance per unit length of the Bergeron line model	Δt	Time-step of the fast subsystem
d	Length of the Bergeron line	$r_{\mathrm{CR},i}$	Capital recovery factor of equipment i
τ	Propagation delay time	r	Discount rate
Z	Surge impedance of the Bergeron line model	l_i	Lifetime of equipment i

Chapter 1 Introduction of Multi-Energy Microgrids

1.1 Definition, Composition and Structure of Multi-Energy Microgrids

Multi-energy microgrid (MEMG) is an energy system that can run autonomously. The system consists of energy management devices, distributed energy sources, energy storage devices, energy conversion devices, and energy loads; structurally, the MEMG is composed of energy production, conversion, and storage, as well as output components.

A typical MEMG was built based on the energy hub model[1-2], which consisting of a combined cold, heat and power (CCHP) system, a gas heat pump (GHP), a distributed photovoltaic (PV), central air conditioning (CAC), electric energy storage system (ESS), and heat storage (HS) components with power, gas, cold, and heat energies, which is shown in Fig. 1-1. The MEMG contains various equipment units that couple with each other to meet the needs of different energy loads. Power loads are supplied by the CCHP system and PV. The ESS or power grid make up for insufficient outputs; heat loads are supplied by the CCHP and GHP. HS devices make up for insufficient outputs; cold loads are supplied by the CCHP and CAC. In the case of failure, different forms of energy give priority to the supply of energy loads and supplement of energy storage devices of the same kind. Extra energy can be employed for conversion or backup to reflect the differences among energy grades.

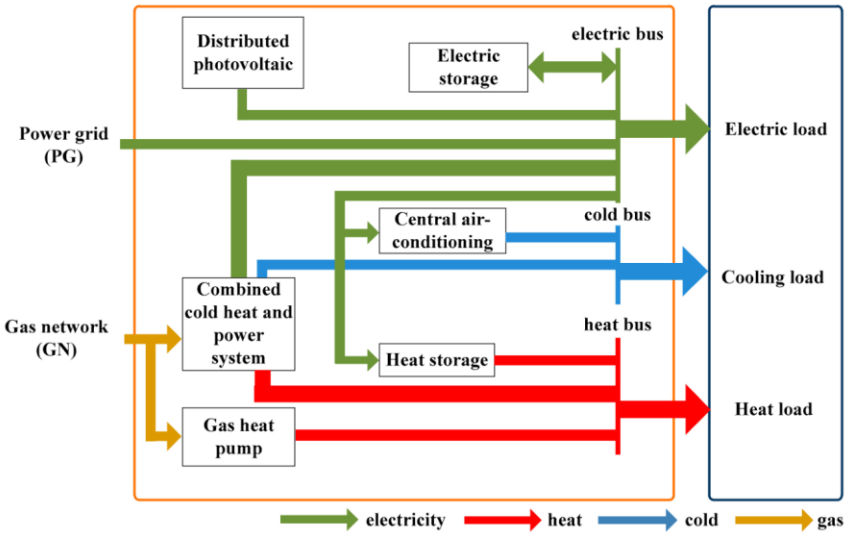

Fig. 1-1 Structure of MEMG[1]

From the perspective of operation, the MEMG, which can operate in the grid connected mode or the electric isolated mode, is an independent and controllable unit of the Energy Internet at the demand side. Its flexible operation capability provided by the coordination of multi-energy can help reduce the energy consumption during transmission and realize the effective utilization of renewable energy sources.

1.2 Connotation and Characteristics of MEMGs

1.2.1 Main Characteristics of MEMGs

A cleaner and more high-efficient energy integration will be created through the complementation among energy of multiple types as well as energies from different regions, especially the combination of traditional and renewable resources. The MEMG has the following characteristics [3]:

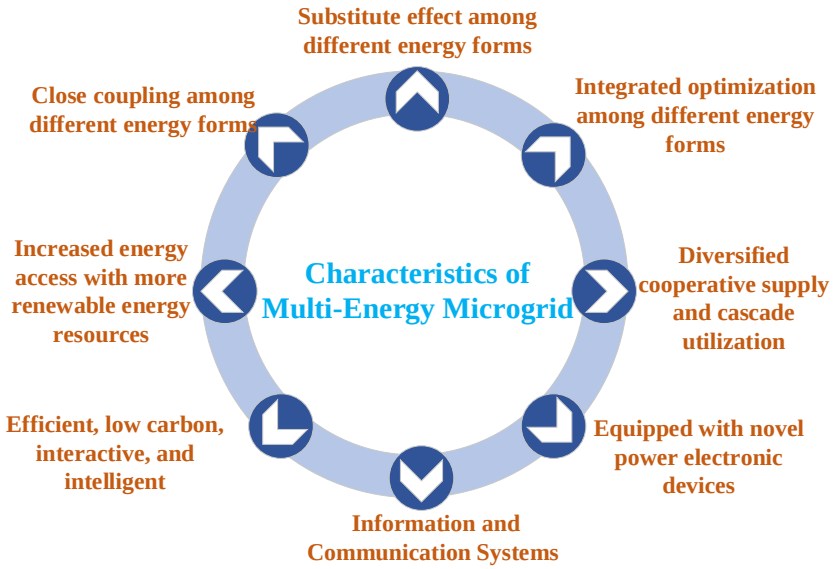

Fig. 1-2 characteristics of MEMG

(1) Closely coupled various types of energy sources

The operational mode of traditional energy system is relatively independent, and there are generally strong barriers between the subsystems. Whereas in the MEMGs, the sources, storages and loads of multi-energy are deeply connected and closely interacted, while in the meantime, the petroleum, natural gas and the generation power of renewable energy in this system are interconnected together on critical energy panel point, so they can be flexibly switched to achieve equal exchange and resource sharing. As a result, in various aspects of the energy industry like

production, transportation, storage and demand, all energy forms are not divided but an organically systemized and integrated ensemble.

(2) An obvious substitution effect exists among all energy forms

In the MEMG, there are non-renewable and traditional fossil fuels, as well as renewable ones like wind and PV. The renewable and non-renewables are not just simply mixed, but with a coordinating control to bundling or to make integrated external output. On the external perspective, the integrated multi-energy appears to be stable and continuous. On the internal point of view, the power output curve caused by the volatility of renewable energy is stabilized by thermal power, energy storage and hydropower, *etc*. All energies involved in the MEMG own the possibility of interconversion and replacement.

(3) Integrated optimization

The MEMG combines multiple types of energies like wind, PV, hydropower, and thermal power *etc*., making it possible to convert the energy product from demand side for electricity, cooling and heating through cooling-heating-electricity combined generation, hydrogen manufacturing/gas production, electricity-heating and electricity-cooling devices. In the coordinating planning layout and operation control, it's possible to achieve an intensive control to reach the integrated result. Therefore, integrated optimization is one of the objectives and critical characteristics.

(4) Diversified coordinating supply and gradient utilization

The terminal consumption of energy mainly includes energy products like cooling, heating and electricity. The multi-energy integration makes a coordinated interaction as "source-load-storage" to change the energy production and supply from singular to multiplex coordinating. By using means like natural gas distributed CCHP, an integrated multi-energy input system is built, and it achieves the synchronized multi-energy supply involving traditional energy and wind power, solar energy, geo-thermal and biomass energy. The system improves the distribution of electricity, gas, heating and cooling, and makes full use of all these resources based on grade. The MEMG can satisfy diversified energy supply within the system, while effectively improving the economic benefits of the system itself.

(5) High efficiency, low carbon, interaction, open, and smart

The MEMG can effectively improve energy efficiency, and reduce the carbon emission of the system by complementing advantages of sources, optimizing the grid structure, along with proactive control and services. Meanwhile, the system comprehensively makes use of technologies like information and communications technology (ICT), cyber physical system (CPS), big data and demand response (DR), and it's an interactive, open and intelligent system.

(6) Be adapted to higher penetration rate for renewable energy to switch in

In recent years, the issue of wind power and solar power curtailment has become quite serious. Electricity generated by wind and PV often suffers from randomness and fluctuation, therefore causes a severe negative impact on the stability of power grid. The implementation of MEMG is to coordinate power generated by wind, PV, thermal and hydro energy, and complements with ESSs to form an energy supply that matches users' demand. In this way, the local consumption and bundling transmission can be effectively improved, and it also can meet a higher switching-in rate for renewable energy.

(7) Novel power electronics with great controllability

Power electronic converters play an essential role in the MEMG and bring increased controllability of active and reactive power flows. The main function of power converters in MEMG is to provide interfaces for distributed generation (DG) units and ESSs. Depending on the characteristics and role of DG or ESS, specific control strategies are designed for their associated power converters, such as constant active/reactive power control, constant voltage/frequency control and droop control. It is usual that these strategies are arranged to perform smooth switching between different operating conditions. In addition to providing interfaces for different types of DG units and ESSs, power converters can also be used as devices that replace traditional transformers, switches, and provide services such as voltage regulation, power flow control, reactive power compensation and harmonic control. A soft open point (SOP) in a medium or low voltage network, which is often based on back-to-back power converters, is a typical example. It is used to replace a conventional switch connecting two feeders and thereby provides a way to optimize the operating condition of MEMG by controlling the power flow between the two circuits.

In summary, the research and development of power electronic devices has become a critical issue for MEMGs.

(8) Sophisticated information and communication systems

A powerful information and communication system is fundamental to the MEMG to manage tasks such as state awareness, information collection and broadcasting of commands. Compared with conventional independent energy systems, the information and communication system of the MEMG has evolved considerably into a sophisticated assembly of advanced measurements, two-way, high-speed communication and big data management that stores and analyses information about power distribution and consumption. The results provide support and data for the planning and design, optimal operation, simulation and analysis of the MEMGs.

1.2.2 Typical Applications of MEMGs

As a system that provides customized power supply services, a MEMG can be applied to various scenarios with different components, structures and operational characteristics, including:

(1) Independent MEMG on islands or in remote areas: It is difficult and expensive to construct a conventional power grid on islands or in remote areas, so a MEMG can be attractive. For a MEMG in an island or remote area, the components and structures should be decided based on local environmental conditions. For example, when there are abundant wind and solar resources, the MEMG can be composed of wind turbine generators (WTGs), PV arrays, diesel generators and batteries. This kind of MEMG then operates in islanded mode. Although diesel generators are still needed considering the uncertainty of wind and solar energy, both annual operating hours and diesel consumption are reduced significantly.

(2) Renewable energy dominated MEMG in areas with a high penetration of renewables: in areas with abundant solar/wind energy, overvoltage issues may occur if large amounts of solar/wind generation are connected to the distribution network directly. Therefore, a renewable energy dominated MEMG at the user or community level can be built to improve the capability of the power grid to integrate distributed renewable energy. This kind of MEMG is mainly composed of solar/wind generation and batteries, and usually operates in grid connected mode. It can also operate in islanded mode to supply users independently when needed.

(3) MEMG in areas with diverse energy sources and demands: When there are abundant energy sources and diverse demands like cooling/heating/electricity demands, an MEMG can be constructed to serve large public buildings, schools or hospitals. The main purposes of the MEMG is to integrate building/community energy saving technology, improve integrated energy utilization and realize efficient use of energy. In such MEMG, electrical energy is generated by solar, wind, geothermal or biomass energy and is stored in electrical or thermal ESSs. In addition, CCHP is a typical characteristic of such MEMGs.

(4) MEMG in distribution networks with extensive distributed energy resources (DERs): This kind of MEMG is an important part of smart distribution networks. Because DG units like PV systems and WTGs that are directly connected to the distribution network cannot supply loads independently, they have to be shut down when there are faults in the distribution network. By integrating distributed generators into branch-level, feeder-level and substation-level MEMGs in distribution networks, DG units can supply key loads when there are faults in the upstream power grid during disasters, and can improve the self-healing ability of distribution networks.

1.3 Worldwide Research and Demonstration Progress of MEMGs

Due to the fact that the MEMG is an effective way to improve comprehensive efficiency for energy system, to improve coordination capability of power supply and demand and to promote an effective way for cleaner and renewable energy to achieve a nearby digestion and high efficient usage rate, the US, EU and many economies in Asia Pacific regions have initiated relevant academic and applicable studies. Especially in China, since 2011, some areas in western China have severe issues on wind power, solar power and hydropower curtailment after a massive development of renewable resources. In order to solve the electricity digestion issue of renewable energy, the Chinese government has launched a series of industrial policies to promote the development of the MEMG and has published the first batch of 23 demonstration projects on MEMG in 2017.

According to Navigant Research, which has tracked MEMG deployment since 2011, the US has been the historical leader in deployed capacity; today, though, the US and Asia have roughly the same capacity of operating, under development, and proposed MEMGs, each with 42% of the market. EU trails with 11%, Latin America with 4%, and the Middle East and Africa currently

have just a 1% share. Total capacity was approximately 1.4 GW in 2015 and is expected to grow to roughly 5.7 GW (considered a conservative estimate) or 8.7 GW (under an "aggressive" scenario) by 2024[4].

1.3.1 EU

From 1998 to 2002, the MICROGRIDS in the 5th Framework Program: Large Scale Integration of Micro-Generation to Low Voltage Grids activity was funded at €4.5 million. The Consortium, led by the National Technical University of Athens (NTUA), included 14 partners from seven EU countries, including utilities such as EdF (France), PPC (Greece), and EdP (Portugal); manufacturers, such as EmForce, SMA, GERMANOS, and URENCO; plus research institutions and universities such as Labein, INESC Porto, the University of Manchester, ISET Kassel, and Ecole de Mines. The EU MICROGRIDS project explored the technical challenges such as safe islanding and reconnection practices, energy management, control strategies under islanded and connected scenarios, protection equipment, and communications protocols. The objectives of project were: study the operation of MEMGs to increase penetration of renewable and other DERs while reducing carbon emissions; study the operation of MEMGs in parallel with the grid and islanded, as may follow faults; define and develop control strategies to ensure efficient, reliable, and economic operation and management of MEMGs; define appropriate protection and grounding policies to assure safety, fault detection, separation, and islanded operation; identify and develop the required telecommunication infrastructures and protocols; determine the economic benefits of MEMG operation and propose systematic methods to quantify them; simulate and demonstrate MEMG operation on laboratory scales. The project was successfully completed, providing several innovative technical solutions.

From 2002 to 2006, a follow-up project titled More Microgrids: Advanced Architectures and Control Concepts for More Microgrids within the 6th Framework Program was funded at €8.5 million. This second consortium, again led by NTUA, comprises manufacturers, including Siemens, ABB, SMA, ZIV, I-Power, Anco, Germanos, and EmForce; power utilities from Denmark, Germany, Portugal, the Netherlands, and Poland; and research teams from Greece, the United Kingdom, France, Spain, Portugal, and Germany. This project focused on the investigation of new DER controllers to provide effective and efficient operation of MGs, and studying the

impact on power system operation, including benefits quantification of MEMGs at regional, national, and EU levels of reliability improvements, reduction of network losses, environmental benefits, *etc* [5].

There are also EU pilot projects of MEMG. In Netherlands, Continuon's MV/LV facility project was carried out. With the MEMG islanded, this project uses power electronic flexible AC distribution systems and storage to make the improvements in power quality. In Germany, the project of MVV Residential Demonstration at Mannheim-Wallstadt has been prepared for a continuous long-term field test site for the More Microgrids project. Greece has also taken on the pilot project of the Kythnos Island MEMG [4].

1.3.2 US

In the US, systematic research and development programs of MEMGs began with the CERTS effort [6-7]. Formed in 1999, CERTS supported by Department of Energy (DOE) has been recognized as the origin of the modern grid connected MEMG concept. It envisioned a MEMG that could incorporate multiple DERs yet present itself to the existing grid as a typical customer or small generator, in order to remove perceived challenges to integrating DERs. Emphasis was placed on seamless and automatic islanding and reconnection to the grid and on passive control strategies such as reactive power versus voltage, active power versus frequency, and flow versus frequency. The goals of these strategies were: 1) to remove reliance on high-speed communications and master controllers, yielding a "peer-to-peer" architecture; and 2) to create a flexible "plug-and-play" system that would not require extensive redesign with the addition or removal of DERs, in order to lower system capital costs and provide the freedom to locate co-generation facilities near thermal loads. The CERTS MG concept has been deployed in a test-bed setting and in real world MEMG projects[8-10]. Two major products of CERTS are the μGrid Analysis Tool (μGrid), under development at the Georgia Institute of Technology, and the Distributed Energy Resources Customer Adoption Model (DER-CAM) in use at Lawrence Berkeley National Laboratory (LBNL) and several other RD&D facilities worldwide. While the initial motivation of CERTS was to improve reliability rather than to reduce greenhouse gas (GHG) emissions, per se, CERTS MGs can incorporate renewable micro generation sources.

General Electric (GE) also co-funds with DOE in an approximately $4 million USD MG

program. GE aims to develop and demonstrate a MEMG energy management framework for a broad set of MEMG applications that provides a unified controls, protection, and energy management platform. This program is complementary to many of the concurrent research programs in this area.

In 2008, the Renewable and Distributed Systems Integration (RDSI) program was supported by the Office of Electricity Delivery and Energy Reliability (OE) [11]. It was the OE's first major program, including nine projects. Projects totaling $100 million USD, typically with 50–50 DOE co-funder financing, were primarily intended to achieve a minimum of 15% peak load reduction, which was generally required by an RDSI program [12].

In 2010, the Smart Power Infrastructure Demonstration for Energy Reliability and Security (SPIDERS) programs was carried out. Jointly funded by DOE, these projects aim to provide highly reliable and resilient power to military bases, which are often in remote locations and are poorly served by the mega grid [13].

In the period of 2011-2012, interest by state and local government in the resilience benefits of MEMGs has spawned MEMG programs of varying size and complexity in all of the states affected by super storm Sandy and Japan Earthquake. The State of New York's Prize program, managed by the State Energy Research and Development Administrations, was the most extensive. The New York Prize program was an ambitious $60 million USD grant program with additional leverage opportunities designed in three stages [14-15].

Other activities of MEMGs are in progress. Primarily funded by the California Energy Commission (CEC), the first full scale integration test of commercial grade utility grid interactive DERs in the U. S., the Distributed Utility Integration Test (DUIT) addresses a key technical issue, namely the electrical implications of operating multiple and diverse DERs at high penetration levels in utility distribution networks. Northern Power and the National Renewable Energy Laboratory (NREL) also have completed a project that examines the regulatory and technical issues associated with installation and operation of a MEMG in rural Vermont. Northern Power worked with the local electricity utility to predict the impact and effects of the MG at the end of a low capacity distribution feeder with the poor PQR typical of rural areas [16].

1.3.3 Japan

Japan is an economy that greatly relies on energy importation therefore is the earliest economy in Asia that starts to study MEMGs.

In September of 2009, the government of Japan announced their emission reduction objectives on the years of 2020, 2030 and 2050, and the intention to put efforts into building MEMGs to cover the whole economy so as to optimize energy structure and improve energy efficiency while facilitating the exploration on renewable energy in a large scale. Under the boosting of the government, main energy study agencies in Japan have all started such research and have generated different study solutions. For example, the Japan Smart Community Alliance, (JSCA) [17], launched and founded in April of 2010 by New Energy and Industrial Technology Development Organization (NEDO), mainly dedicates in the study and demonstration on Smart Community technology. The Smart Community achieves an all-in-one system integration of transportation, water supply, information and medical treatment based on the community MEMGs (including electricity, gas, heating power, renewable resources *etc.*). Tokyo Gas came up with a more advanced solution on MEMGs [18]. On the basis of traditional MEMGs (electricity, gas and heating power), a hydro energy supply grid which covers the whole society will be built. In this way, a terminal MEMG is formed and it will be composed by terminals of energy network, different energy using devices and transferring storing units of powers.

After the severe earthquake in 2011, all walks of life in Japan paid more attention to the development of DER and MG with extended definitions. They've tried to build distributed energy system in urban areas like Shinjuku, Harajuku and Roppongi based on smart grid in the purpose of big improvement on the reliability of power infrastructure and the capability against catastrophic risks. The representing projects include: distributed energy system in Hachinohe area of Aomori Prefecture, ECO energy project in Kyoto, distributed energy system at World Expo in Aichi Prefecture, municipal type energy supply system in Roppongi [19].

Currently, Japan has become the pioneer in MEMG demonstration projects. The Japanese government has set ambitious targets for increasing the contribution of renewable energy sources, such as WTG and PV, but the fluctuating power of renewable energy sources might degrade the country's outstanding power quality and reliability. Traditionally, customers that operate fossil fuel fired DERs, such as CHP units for compensating the fluctuations. Others that use intermittent

renewable sources balance supply and demand through purchased grid power. In either case, residual purchases from the grid are volatile. Conversely, a MEMG can contribute load following capability to a utility grid by balancing its own energy requirement using the coordination of multi-energy to balance fluctuating load and renewable output. For example, a MEMG with electrical storage and/or gensets can potentially fully compensate for its intermittent renewable supply and present itself to the grid as a constant load. This principle has motivated much of the research, development, and demonstration in Japan, and has led to an emphasis on controls and electrical storage.

(1) NEDO MG Projects

NEDO, research funding and management agency of the Ministry of Economy, Trade, and Industry, started three demonstration projects under its Regional Power Grid with Renewable Energy Resources Project in 2003. These field tests focused on the integration of new energy sources into a local distribution network. Proposed MEMG projects in Aomori, Aichi, and Kyoto Prefectures qualified for the program, and all have a significant renewable energy component.

(2) The Aomori Project in Hachinohe

This MEMG was put into operation in October 2005 and was being evaluated for PQR, cost effectiveness, and GHG emission reductions over a planned demonstration period lasting until March 2008. A central feature of the system is that only renewable energy sources, including PV, WTGs (together totaling 100 kW), and biomass, were used to supply electricity and heating. The controllable DERs consist of three 170 kW gensets (510 kW total) burning sewage digester gas, a 100 kW lead acid (LA) battery bank, and a 1.0 t/h woody biomass boiler. The MG serves seven City of Hachinohe buildings. These facilities are interconnected through a 6 kV, 5.4 km duplicate distribution line, with the whole system connected to the commercial grid at a single point of common coupling (PCC). From November 2005 and July 2006, primary energy consumption was reduced by 57.3%, thanks to reduced electricity purchases, while carbon emissions were also reduced by 47.8% [19].

(3) The Aichi Project near the Central Japan Airport

The first NEDO demonstration project started operation at the site of the 2005 World Exposition in March 2005. The system was moved to the Central Japan Airport City near Nagoya

in 2006, where it began operation in early 2007. It now supplies a Tokoname City office building and a sewage plant via a private distribution line. Its main feature is a combination of the following fuel cells as the main sources: two 270 kW and 300 kW molten carbonate fuel cells (MCFCs), four 200 kW phosphoric acid fuel cells (PAFCs), and a 50 kW solid oxide fuel cell (SOFC). The MCFCs use biogas generated from high temperature (1,200 °C) treatment of wood waste and plastic bottles. Both the MCFCs and SOFC are base loaded while the PAFCs load follow. Total PV capacity is 330 kW, and a 500 kW sodium sulfur battery was used for balancing. Experiment results of intentional islanding mode have also been obtained.

1.3.4 China

China started its MEMG development through the 12th Five Year Plan (FYP, from 2011 to 2015). The primary goal is to find a distributed clean energy way which can relieve China's dependence on centralized coal power, reduce carbon emission, and improve air quality. Chinese central government targeted to build 30 MEMG demonstration projects in the 12th FYP and this work was further extended to the 13th FYP (from 2016 to 2020). In order to support the economy's development projects, MEMGs were further defined as three types: island, remote and city MEMGs, with each type including recommendations of energy system configuration applicable in China.

Since 2011, along with massive development on renewable energy in China, wind, solar, and hydropower curtailment have become very serious in western regions. In order to solve the digestion on renewable energy like wind power, PV and hydro energy, China has released a series of industrial policies as shown in Table 1-1 that can promote the development of MEMGs.

Table 1-1 Relevant policies in China regarding MEMGs (2011-2018) [20]

No.	Policy Name	Releasing Time
1	Guidance Regarding Developing Energy on Natural Gas [No.2196 NDRC Energy(2001)]	October 9th 2011
2	Temporary Administrative Measures on Distributed Generation [No. 1381 NDRC Energy(2013)]	July 18th 2013
3	Implementing Regulations of Distributed Energy Demonstration Projects on Natural Gas Distributed Energy [No. 2382 NDRC Energy(2014)]	October 23rd 2017
4	Guidance Regarding the Promotion of Smart Grid Development [No. 1518 NDRC Operation(2015)]	July 6th 2015
5	Guidance Regarding Promoting the Construction of New Energy Micro Grid Demonstration Project [No. 265 NEA New Energy(2015)]	July 13th 2015

6	Guidance Regarding Promotion on Developing "Internet+" Intelligent Energy [No. 392 NDRC Energy(2016)]	February 25th 2016
7	Suggestions on the Implementation of Facilitating Integrated Multi-energy System Demonstration Projects [No. 1430 NDRC Energy(2016)	July 4th 2016
8	Guidance Reagrding the Promotion Technological and Industrial Development on Energy Storage Technique [No. 1701 NDRC Energy(2017)]	September 22nd 2017

In December of 2016, National Development and Reform Commission (NDRC) and National Energy Administration (NEA) jointly published Energy Production and Consumption Revolution Strategy (2016-2030). The strategy brought up the objective to fully establish "Internet+" intelligent energy; reinforce the smart infrastructure of power grid to effectively connect to oil and gas pipeline, heating pipeline and other energy grids; promote the interconnection of multiple types of energy flow, and transformation of different energy forms; build up a coordinated "source-grid-load-storage" and integrated multi-energy network.

On January 25th of 2017, NEA published Notification Regarding the First Batch of Integrated Multi-energy System Demonstration Projects [No. 30 NEA Planning (2017)] and the first batch of MEMG demonstration projects was announced. There were 23 projects arranged in this demonstration plan, among which contains 17 MEMGs at user side, and 6 MEMGs at power source side.

Table 1-2 First Batch of MEMGs Demonstration Projects in China (Jan. 2017)

Mode I: MEMGs at End-user Side	
No.	**Project Location**
1	Beijing Lize Financial Business District, Beijing
2	Guyuan County, Zhangjiakou, Hebei Province
3	Langfang Economic Development Zone, Langfang, Hebei Province
4	Xianghe County, Langfang, Hebei Province
5	Datong Economic & Technical Development Zone, Datong, Hebei Province
6	Zhalute Zhahazhuoer Industrial Park, Tongliao, The Inner Mongolia Autonomous Region
7	Suzhou Industrial Park, Suzhou, Jiangsu Province
8	Chengnan Economic New Zone, Gaoyou, Jiangsu Province
9	Hefei Airport Economic Demonstration Area, Hefei, Anhui Province
10	Qingdao Economic Development Zone, Qingdao, Shandong Province
11	Future Science and Technology City, Wuhan East Lake High-tech Development Zone, Wuhan, Hubei Province
12	Shenzhen International Low Carbon City, Shenzhen, Guangdong Province
13	Jingbian Industrial Park for Comprehensive Utilization of Energy and Chemical Industry, Yulin, Shanxi Province
14	Yanan New town, Yanan, Shanxi Province

15	Ansai District, Yanan, Shanxi Province
16	Fuping County, Weinan, Shanxi Province
17	The Xinjiang Production and Construction Corps Twelfth Division, Xinjiang Province

Mode II: MEMGs at Power Source Side

No.	Project Location
1	Zhangbei County, Zhangjiakou, Hebei Province
2	Tumoteyouqi, Baotou, The Inner Mongolia Autonomous Region
3	Kala Town, Muli County, Liangshan, Sichuan Province
4	Longmen Economic & Technical Development Zone, Hanchen, Shanxi Province
5	Geermu county, Haixizhou, Qinghai Province
6	Hainanzhou, Qinghai Province

1.3.5 APEC Economies

Up to 2018, APEC projects applied by APEC economies in the field of MEMGs are listed in Table 1-3. In order to boost the concentrated integration and high efficient use of new energy and renewable energy in APEC economies, 10 economies including China, US, Chinese Taipei, Thailand, Russia, Japan, Australia, Chile, New Zealand and Vietnam *etc*. have totally applied 22 APEC Projects regarding integrated multi-energy from 2006 to nowadays. The projects involve smart grid, integrated energy system, distributed energy and MEMGs *etc*. Fig. 1-3 shows the distribution of APEC projects in the MEMGs field. In total, there were 10 economies applied relevant projects during 2009-2018. China and US were the two economies that declared the most projects in the field with respectively 5 and 4 items (2 of them were jointly applied with Chinese Taipei); Thailand and Chinese Taipei separately applied 3 items (2 of them were jointly applied with US); Russia applied 2 items, while one item was declared by 5 other economies respectively by Australia, Chile, Japan, New Zealand and Vietnam.

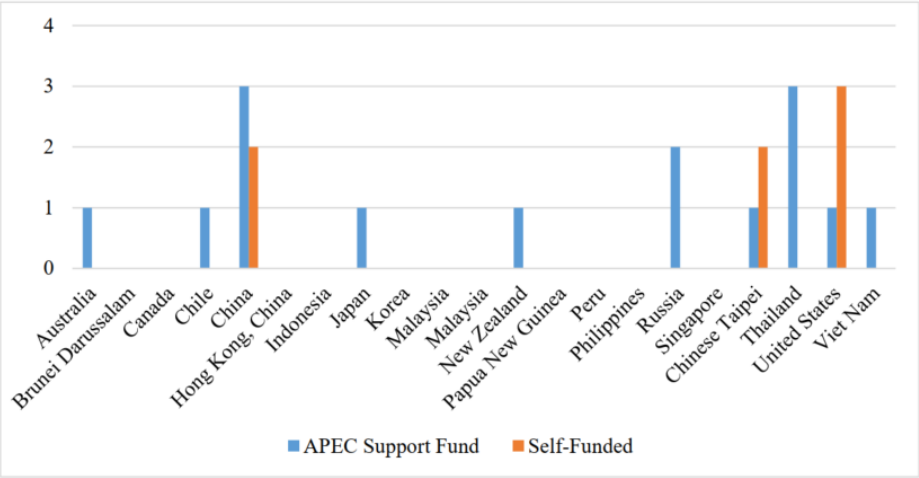

Fig. 1-3 Distribution of APEC Projects in the Field of MEMGs

1) Most of the researches were related to the key word "Smart", including "smart grid", "intelligent microgrid", "grid integration", "energy smart community", "smart DC community" and "green energy smart farm". There were 14 relevant research projects in total (and "smart grid" owns the most related project, 7 of them were of this category).

2) The key words that were related to "integrated energy" are "grid-interconnection", "integrated energy system" and "integrated multi-energy system". 3 projects were related to them.

3) 3 projects used "distributed energy" as key word.

4) 2 projects used "multi-energy" as key word.

We can see that "smart grid" has always been the critical and hot point of research in APEC economies. They still widely develop the application research and practical promotion in this field from aspects like "MEMGs", "integrated energy", "distributed energy".

Table 1-3 Summary of APEC Projects in the Field of MEMGs (2006-2018) [21]

NO.	Year	Proposing Economy(ies)	Co-Sponsoring Economies	Project No.	Project Title
1	2019	US	Australia; Indonesia; Japan; Singapore; Chinese Taipei; Thailand; Vietnam	EWG 01 2009S	Using Smart Grids to Enhance Use of Energy Efficiency and Renewable Energy Technologies
2		Japan	New Zealand; US	EWG 02 2009	Addressing Grid-Interconnection Issues in Order to Maximize the Utilization of New and Renewable Energy Sources

3	2011	Russia	Canada; Japan; Korea; Singapore; Chinese Taipei; Thailand; US	EWG 15 2011A	Piloting Smart-Microgrid Projects for Insular and Remote Localities in APEC Economies
4		China	China	IST 01 2011A	Cooperative Study on Efficient Renewable Resources Integration and Distribution Technologies for Smart Grid Construction
5		US	China; Japan; Korea; Chinese Taipei	CTI 30 2011T	Workshop on Regulatory Approaches to Smart Grid Investment and Deployment
6	2012	Vietnam	New Zealand; Chinese Taipei; US	EWG 05 2012A	Small Hydro and Renewable Grid Integration Workshop
7		China	Australia; Chile; Hong Kong, China; Indonesia; Korea; Chinese Taipei; Thailand; US	EWG 04 2012A	Study of Demand Response's Effect in Accommodating Renewable Energy Penetration in the Smart Grid
8		New Zealand	Chinese Taipei; Thailand; US	EWG 08 2012	Urban Development Smart Grid Roadmap - Christchurch Recovery Project
9		Russia	China; Indonesia; Japan; US	EWG 09 2012	Combined Heat and Power (CHP) Technologies for Distributed Energy Systems
10	2013	China	Canada; Hong Kong, China; Singapore; Thailand; Japan; New Zealand; US	EWG 03 2013A	Building Code Harmonization in Energy Smart Community
11		Thailand	Chinese Taipei; US; China; Hong Kong, China; Malaysia; Indonesia; Vietnam	EWG 06 2013A	APEC Smart DC Community Power Opportunity Assessment
12	2014	Thailand	China; US	EWG 07 2014A	Realization of APEC Low Carbon Model Town through Smart Grid Development (LCMT-SGD)
13		US	Canada; Singapore	EWG 02 2014S	Cyber-Energy Nexus Study - Opportunities, Challenges and Best Practices for Smart Energy Technology
14	2015	Chinese Taipei	China; Korea; Thailand; US	EWG 23 2015A	Best Practices for Developing the Green Energy Smart Farm in the APEC Region
15		Chinese Taipei; US		EWG 03 2015S	2015 Energy Smart Community Initiative (ESCI) Best Practices Awards Program
16	2016	Chinese Taipei; US		EWG 04 2016S	2017 Energy Smart Communities Initiative (ESCI) Best Practices Awards Program
17	2017	Thailand	Chinese Taipei; US; Japan; Philippines	EWG 11 2017A	Empowering a Distributed Energy Resource Future through Regulatory and Market Reforms

18		Australia	Philippines; New Zealand; Indonesia; Japan	EWG 13 2017A	Integrated Energy System Planning for Equitable Access to Sustainable Energy for Remote Communities in the APEC Regions using North Sulawesi as a Pilot Project/Test Bed
19		Chile	Japan; Mexico; Singapore; Chinese Taipei; US	EWG 16 2018A	Distributed Energy Resources Regulation and Rate Design
20		China		EWG 03 2018S	Establishment of a Cloud-based Sharing Platform of Multi-Energy Microgrids for APEC Economies
21	2018	US		EWG 09 2018S	APEC Energy Resilience Smart Grid Workshop
22		China		EWG 10 2018S	Research on Integrated Multi-Energy System to Improve Energy Efficiency and Enhance Technological Progress of Renewable Energy in APEC Region

(1) Singapore Renewable Energy Integration Demonstration

Fig. 1-4 shows the Singapore Renewable Energy Integration Demonstration diagram. This Renewable Energy Integration Demonstration (REIDS) MEMG in Singapore is a research and development site designed to test out various, cutting edge integration strategies to create 100% renewable energy MEMGs. It was being recognized as the largest MEMG demonstration platform in the tropics. The project was led by ENGIE, a large energy company based in France. Formerly known as GDF Suez, it was France's natural gas utility and was heavily invested in large centralized plants. However, realizing that the energy industry was changing, and responding to deregulation trends sweeping across EU, the company took on a new name, made a series of acquisitions, and refocused its business strategy as a global developer of DER, including MEMGs.

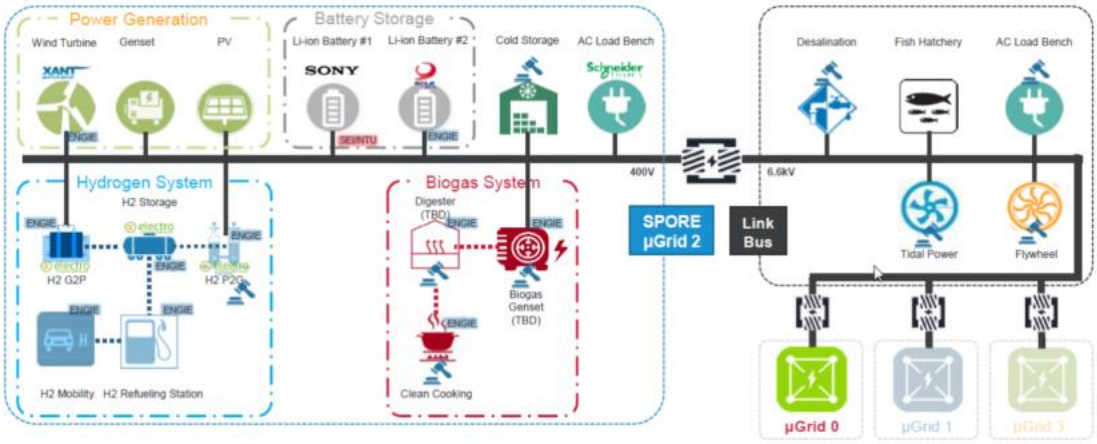

Source: ENGIE

Fig. 1-4 Singapore Renewable Energy Integration Demonstration Diagram

(2) Yellowknife Township Demonstration Project, Canada

The Integrated Community Energy Solutions (ICES) research program initiated by the Canadian government focuses on the application of MEMG technology in various community energy supply links, with special emphasis on the integrated use of various types of distributed energy and community public facilities (transport, medical, communications, *etc*.) mutual support. Under the funding of the ICES project, Canada has established many demonstration projects including Kasabonika MEMG, Bella Coola MEMG, Ramea MEMG, Nemiah MEMG, Quebec MEMG, Utility MEMG, Hydro Boston Bar MEMG, and Calgary MEMG, *etc*. It plans to build more than 2,000 MEMGs across the economy by 2020.

Yellowknife Town has a population of about 20,000, dominated by tourism, has large surrounding waters, and has a long heating period throughout the year (about 200 days). The main problems in the town are as follows: there is no relatively complete municipal heating network system, energy efficiency is ignored, local renewable energy is not fully utilized, and residents' awareness of energy conservation is weak. With the help of ICES, the town of Yellowknife combined the concept of MEMG to transform the energy system of the town. Local industrial, commercial and agricultural industries use energy management centers to comprehensively manage and utilize various energy sources. Use residual heat, waste heat and geothermal heat to reduce waste emissions and increase recycling of waste. Taking heating as an example, in addition to the traditional heating system, the town heating system has also added ground source heat pumps

(GSHP), hydropower heating, solar hot air systems, and passive solar heating. This greatly improves the efficiency of energy use and the utilization of renewable energy [22].

1.4 Standard and Software Development of MEMGs

1.4.1 Standard of MEMGs

IEEE 1547.4 was acknowledged as the baseline standard for MGs [23], while P1547.8 will help broaden and support the IEEE 1547 standard in the future. P2030 was also cited as an important standard with respect to interoperability in MEMGs. There were 18 R&D areas identified for standards and protocols, some of which were then eliminated, followed by voting on the remaining areas for priority and finally consolidation into two key areas that are described below:

(1) Universal MEMG communications and control standards

1) Description of the R&D scope: Clearly define an end-to-end communications and control standard (schema or data structures) that links DG, loads, and utility connections, for instance, energy management systems (EMSs), building automation systems (BASs), utilities, MEMG controller, industrial metering, and market participation, with standardized component capabilities including DR, BAS, diesels, loads, *etc*., consistent with applicable cyber security standards.

2) Technical performance baselines and R&D target: Current MEMG communications and control are bespoke, and are thus costly and risky to scale up. There are not consistent capabilities from DER and BAS. The R&D target should focus on interoperability, easier BAS integration, response to ancillary signals and optimized system operations with low integration and design costs, as well as standardization for easy and affordable scaling.

3) Cost baselines and R&D target: The current costs are about $100,000 USD to integrate each DER/BAS, while the targeted costs should be probably as low as $10,000 per DER/BAS.

4) The milestones include developing a plan to address interoperability of legacy equipment, BAS integration, DER fleet, and external signals with MGs in year 1, followed by deployment in years 2 and 3.

5) The synergistic developments for this activity are being carried out by IEEE SCC21 Projects (1547 and 2030) and NIST Smart Grid Interoperability Panel.

6) A caveat is that Standards Development Organizations (SDOs) take considerable time to

reach consensus for the final standards approval, so it may be best to publish best practices based on real world examples in the interim.

(2) MEMG protection, coordination, and security

1) Description of the R&D scope:

i. Modify existing anti-islanding DER techniques to operate correctly in MEMG operations. Develop new unintentional islanding techniques to handle larger numbers of DERs in MEMG. Define acceptable anti-islanding requirements for MEMGs that export power.

ii. Develop new protection and coordination methods to handle faults and abnormal conditions when grid connected and inside the MEMG.

iii. Coordinate disturbance response with utility.

iv. Develop protection and coordination practice in MEMGs with high levels of inverter-based DERs.

2) Technical performance baselines and R&D target: The currently used standards are limited to IEEE 1547, with a lack of standard for protection of MEMGs with multiple DER units. There is a need for a standard that addresses protection, reverse power flow, and anti-islanding with multiple DERs and to have a standard way to implement protection with inverter based DERs for various MEMG markets.

3) Cost baselines and R&D target: As the current costs are in the range of hundreds of thousands of dollars (that is 100% of MEMG costs for under 4 MW) to perform interconnection studies, the targeted cost should be less than 5% of MEMG costs to make their implementation feasible.

4) The milestones include developing a plan to address protection, coordination, and security with MEMGs in year 1, followed by deployment in years 2 and 3, and publishing best practices at the end of year 3.

5) In terms of synergistic developments, R&D work has been done in the field of MEMG protection by the CERTS and RDSI projects.

1.4.2 Software Development of MEMGs

Simulation in software is a fundamental tool for MEMGs. It plays an important role in the

operational optimization, protection, control, and R&D of novel MEMG equipment. Depending on the time scale, simulations of a MEMG can be divided into steady state and transient studies. Steady state simulation is based on power flow calculations and provides support to more advanced functions including short circuit and reliability analysis, operational optimization, and self-healing control. Transient simulation algorithms need to be accurate and stable for non-linear problems in order to handle the properties of MEMG models such as the highly coupled dynamics of different energy sources and equipment. The simulation tools should provide access for flexible user defined models to keep up with the rapid development of novel devices. Mathematically, the optimization of a MEMG is usually a large-scale, non-linear optimization problem. Based on the different decision variables, this type of problem can be divided into two categories: continuous and discrete. The former solves continuous problems, the latter solves discrete problems such as the optimization of connection switch status, which are more suitable for artificial intelligence (AI).

Several software programs are available for MEMG planning and design. In HOMER developed by NREL [24], capacity of DG units, operation schedule and tie-line power exchange can be optimized to minimize the MG life-cycle cost. DER-CAM [25], developed by LBNL, focuses on optimal configuration either for individual customer sites or MGs. Annual costs or CO_2 emissions are taken as objectives, and various types of CHP technologies are considered. PDMG [26], a software developed by Tianjin University, combines planning, design and operation dispatch in a two-stage optimization. Considering the basic role of the power system as a link, the existing research on the MEMGs dynamic characteristics mostly adopt the idea of adding thermal, gas and renewable energy equipment models directly into the power analysis platform. Generally, MATLAB/Simulink Power System Block, PSCAD, Digsilent Power Factory and SSDG, TSDG, are used [27-28]. In the above modeling process, other aspects besides electricity are greatly simplified, for the researchers focus on demand side of power system.

In order to consider the dynamic characteristics of gas and thermal networks as well as the steady state model of the MEMG. Several research have been conducted on interaction between electrical network and gas network. The models are built in commercial software Sincal to realize real-time co-simulation of coupled multi-energy systems [29]. In the building energy area, the software Energy Plus is used in the electrical-heating system modeling to effectively reduce

building energy consumption and improve household comfort [30]. Traditional MEMG system analysis, optimization and planning issues are often based on the basic physical principles of each energy system to establish its physical model, and then through numerical calculation or optimization methods to obtain the comprehensive energy system operation data. The idea of data-driven modeling arises these years to obtain unknown models through collecting a large number of observation data and describe the relationship between these statistics by using machine learning, deep learning as well as data mining technology. The commonly used statistical modeling methods include regression analysis modeling method, neural network modeling method, support vector machine method, decision tree modeling method and hybrid modeling method. Data-driven modeling methods have been applied to various fields related to the urban built environment, including prediction of solar and wind energy [31] and prediction of building energy consumption [32].

1.5 Significance and Challenges of developing MEMGs

1.5.1 Significance of Developing MEMGs

The development of MEMGs has the following significances [3]:

(1) Facilitate the accommodation of renewable energy

Due to the randomness and fluctuating feature of wind and PV power, implementing a coordinating operation of wind power, PV power together with micro gas turbine will decrease the power control because of the wind, solar and hydropower curtailment. It also will effectively promote the accommodation capability of renewable energy. By increasing the supply proportion of renewable energy, reducing consumption of fossil fuels and cutting down carbon emission, the power grid can run safely, steadily and economically and the sustainable development of energy and environment will be achieved.

(2) Realize gradient utilization and energy efficiency improvement

The gradient utilization can be achieved by developing gas turbine based cooling, heating and power generation system in MEMGs, and it will effectively transfer and use the power from fossil energy. It is an inevitable choice to enhance utilization ratio of the energy.

(3) Push the innovation and development of energy technology

MEMGs push the energy technology to be continuously innovated. The realization of

MEMGs has high requirements on technologies like ESS, energy replacement, response at user side, virtual power plant (VPP), CPS and multi-energy flow scheduling and control *etc*. This situation makes it a popular technological topic for research nowadays. Many innovative results have emerged and they have greatly pushed the development of energy technologies.

(4) Solve the problem on power supply in areas without electricity

In undeveloped places such as agricultural and stock raising areas, remote regions and islands, the connection to the grand power grid is weak, whereas the power generation investment is high and the power is generally insufficient. The power grid even can't cover the whole area. Using the MEMG technology will create a regional energy system and use the local resources. By doing this, the generation, dispatch and utilization of the electricity in such region can be independent from the main grid and the cost will be reduced. This new MEMGs can also connect to existing grid to offer support and share load so problems like insufficient power supply and unstable voltage will be solved in these regions.

1.5.2 Challenges of Developing MEMGs

(1) Technical issues

MEMGs include many kinds of energy supply methods, so it is necessary to coordinate its relationship to ensure the quality of power provided by MEMG, and ensure its safe and stable operation. What kind of control strategy should be adopted in different situations, such as what kind of power distribution strategy should be adopted in MEMGs when solar energy and wind energy are sufficient, and what kind of distribution strategy should be adopted when solar energy and other new energy are insufficient, so as to ensure the normal supply of power. These all need more detailed investigation and analysis.

(2) Legal and regulatory uncertainty

There are two key legal issues affecting the MEMGs: first, they are considered as distribution utilities and therefore supervised by state regulators; second, are they in line with the existing legal framework on electricity trading and generation and distribution rights? It is necessary to have a clear legal identity for the MEMGs to achieve the regulatory certainty required for the "banking" of the MEMG project, otherwise the potential cost is too high and the income is too uncertain to prove the rationality of the investment time and funds.

(3) Interconnection policy

The interconnection between MEMGs and power grid is the most important consideration: if the MEMGs cannot be connected to the public grid, they must operate permanently in island mode, lose the opportunity to obtain income from the grid services they could have provided, and damage their revenue. So how to integrate distributed energy into the grid in a safe way? How to ensure operation in grid connection mode, transition to intentional islanding mode, operation in islanding mode and reconnection to the grid, and specify the correct voltage, frequency and phase angle? To eliminate the possible problems in the MEMGs interconnection, we need standardized technical and dimensional requirements, clear review process, testing and certification procedures, set costs and simplified application process.

(4) Utility regulation

MEMGs are likely to be considered as a power company if it intends to serve multiple other unrelated retail customers. If the MEMGs are considered as a distribution facility, it may be obligated to provide services, which means it will be required to provide services at the written or oral request of a potential retail customer. In addition, MEMGs sold to retail customers may have to comply with various consumer protection laws. However, the MEMG does not fully meet the market participant categories defined by the restructuring, which may be because they exceed the categories of generation, transmission and distribution. Therefore, further efforts are needed to integrate it into the regulatory legal structure.

Chapter 2 Key Technologies of MEMGs

2.1 Modeling of MEMGs

In this section modeling for common components of MEMG are presented, including wind energy conversion system, solar PV system, CHP generation and fuel cells. Understanding the models are critical in analyzing the characteristics and performance of MEMGs.

2.1.1 Wind Energy Conversion System

As an energy conversion system that converts wind energy into electrical energy, various wind energy conversion systems (WECSs) technologies have become mature. According to whether the rotational speed of WTGs can be adjusted with the wind velocity, WECSs are mainly divided into two types: fixed speed WECSs and variable speed WECSs.

(1) Fixed speed WECS

In the fixed speed WECS, WTGs are directly connected to the power system, and stall control is adopted to maintain the rotational speed constant when the wind velocity changes. A typical fixed speed WECS is shown in Fig. 2-1, which is mainly composed of an aerodynamic system, a pitch control module, an induction generator and a shafting module.

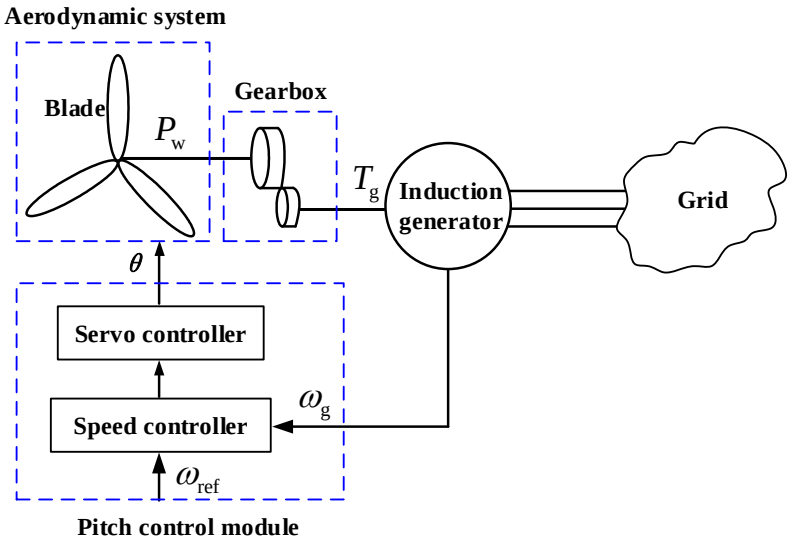

Fig. 2-1 Configuration of the fixed speed WECS

1) Aerodynamic system

The aerodynamic model describes the process by which a wind turbine converts wind energy into mechanical energy, and the power captured from the wind is given by:

$$P_{\mathrm{w}} = P_{\mathrm{wind}} C_{\mathrm{p}} = \frac{1}{2} \rho \pi R^2 v^3 C_{\mathrm{p}} \tag{2-1}$$

where ρ is the air density; R is the length of rotor blades; v is the wind velocity; C_{p} is the wind energy conversion efficiency, which is usually represented as a nonlinear function of blade tip speed ratio α and blade pitch angle β, and the blade tip speed ratio α is defined as:

$$\alpha = \frac{\omega R}{v} \tag{2-2}$$

Here, ω is the rotation speed of the rotor blades.

For a fixed pitch wind turbine, C_{p} is only related to α, which results in that the aerodynamic system can only obtain the maximum wind energy conversion efficiency when operating at a certain wind velocity. While the wind energy conversion efficiency C_{p} varies with blade tip speed ratio α and blade pitch angle β for a variable-pitch wind turbine. Through variable-pitch control, the wind turbines can always run at the maximum wind energy conversion efficiency.

2) Pitch control module

The pitch control module can continuously adjust the blade angle of wind turbine as the wind velocity changes, so that WECS can obtain a relatively stable power input. Active stall control is generally applied for variable pitch control of the fixed speed WECS. When the wind velocity is below the rated value, the controller sets the pitch angle to 0°, and the output power changes with the wind velocity according to the aerodynamic performance of the blade. When the wind velocity exceeds the rated velocity, the pitch angle control can prevent the rotational speed and output power from exceeding the rated value. The diagram of active stall control using the generator's rotational speed ω_{g} as a input signal is shown in Fig. 2-2.

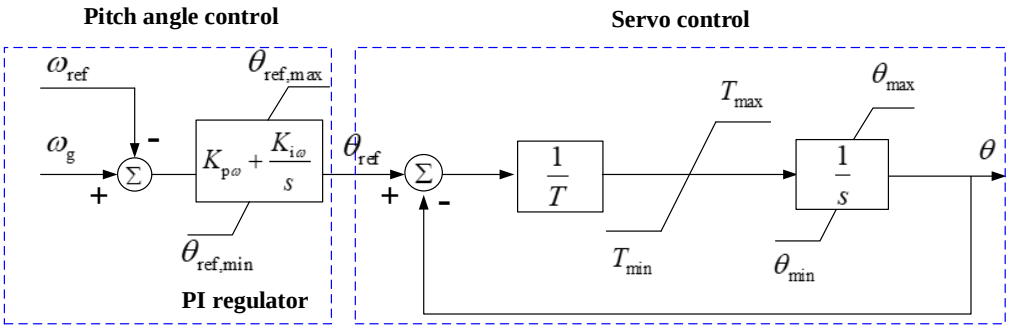

Fig. 2-2 Block diagram of active stall control module

The lower limit of the PI regulator is generally set to zero, so when the generator rotational speed ω_g is lower than the rated speed ω_{ref}, the output of the PI regulator is zero, and the pitch angle θ is controlled at 0° accordingly. When the generator rotational speed ω_g exceeds the rated speed, the output of the PI regulator is greater than zero, and the servo controller operates to adjust the pitch angle.

3) Shafting module

The shafting module of WECSs is mainly composed of three parts: a wind turbine mass, a gearbox mass, and a generator mass, in which the gearbox mass is used to mesh the wind turbine and the generator together. Due to the large inertia difference within these masses, the shafting module of WECSs is mainly divided into a three-mass model, a two-mass model, and a single-mass model. Here, the two-mass model is employed for description [1], and its schematic is shown in Fig. 2-3.

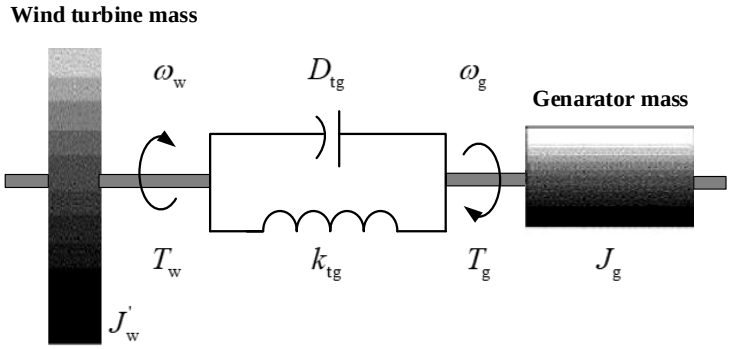

Fig. 2-3 Two-mass model schematic

In the two-mass model, the inertia of the gearbox is ignored because of its smaller inertia than that of the other two masses. Assuming that $J_{\mathrm{gear1}} = J_{\mathrm{gear2}} = 0$, variables related to the low-speed shaft can be converted to the high-speed shaft, and the corresponding state equation is as follows

$$\begin{cases} T_{\mathrm{w}} = J'_{\mathrm{w}} \frac{d\omega_{\mathrm{w}}}{dt} + D_{\mathrm{tg}}(\omega_{\mathrm{w}} - \omega_{\mathrm{g}}) + k_{\mathrm{tg}}(\theta_{\mathrm{w}} - \theta_{\mathrm{g}}) \\ -T_{\mathrm{g}} = J_{\mathrm{g}} \frac{d\omega_{\mathrm{g}}}{dt} + D_{\mathrm{tg}}(\omega_{\mathrm{g}} - \omega_{\mathrm{w}}) + k_{\mathrm{tg}}(\theta_{\mathrm{g}} - \theta_{\mathrm{w}}) \end{cases} \tag{2-3}$$

where, J'_{w} is the inertia constant of the wind turbine after conversion; D_{tg} and k_{tg} denote the damping coefficient and stiffness coefficient of the wind turbine after conversion, respectively.

(2) Variable speed WECS

Two main types of variable speed WECS are doubly-fed induction generator (DFIG)-based WECS and permanent magnet synchronous generator (PMSG)-based WECS. Since these two WECSs have similar structures, here the more widely used PMSG-based WECS is employed for introduction. A typical PMSG-based WECS is shown in Fig. 2-4, where PMSG is connected to the grid through a full-scale back-to-back converter.

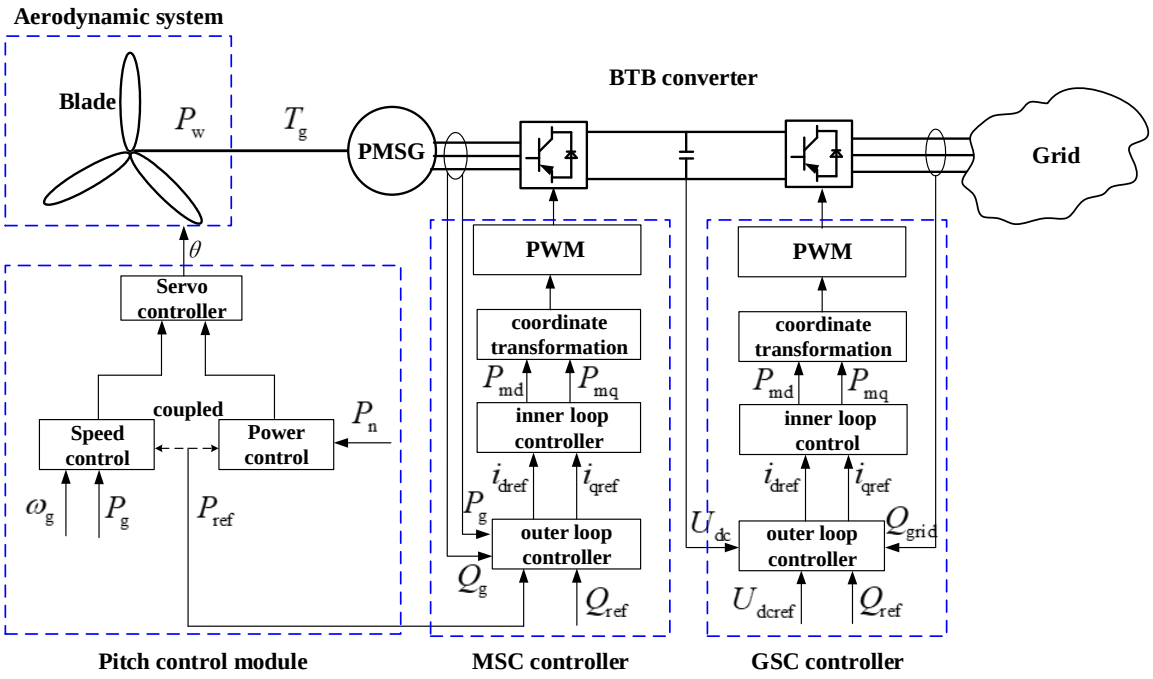

Fig. 2-4 Configuration of the PMSG-based WECS

1) PMSG model

The PMSG is modeled based on the d-q reference frame [2], and the terminal voltages of its stator can be expressed by the following equation:

$$v_{\mathrm{d}} = L_{\mathrm{d}} \frac{\mathrm{d}i_{\mathrm{d}}}{\mathrm{d}t} + Ri_{\mathrm{d}} - p\omega L_{\mathrm{q}} i_{\mathrm{q}} \tag{2-4}$$

$$v_{\mathrm{q}} = L_{\mathrm{q}} \frac{\mathrm{d}i_{\mathrm{q}}}{\mathrm{d}t} + Ri_{\mathrm{q}} + p\omega(L_{\mathrm{d}} i_{\mathrm{d}} + \lambda) \tag{2-5}$$

where v_{d} and v_{q} represent the terminal voltages of the stator in d/q axes, respectively; i_{d} and i_{q} are the stator currents in d/q axes, respectively; L_{d} and L_{q} denote the d/q axes inductance; R is the resistance of the stator winding; p is the pole pair number; ω represents the motor rotational speed; and λ denotes the permanent magnet flux linkage.

The mechanical equations of the PMSG mainly include:

$$T_{\mathrm{e}} = 1.5p[\lambda i_{\mathrm{q}} + (L_{\mathrm{d}} - L_{\mathrm{q}}) i_{\mathrm{d}} i_{\mathrm{q}}] \tag{2-6}$$

$$\frac{\mathrm{d}\omega}{\mathrm{d}t} = \frac{1}{J}(T_{\mathrm{m}} - T_{\mathrm{e}}) \tag{2-7}$$

Here, T_{e} and T_{m} are the electromagnetic torque and mechanical torque of the generator, respectively.

2) MSC Controller model

The MSC controller adopts stator voltage directional control, and the detailed control diagram is shown in Fig. 2-5. Because the WTG is modeled in the rotor reference coordinate system (RRF), the stator current i'_{sq} and i'_{sd} need to be transformed into the stator voltage reference coordinate system (SVRF) by the coordinate transformation in the dashed box ②. The output active power P_{g} and reactive power Q_{g} of the generator are filtered by a low-pass filter to remove high-frequency harmonics. The difference between the filtered power and the reference value is input to the PI regulator, so as to output the control command of the current inner loop, as shown in ③. Then the PWM modulation coefficient P'_{md} and P'_{mq} can be calculated by another PI regulator in the current inner loop control. In order to prevent the output modulation signal from being saturated, it is necessary to limit the modulation signal through the limiter in ⑤. Based on the modulated signals P_{md} and P_{mq}, the stator voltage can be modulated, and the RMS of the fundamental line-to-line voltage is given by:

$$\begin{cases} u_{\mathrm{gq}} = \frac{\sqrt{3}}{2\sqrt{2}} P_{\mathrm{mq}} U_{\mathrm{dc}} \\ u_{\mathrm{gd}} = \frac{\sqrt{3}}{2\sqrt{2}} P_{\mathrm{md}} U_{\mathrm{dc}} \end{cases} \tag{2-8}$$

where u_{gq} and u_{gd} denote the q-axis and d-axis component of the generator terminal voltage, respectively.

3) GSC Controller model

The GSC controller adopts grid converter voltage reference frame (GCVRF) control, in which the GSC voltage vector is set on the d-axis to implement the d/q axes decoupling control.

In the control diagram of GSC controller shown as Fig. 2-6, the capacitor voltage U_{dc} is filtered by a low-pass filter to remove high-frequency harmonics, and then the difference between the filtered voltage and the reference is input to a PI regulator, as shown in ②. Considering that the PMSG-based WECS generally adopts unit power factor control, the q-axis reference current is set to 0. Similar to MSC controller, the PWM modulation coefficient P'_{md} and P'_{mq} can be calculated by another PI regulator in the current inner loop control, and a limiter shown in ④ is employed to limit the modulation signal. Then, the stator voltage can be modulated based on the modulated signals P_{md} and P_{mq}, and the RMS of the fundamental line-to-line voltage is given by:

$$\begin{cases} u_{\mathrm{acd}} = \frac{\sqrt{3}}{2\sqrt{2}} P_{\mathrm{md}} U_{\mathrm{dc}} \\ u_{\mathrm{acq}} = \frac{\sqrt{3}}{2\sqrt{2}} P_{\mathrm{mq}} U_{\mathrm{dc}} \end{cases} \tag{2-9}$$

where u_{acq} and u_{acd} denote the q-axis and d-axis component of the GSC grid-connected bus voltage, respectively.

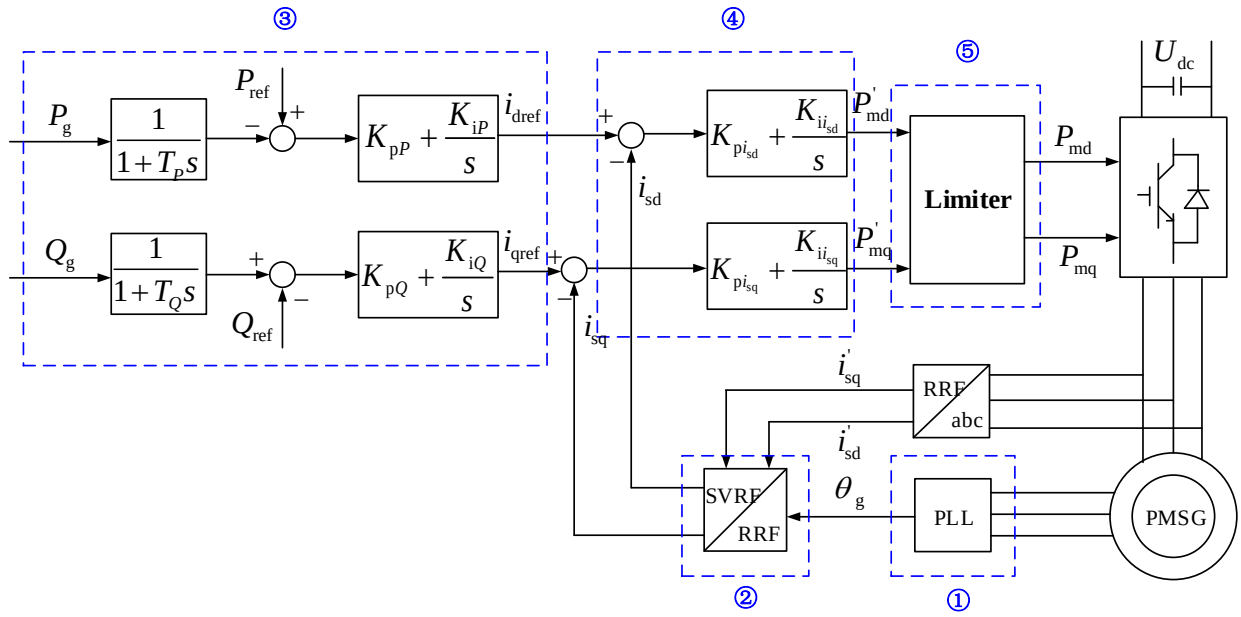

Fig. 2-5 Control diagram of MSC Controller

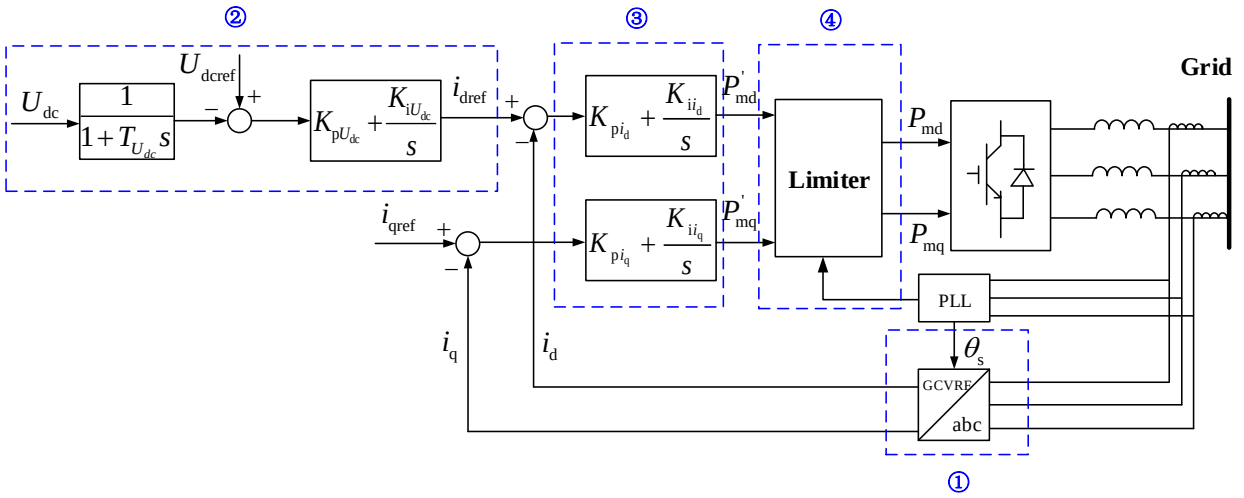

Fig. 2-6 Control diagram of GSC Controller

4) Pitch control module

The pitch control module is a key to controlling the WECS to track the maximum wind power, thereby effectively improving the wind energy utilization. The stable power output is mainly achieved through the following three paths [3]:

i. When the wind velocity is lower than the rated velocity, the pitch control module cooperates with the converter controller for optimal power control;

ii. When the WTG's rotational speed exceeds the rated speed, the rotational speed is

limited to maintain the rated value;

iii. When the wind velocity exceeds the rated velocity, power limit control is performed to maintain the output power at the rated value.

In addition, the aerodynamic system of the PMSG based WECS is the same as that of the fixed speed WECS, and is not be described here.

2.1.2 Solar PV System

Solar PV system is the most common way to convert energy from the sun directly into electricity. In recent years, installations of grid-connected PV systems have been growing at an ever-increasing rate, due to government incentives and the rapid fall in costs [4].

A PV cell is the most basic unit in PV energy system. The power generated by a single PV cell is usually too low, so PV cells are connected in series and in parallel to form a PV module, with output voltage in the range of tens of volts. Multiple PV module can be grouped into PV array, which is the core component of a PV energy system. PV cell generates DC power. Its equivalent circuit is shown in Fig. 2-7 [5]. The diode used here is not an idealized component, but represents non-linear voltage-current relationship of the PV cell. The bulk resistance of the semiconductor material adds a series resistance to the ideal forward-biased diodes, and non-ideal partial short-circuiting near the junction introduces a shunt resistance.

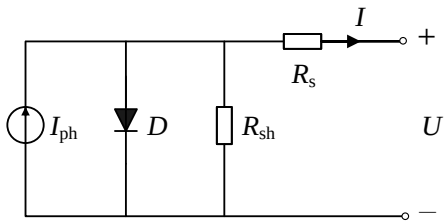

Fig. 2-7 Equivalent circuit of PV cell with single diode model

The output current of the PV cell for this equivalent circuit can be given below:

$$I = I_{\text{ph}} - I_{\text{s}}\left(\text{e}^{\frac{q(U+IR_{\text{S}})}{AkT}} - 1\right) - \frac{U+IR_{\text{s}}}{R_{\text{sh}}} \tag{2-10}$$

where U is the output voltage, I is the output current, I_{ph} is the light generated current, I_s is the dark saturation current, q is the charge of an electron ($1.60217662 \times 10^{-19}$ C), k is Boltzmann's constant (1.381×10^{-23} J/K), T is the absolute temperature of the PV cell, A is a constant between 1 and 2.

When identical PV cells are connected to form a PV array, ignoring the resistance of the connection cable and assuming the parameters of these PV cells are identical, the equivalent circuit of a PV circuit is shown in Fig.2-8 [6]:

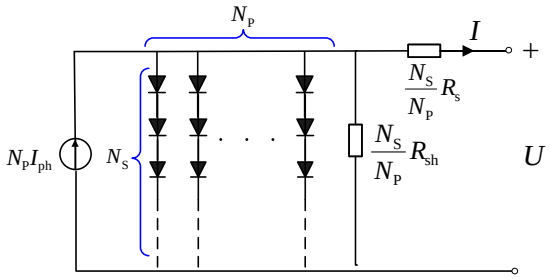

Fig. 2-8 Equivalent circuit of PV array with single diode model

From the equivalent circuit the voltage-current relationship of the solar array can be derived:

$$I = N_P I_{ph} - N_P I_s \left(e^{\frac{q}{AkT}\left(\frac{U}{N_S}+\frac{IR_S}{N_P}\right)} - 1 \right) - \frac{N_P}{R_{sh}}\left(\frac{U}{N_S}+\frac{IR_S}{N_P}\right) \quad (2\text{-}11)$$

where N_P is the number of PV cells connected in parallel in the solar array, N_S is the number of PV cells connected in series in the solar array.

2.1.3 CHP Generation

CHP plant can generate heat in addition to electricity by reusing waste heat, which is produced as a by-product of electricity generation, for industrial and residential uses. With the ability to meet heating, cooling and electricity demand of its users, CHP plant reduces fuel consumption and improves energy efficiency. Designed for domestic and commercial applications, microturbines are small gas turbines that is convenient to install and maintain, yet achieves high energy efficiency and low pollutant emission. Microturbine energy plant mainly consists of compressor, combustor, gas turbine and generator.

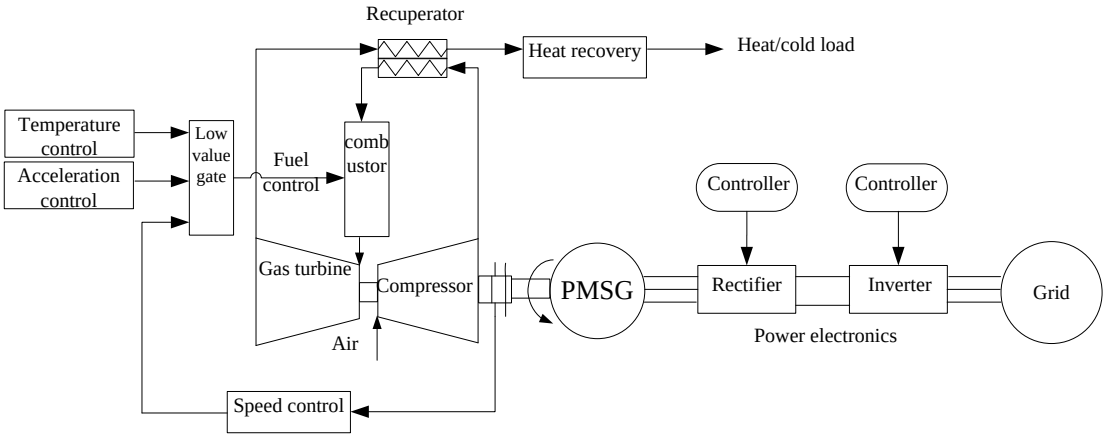

Fig. 2-9 Composition of Microturbine CHP system

Rowen turbine model [7], as shown in Fig. 2-10, is a common model used in transient stability simulation. The model contains speed controller, fuel controller, gas turbine and temperature controller.

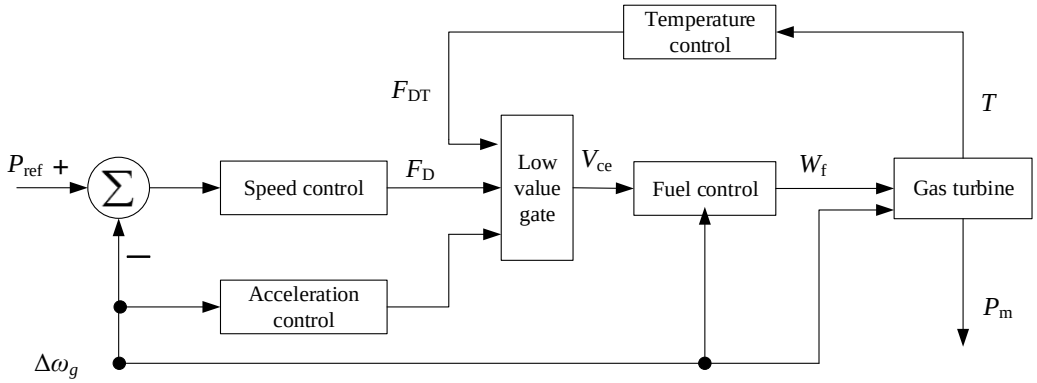

Fig. 2-10 Model of Microturbine CHP system

The detailed transfer function for microturbine energy plant is shown in Fig. 2-11. The speed controller controls fuel intake in order to maintain the stability of turbine rotation speed. The acceleration controller limits the acceleration rate of turbine when the microturbine system starts, and is shutdown when the system has reached operational rotation speed. The fuel controller receives input of V_{ce} and $\Delta\omega_g$ and controls the flux of fuel valve. The gas turbine module models the characteristics of combustion system and gas turbine, produces the value of gas temperature and mechanical power generated by the turbine. The temperature controller models the protective

system that protects the microturbine system by monitoring the exhaust temperature and reducing fuel intake when the temperature goes too high [8].

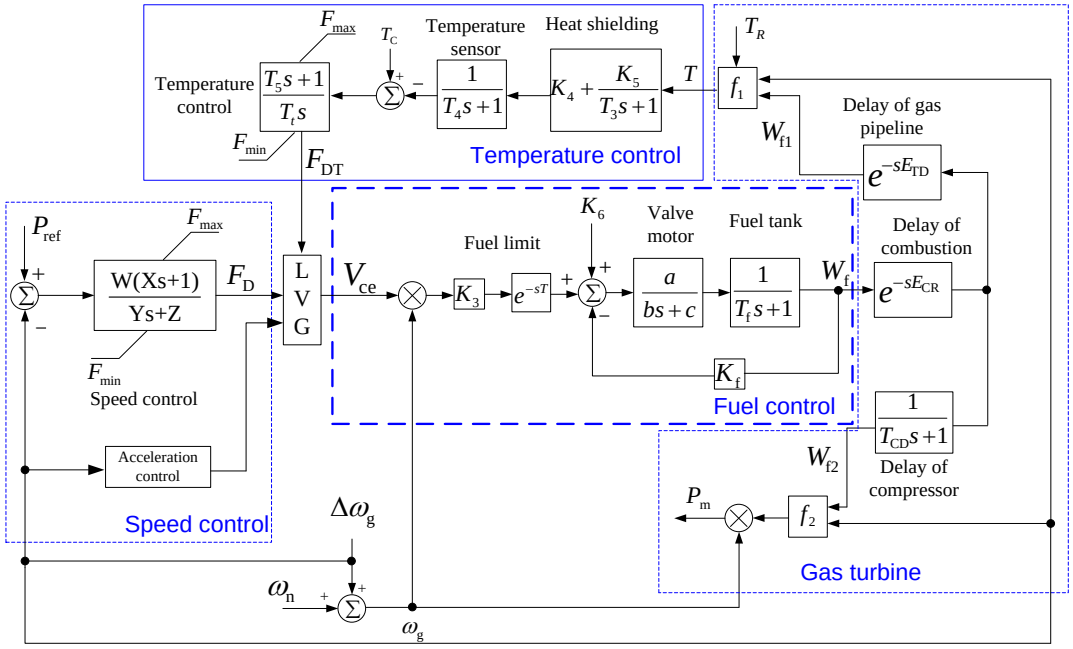

Fig. 2-11 Control system of Microturbine CHP system

The generator is interfaced with VSC AC-DC-AC converter to convert the high frequency power into grid frequency. The controller used include outer loop control, inner loop control and pulse width modulation. The control methods used with microturbine include $i_{sd} = 0$ control, output voltage control, $\cos\varphi = 1$ control and maximum output power control.

2.1.4 Fuel Cells

Fuel cells are efficient, environmentally friendly and quiet energy conversion system that directly converts chemical energy in fuel into electrical energy through electrochemical reactions. It has many advantages due to the lack of combustion process when converting chemical energy into electrical energy. Fuel cell models can be divided into three types based on the time scale of dynamic processes: (1) Short-term dynamic model considering electric double layer effect; (2) Medium-term dynamic model considering electrochemical process of reactant gas pressure change; (3) Long-term dynamic model considering thermodynamic process of temperature change.

In the short-term dynamic simulation of fuel cells, because the simulation time is relatively short, the time constants of the gas partial pressure and temperature are generally considered in

minutes, and the gas partial pressure and temperature can be considered constant in the short-term dynamic simulation. The equivalent circuit model for a single fuel cell is shown in Fig. 2-12. This is the most widely used equivalent circuit model. It can be used to represent low-temperature fuel cells, and also high-temperature fuel cells with slightly different calculation of parameters [9].

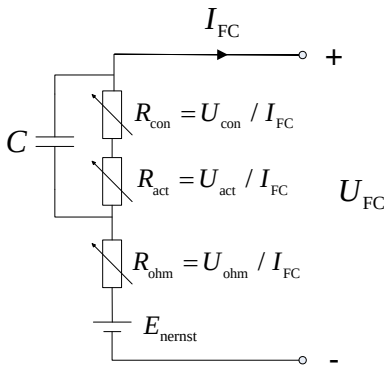

Fig. 2-12 The equivalent circuit model for a single fuel cell

In Fig. 2-12, U_{FC} and I_{FC} are the voltage and current of the fuel cell; $E_{\mathrm{enerst}}$is the reversible open circuit voltage of the battery, also known as "Nernst voltage"; R_{ohm} is the ohmic overvoltage equivalent resistance, and its voltage drop U_{ohm} is called the ohmic overvoltage; R_{act} is the activation overvoltage equivalent resistance, and its voltage drop is U_{act}; R_{con} is the concentration overvoltage equivalent resistance, and its voltage drop is U_{con}; C is the equivalent capacitance reflecting the electric double layer effect of the fuel cell. Delay characteristics due to activation and concentration overvoltage. The time constant τ of the electric double layer effect delay characteristic can be expressed by $\tau = CR_{\mathrm{a}}$, where R_{a} is the equivalent resistance (Ω), which is determined by the operating current and activation, concentration overvoltage:

$$R_{\mathrm{a}} = \frac{U_{\mathrm{act}}+U_{\mathrm{con}}}{I_{\mathrm{FC}}} \tag{2-12}$$

When N single fuel cells are connected in series to form a fuel cell stack, and it is assumed that the parameters of each cell are the same, the equivalent circuit model for a fuel cell stack is remaining the same in Fig. 2-12 with adjusted parameters according to the series circuit law [10].

When considering the effect of changes in gas partial pressure on the dynamic characteristics of the fuel cell, and the dynamic process time is not long enough for temperature to significantly

affect the system dynamic characteristics, the temperature of the fuel cell can still be regarded as a constant. The fuel cell model at this time is called the medium term dynamic model [11-12].

When the simulation time scale of the dynamic process is so large that the effects of temperature changes need to be considered, the fuel cell needs a long-term dynamic model, it can be assumed that the dynamic process of electric double layer effect and gas pressure change has ended, and only the dynamic process caused by temperature change is considered.

In the long-term dynamic modelling process, it is assumed that each part of the fuel cell stack has the same temperature, and the temperature difference between adjacent battery cells is ignored. It can be determined by the energy conservation equation [13-15].

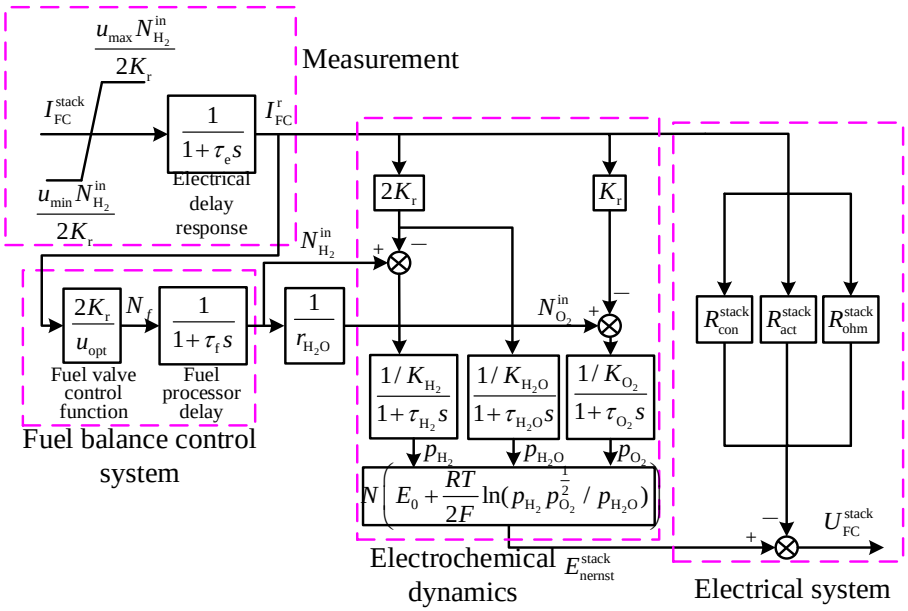

Fig. 2-13 Block diagram of typical mid-term dynamic model of a fuel cell stack

2.1.5 Battery Storage Systems

Electrochemical batteries are energy storage devices that store and release electricity by alternating between the charge–discharge phases. They can efficiently store electricity in chemicals and reversibly release it according to demand, without harmful emissions or noise, and require little maintenance. A variety of such batteries is available in the market, such as LA, Na-S, nickel-cadmium (Ni-Cd), nickel-metal hydride (Ni-Mh) and lithium-ion batteries. Their main advantages are energy density and technological maturity. Their main disadvantage however is their relatively low durability for large-amplitude cycling (a few 100 to a few 1000 cycles).

One of the important parameters of a battery is its state of charge (SOC). It is defined as

$$\mathrm{SOC} = \frac{Q_\mathrm{r}}{C} \tag{2-13}$$

where Q_r is the residual capacities of the battery in Ah, and C is the capacity of the battery in Ah.

Some of the commonly used battery technologies are LA batteries, lithium-ion batteries, Ni based batteries and Na-S batteries. LA energy storage cells are the most well-known and commercially mature (deployed since about 1890) rechargeable battery technology. A good combination of power density and low price make LA batteries suitable for many applications such as emergency power supply systems, stand-alone systems with PV, and mitigation of output fluctuations from wind power. Their disadvantages include relatively heavy weight, cycle life limitations and maintenance requirements.

Common battery charge and discharge dynamic models include electrochemical models and equivalent circuit models. For LA batteries, common equivalent circuit models currently include simple equivalent circuit models, Thevenin equivalent circuit models, third-order dynamic models, and fourth-order dynamic models [16], *etc*. The most detailed model is the fourth-order dynamic model proposed by Giglioli *et al*. in 1990 [17].

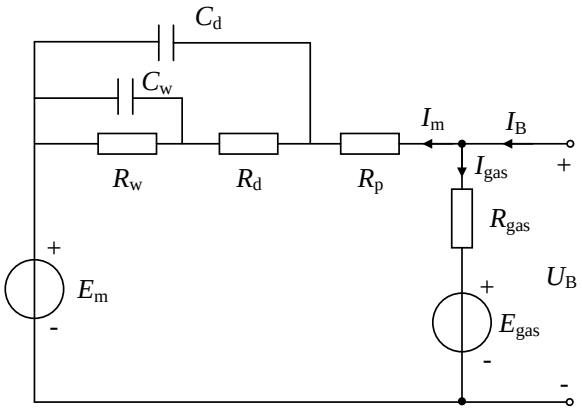

Fig. 2-14 The fourth-order dynamic model.

Considering the different time scales of the realistic problem, the fourth-order dynamic model shown in Fig. 2-14 can be simplified according to the needs of the research. This section focuses on the short-term battery discharge model.

Since the temperature of the electrolyte can be considered constant in short-term dynamic simulation, and its self-discharge and diffusion effects can be ignored. The short-term discharge

process of the battery can be described using the equivalent circuit model shown in Fig. 2-15 [18]. This is a Thevenin equivalent circuit model that can accurately describe the short-term discharge characteristics of LA batteries.

In Fig. 2-15, U_{B} is the terminal voltage of the battery (V); I_{B} is the discharge current of the battery (A), which is positive when the battery is discharged; E_{m} is the open circuit voltage of the battery (V); $R_{\mathrm{p}}$is the ohmic polarization resistance (mΩ), which reflects the voltage drop caused by internal resistance; $R_{\mathrm{o}}$is the discharge overvoltage resistance (mΩ), which reflects the energy loss caused by charge transfer in the electric double layer; C_{o} is the discharge overvoltage capacitor (F), which describes the dynamics of the electric double layer effect of the battery. Assume τ_{o} is the time constant (s) of the electric double layer effect. Generally, $\tau_{\mathrm{o}} = R_{\mathrm{o}}C_{\mathrm{o}}$ is less than 1s. Assuming the battery parameters are constant, the terminal voltage of the battery during discharge can be calculated by the following formula:

$$U_{\mathrm{B}}(t) = E_{\mathrm{m}} - I_{\mathrm{B}}\left(R_{\mathrm{p}} + R_{\mathrm{o}}\right) + I_{\mathrm{B}}R_{\mathrm{o}}e^{-\frac{t}{\tau_{\mathrm{o}}}} \tag{2-14}$$

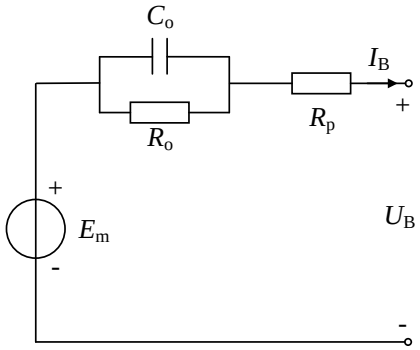

Fig. 2-15 The short-term batteries discharge equivalent circuit.

2.2 Transient Simulation of MEMGs

MEMGs include renewable energy generation, distributed energy storage, multiple energy conversion device, and the advent of novel power electronic equipment. It is important to study the transient behavior of such MEMGs as stability and reliability may be compromised due to the variation of renewable generation and switching of power electronic equipment. This chapter addresses the transient analysis of MEMGs through electromagnetic transient simulations.

2.2.1 Nodal Analysis for Transient Simulation

For electromagnetic transient simulations, two approaches are used, i.e. the nodal analysis and the state space analysis. The basic process of nodal analysis is to establish a set of differential equations (state equations) that describes the dynamics of the system, and then apply certain numerical integration formula to the differential equations as a whole. The major advantage of the state space analysis is the flexibility in choosing the integration algorithms. However, the formation of the state equations for a large power system could be challenging. The nodal analysis on the other hand uses a bottom-up modeling approach that applies the integration formulas at the branch level, which significantly simplifies the modeling process. Many commercial electromagnetic transient simulation programs use the nodal analysis approach, and they are commonly referred as EMTP-type programs. The following part of this chapter focuses on the nodal analysis approach.

(1) Electrical System Element Modeling

A numerical integration formula is used to discretize the differential equations corresponding to each element into algebraic equations. These algebraic equations are represented in the form of equivalent circuits of the elements. The ensemble circuit formed by connecting the equivalent circuits of each element is then analyzed using the nodal analysis method and a set of algebraic equations are derived. These equations are then solved using proper numerical methods.

The implicit trapezoidal method is the most commonly used integration formula in the nodal analysis framework. The discretization rule can be summarized as:

1) replace variable px with $(x(t) - x(t-\Delta t))/\Delta t$, where p is the differential operator;

2) replace variable x with $(x(t) + x(t-\Delta t))/2$;

3) constants and constant coefficients remain unchanged.

Take the inductor branch shown in Fig. 2-16(a) as an example, the *V-I* relationship of the branch is described by

$$L \cdot \mathrm{p} i_{\mathrm{km}} = u_{\mathrm{k}} - u_{\mathrm{m}} \tag{2-15}$$

(a) inductor branch **(b) equivalent circuit**

Fig. 2-16 Inductor branch and its equivalent circuit

Applying the discretization rule of the trapezoidal method, the resultant algebraic equation is

$$L\left[\frac{i_{km}(t)-i_{km}(t-\Delta t)}{\Delta t}\right]=\frac{u_k(t)+u_k(t-\Delta t)}{2}-\frac{u_m(t)+u_m(t-\Delta t)}{2} \tag{2-16}$$

This equation can be rearranged as

$$i_{km}(t)=\frac{\Delta t}{2L}\big(u_k(t)-u_m(t)\big)+I_h(t-\Delta t) \tag{2-17}$$

where $I_h(t\text{-}\Delta t)$ is referred as the history current source, with the form:

$$I_h(t-\Delta t)=i_{km}(t-\Delta t)+\frac{\Delta t}{2L}\big(u_k(t-\Delta t)-u_m(t-\Delta t)\big) \tag{2-18}$$

The difference formula (2-17) can be viewed as a Norton equivalent circuit with an equivalent conductance of $G_{eq} = \Delta t/2L$ paralleled with the history current source, as shown in Fig. 2-16(b).

Among the multi-phase elements with mutual coupling, the coupled inductor element shown in Fig. 2-17 is most frequently seen. Using the familiar implicit trapezoidal method as the discretization rule, the characteristic equation of the element, equivalent conductance and history current source for the multi-phase elements can be expressed in a similar way to the single-phase elements in matrix-vector notation:

$$\boldsymbol{L}\cdot \mathrm{p}\boldsymbol{i}_{km}=\boldsymbol{u}_k-\boldsymbol{u}_m \tag{2-19}$$

$$\boldsymbol{G}_{eq}=\Delta t\boldsymbol{L}^{-1}/2 \tag{2-20}$$

$$\boldsymbol{I}_h(t-\Delta t)=\boldsymbol{i}_{km}(t-\Delta t)+\Delta t\boldsymbol{L}^{-1}\big(\boldsymbol{u}_k(t-\Delta t)-\boldsymbol{u}_m(t-\Delta t)\big)/2 \tag{2-21}$$

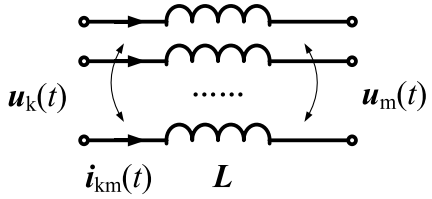

Fig. 2-17 Multi-phase coupled inductor branch

Discretization on the element level requires the utilized numerical integration formula to have a simple form, so that the expression of the equivalent conductance and history current source is not too complicated, and with good numerical stability and accuracy. The implicit trapezoidal formula is usually a good choice for the electromagnetic transient simulation.

(2) Modeling and Simulation at the System Level

After assembling an equivalent circuit comprised of voltage sources, current sources, conductance and switches, the nodal analysis is applied to establish a set of equations that represent the nodal voltage and branch current constraint, alongside with the equations of each element. This set of equations is the fundamental equation of the electromagnetic transient simulation of the distribution systems and is in the form of (2-22):

$$\boldsymbol{Gu} = \boldsymbol{i} \tag{2-22}$$

where the $\boldsymbol{G}$ matrix and $\boldsymbol{i}$ vector are comprised of the equivalent conductance G_{eq} and the history current source I_h. For illustration, the contribution to the $\boldsymbol{G}$ matrix and $\boldsymbol{i}$ vector from a single phase element that is connected between node k and m is shown in Fig. 2-18(a), and the contribution from a three-phase element connected between $\{k_1, k_2, k_3\}$ and $\{m_1, m_2, m_3\}$ is shown in Fig. 2-18(b).

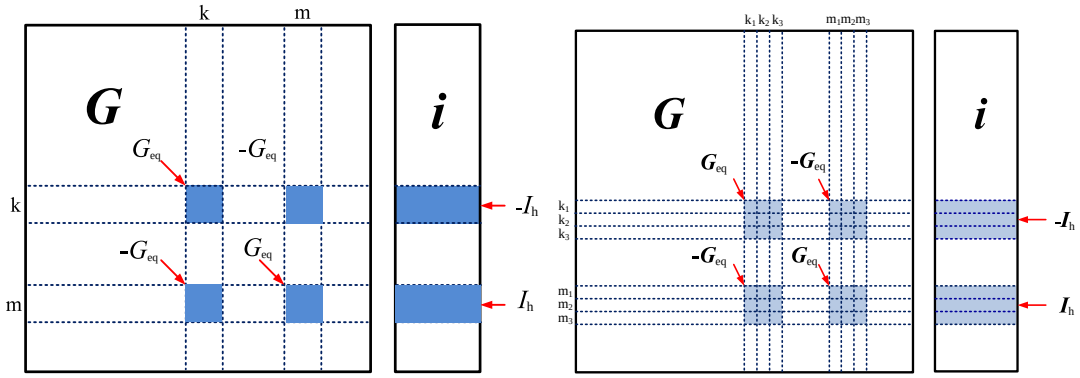

(a) single phase element **(b) multi-phase coupled element**

Fig. 2-18 Formation of the nodal conductance matrix and current source vector

The solution of Equation (2-22) gives the transient response of the system at the specified time instant. As Equation (2-22) is in the form of a linear system $\boldsymbol{Ax} = \boldsymbol{b}$, a sparse library such as Sparse [19], KLU [20], *etc*. can be used to solve it.

Modeling with the nodal analysis formulation has certain limitations, such as the inconvenience in handling current-dependent elements (e.g. the ideal transformer model) and ungrounded ideal voltage sources. The electronic circuit simulation program SPICE has utilized the Modified Nodal Approach (MNA) to address above issues of the program [21]; on this basis, the Modified Augmented Nodal Analysis (MANA) further enhances the handling of ideal switch branches [22]. The fundamental equation under the MANA framework is shown as follows:

$$\begin{bmatrix} \boldsymbol{Y}_{\mathrm{n}} & \boldsymbol{V}_{\mathrm{c}} & \boldsymbol{D}_{\mathrm{c}} & \boldsymbol{S}_{\mathrm{c}} \\ \boldsymbol{V}_{\mathrm{r}} & \boldsymbol{V}_{\mathrm{d}} & \boldsymbol{D}_{\mathrm{VD}} & \boldsymbol{S}_{\mathrm{VS}} \\ \boldsymbol{D}_{\mathrm{r}} & \boldsymbol{D}_{\mathrm{DV}} & \boldsymbol{D}_{\mathrm{d}} & \boldsymbol{S}_{\mathrm{DS}} \\ \boldsymbol{S}_{\mathrm{r}} & \boldsymbol{S}_{\mathrm{SV}} & \boldsymbol{S}_{\mathrm{SD}} & \boldsymbol{S}_{\mathrm{d}} \end{bmatrix} \begin{bmatrix} \boldsymbol{v}_{\mathrm{n}} \\ \boldsymbol{i}_{\mathrm{V}} \\ \boldsymbol{i}_{\mathrm{D}} \\ \boldsymbol{i}_{\mathrm{S}} \end{bmatrix} = \begin{bmatrix} \boldsymbol{i}_{\mathrm{n}} \\ \boldsymbol{v}_{\mathrm{b}} \\ \boldsymbol{d}_{\mathrm{b}} \\ \boldsymbol{s}_{\mathrm{b}} \end{bmatrix} \tag{2-23}$$

The MANA formulation (2-23) includes the voltage source branch current $\boldsymbol{i}_{\mathrm{V}}$, the controlled source branch current $\boldsymbol{i}_{\mathrm{D}}$, and the ideal switch branch current $\mathbf{i}_{\mathrm{S}}$ as unknown variables besides the nodal voltage $\boldsymbol{v}_{\mathrm{n}}$. The device equations of these branches are then listed below the nodal equations. For a voltage source connected between node k and m, the branch equation is $v_{\mathrm{k}} - v_{\mathrm{m}} = v_{\mathrm{b,km}}$, which is inserted into (2-23) by adding 1 and -1 in column *k* and *m*, respectively, of matrix $\boldsymbol{V}_{\mathrm{r}}$, and include $v_{\mathrm{b},km}$ in the vector $\boldsymbol{v}_{\mathrm{b}}$. Take an ideal switch connected between node p and q as another example: when the switch is on, equation $v_{\mathrm{p}} - v_{\mathrm{q}} = 0$ is included, which again contributes 1 and -1 to the matrix $\boldsymbol{S}_{\mathrm{r}}$; when the switch is off, the equation $i_{\mathrm{s,pq}} = 0$ is included, which contributes 1 in the corresponding column of $\boldsymbol{S}_{\mathrm{d}}$. The MANA method is used in this chapter in modeling the electrical MEMGs.

2.2.2 Multirate Real Time Simulation of MEMGs

Real-time simulation of MEMGs is capable of reproducing the dynamic behaviors of the real system and testing the system equipment and operation strategies. However, real-time simulation of MEMGs exhibiting a wide range of time-scales puts forward higher requirements for simulation accuracy and efficiency. This chapter presents an extendable method and design for the real-time simulation of MEMGs utilizing high-performance hardware field programmable gate arrays (FPGAs). In the aspect of numerical algorithm, a high-accuracy and stable multirate simulation algorithm is proposed. The entire MEMGs is decoupled into different subsystems by their inherent time-scales and distinct time steps are used to solve the subsystems.

(1) Network decomposition

Generally, the Bergeron line model can't be directly used for the modelling of the short line as the propagation delay time is often not longer than the time-step. Here, the short line is adjusted to have a propagation delay of one or several certain time steps [23]. The short line is essentially modelled by a series resistance-inductance branch as Fig. 2-19(a) shows, where R and L are the lumped resistance and inductance. Assuming that the branch comprises infinitely connected inductances and resistances ($\Delta x \cong 0$), and adding unreal distributed capacitances throughout the line, a Bergeron line model is derived as Fig. 2-19(b) shows, where L' is the inductance, R' is the resistance and C' the capacitance per unit length. The length of the line is set to d artificially.

The characteristic equations of the Bergeron line model at both ends k and m are:

$$\begin{cases} i_{\mathrm{km}}(t) = 1/(Z + R/4)v_{\mathrm{k}}(t) + I_{\mathrm{k}}(t-\tau) \\ i_{\mathrm{mk}}(t) = 1/(Z + R/4)v_{\mathrm{m}}(t) + I_{\mathrm{m}}(t-\tau) \end{cases} \tag{2-24}$$

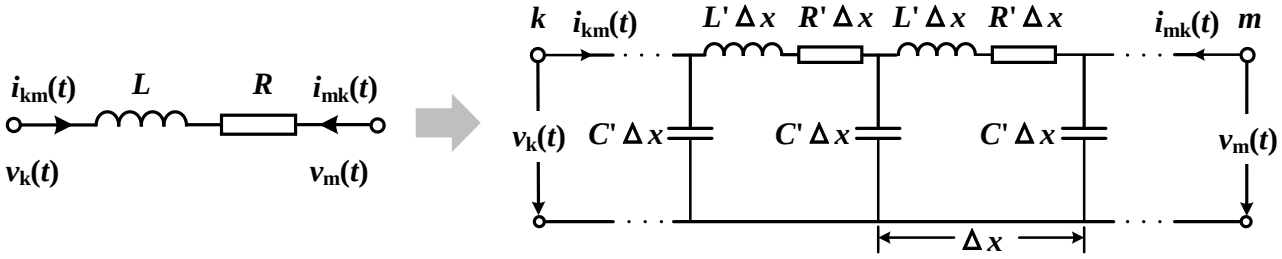

(a) Short line **(b) Bergeron line model**

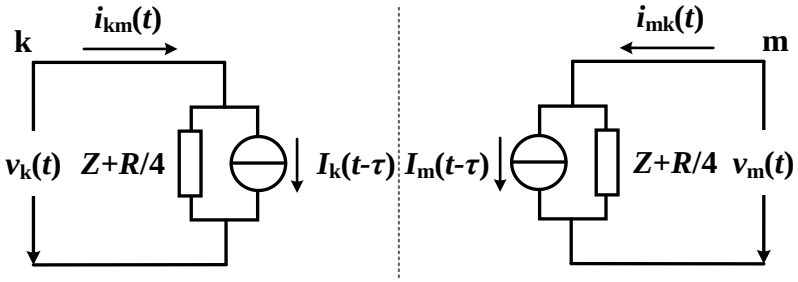

(c) Equivalent circuit of Bergeron line model.

Fig. 2-19 Bergeron line model and its equivalent circuit model

The surge impedance Z and propagation delay time τ are given by:

$$Z = \sqrt{L'/C'} \tag{2-25}$$

$$\tau = d\sqrt{L'C'} \tag{2-26}$$

The history current source I_{k} and I_{m} are computed as:

$$\begin{cases} I_{\mathrm{k}} = (B_1 v_{\mathrm{k}} + B_3 i_{\mathrm{km}}) + (B_2 v_{\mathrm{m}} + B_4 i_{\mathrm{mk}}) \\ I_{\mathrm{m}} = (B_1 v_{\mathrm{m}} + B_3 i_{\mathrm{mk}}) + (B_2 v_{\mathrm{k}} + B_4 i_{\mathrm{km}}) \end{cases} \tag{2-27}$$

where the coefficients B_1, B_2, B_3 and B_4 are given by:

$$B_1 = \frac{-R/4}{(Z+R/4)^2}, B_2 = \frac{-Z}{(Z+R/4)^2}, B_3 = \frac{-R/4(Z-R/4)}{(Z+R/4)^2}, B_4 = \frac{-Z(Z-R/4)}{(Z+R/4)^2} \tag{2-28}$$

Fig. 2-19(c) shows the resulting two-port equivalent circuit model. There is no direct connection between the two terminals, thus decomposition can be performed. Note that C' is a direct consequence of modelling the RL branch as a Bergeron line model and would not normally exist in the circuit. It shouldn't be too large. In general, the value of X_c should be significantly larger than the surrounding impedances. Applying the decomposition approach, the schematic network can be substituted by Fig. 2-20.

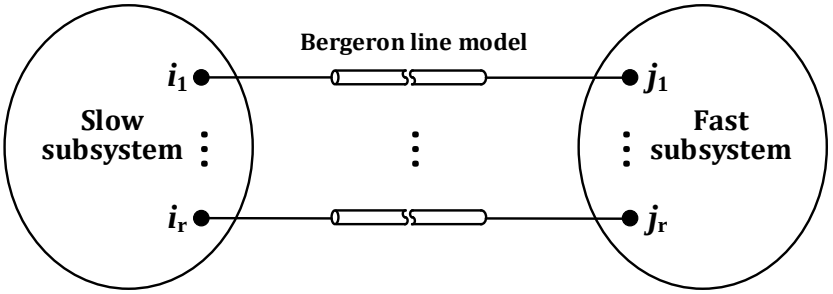

Fig. 2-20 Sample network decoupled by Bergeron line model

The nodal formations for the decoupled slow and fast subsystems using Bergeron line model are derived as

$$\begin{cases} \boldsymbol{G}_{\mathrm{s}} \boldsymbol{v}_{\mathrm{s}}(t) = \boldsymbol{i}_{\mathrm{s}}(t) - \boldsymbol{I}_{\mathrm{h,s}}(t - \Delta T) - \boldsymbol{I}_{\mathrm{IF,s}}(t - \tau) \\ \boldsymbol{G}_{\mathrm{f}} \boldsymbol{v}_{\mathrm{f}}(t) = \boldsymbol{i}_{\mathrm{f}}(t) - \boldsymbol{I}_{\mathrm{h,f}}(t - \Delta t) - \boldsymbol{I}_{\mathrm{IF,f}}(t - \tau) \end{cases} \tag{2-29}$$

where $\boldsymbol{I}_{\mathrm{IF,s}}(t-\tau)$ and $\boldsymbol{I}_{\mathrm{IF,f}}(t-\tau)$ are computed by:

$$\begin{cases} \boldsymbol{I}_{\mathrm{IF,s}}(t-\tau) = \left(\boldsymbol{B}_1 \boldsymbol{v}_{\mathrm{IF,s}}(t-\tau) + \boldsymbol{B}_3 \boldsymbol{i}_{\mathrm{IF,s}}(t-\tau)\right) + \left(\boldsymbol{B}_2 \boldsymbol{v}_{\mathrm{IF,f}}(t-\tau) + \boldsymbol{B}_4 \boldsymbol{i}_{\mathrm{IF,f}}(t-\tau)\right) \\ \boldsymbol{I}_{\mathrm{IF,f}}(t-\tau) = \left(\boldsymbol{B}_1 \boldsymbol{v}_{\mathrm{IF,f}}(t-\tau) + \boldsymbol{B}_3 \boldsymbol{i}_{\mathrm{IF,f}}(t-\tau)\right) + \left(\boldsymbol{B}_2 \boldsymbol{v}_{\mathrm{IF,s}}(t-\tau) + \boldsymbol{B}_4 \boldsymbol{i}_{\mathrm{IF,s}}(t-\tau)\right) \end{cases} \tag{2-30}$$

To simplify the representation, we have:

$$\begin{cases} \boldsymbol{I}_{\mathrm{IF,s}}(t-\tau) = \boldsymbol{I}_{\mathrm{s,s}}(t-\tau) + \boldsymbol{I}_{\mathrm{s,f}}(t-\tau) \\ \boldsymbol{I}_{\mathrm{IF,f}}(t-\tau) = \boldsymbol{I}_{\mathrm{f,f}}(t-\tau) + \boldsymbol{I}_{\mathrm{f,s}}(t-\tau) \end{cases} \tag{2-31}$$

in which

$$\begin{cases} \boldsymbol{I}_{\mathrm{s,s}}(t-\tau) = \boldsymbol{B}_1\boldsymbol{v}_{\mathrm{IF,s}}(t-\tau) + \boldsymbol{B}_3\boldsymbol{i}_{\mathrm{IF,s}}(t-\tau) \\ \boldsymbol{I}_{\mathrm{s,f}}(t-\tau) = \boldsymbol{B}_2\boldsymbol{v}_{\mathrm{IF,f}}(t-\tau) + \boldsymbol{B}_4\boldsymbol{i}_{\mathrm{IF,f}}(t-\tau) \\ \boldsymbol{I}_{\mathrm{f,f}}(t-\tau) = \boldsymbol{B}_1\boldsymbol{v}_{\mathrm{IF,f}}(t-\tau) + \boldsymbol{B}_3\boldsymbol{i}_{\mathrm{IF,f}}(t-\tau) \\ \boldsymbol{I}_{\mathrm{f,s}}(t-\tau) = \boldsymbol{B}_2\boldsymbol{v}_{\mathrm{IF,s}}(t-\tau) + \boldsymbol{B}_4\boldsymbol{i}_{\mathrm{IF,s}}(t-\tau) \end{cases} \tag{2-32}$$

Hence, (2-29) can be rearranged as:

$$\begin{cases} \boldsymbol{G}_{\mathrm{s}}\boldsymbol{v}_{\mathrm{s}}(t) = \boldsymbol{i}_{\mathrm{s}}(t) - \boldsymbol{I}_{\mathrm{h,s}}(t-\Delta T) - \boldsymbol{I}_{\mathrm{s,s}}(t-\tau) - \boldsymbol{I}_{\mathrm{s,f}}(t-\tau) \\ \boldsymbol{G}_{\mathrm{f}}\boldsymbol{v}_{\mathrm{f}}(t) = \boldsymbol{i}_{\mathrm{f}}(t) - \boldsymbol{I}_{\mathrm{h,f}}(t-\Delta t) - \boldsymbol{I}_{\mathrm{f,f}}(t-\tau) - \boldsymbol{I}_{\mathrm{f,s}}(t-\tau) \end{cases} \tag{2-33}$$

As can be seen from (2-33), when solving the slow subsystem, $\boldsymbol{I}_{\mathrm{s,s}}$ is updated with ΔT and $\boldsymbol{I}_{\mathrm{s,f}}$ is updated with Δt. If τ is not a multiple of ΔT and Δt, $\boldsymbol{I}_{\mathrm{s,s}}$ and $\boldsymbol{I}_{\mathrm{s,f}}$ have to be extracted and interpolated to give the correct values. As the propagation time τ can be determined artificially, setting τ to a multiple of ΔT and Δt will prevent this. To reduce the affect brought by the unreal capacitances, τ is set to a minimum multiple of ΔT and Δt. For the sake of simplicity, the integration step of the slow subsystem ΔT is defined as an integer multiple of the fast subsystem Δt. The time delay τ is defined as ΔT.

$$\begin{cases} \tau = \Delta T \\ \Delta T = N\Delta t \end{cases} \tag{2-34}$$

A set of completely discrete system nodal equations can be obtained as

$$\begin{cases} \boldsymbol{G}_{\mathrm{s}}\boldsymbol{v}_{\mathrm{s}}(t) = \boldsymbol{i}_{\mathrm{s}}(t) - \boldsymbol{I}_{\mathrm{h,s}}(t-\Delta T) - \boldsymbol{I}_{\mathrm{s,s}}(t-\Delta T) - \boldsymbol{I}_{\mathrm{s,f}}(t-N\Delta t) \\ \boldsymbol{G}_{\mathrm{f}}\boldsymbol{v}_{\mathrm{f}}(t) = \boldsymbol{i}_{\mathrm{f}}(t) - \boldsymbol{I}_{\mathrm{h,f}}(t-\Delta t) - \boldsymbol{I}_{\mathrm{f,f}}(t-N\Delta t) - \boldsymbol{I}_{\mathrm{f,s}}(t-\Delta T) \end{cases} \tag{2-35}$$

(2) Multirate interfacing method

At the small time steps Δt within the large step ΔT, only the fast subsystem is solved. If the slow subsystem's contribution for the solution of the fast subsystem is completely neglected, incorrect solution will result. Also, at the instant that both the two subsystems are solved, the variation of the fast subsystem solution through the entire ΔT should be considered for the solution of the slow one to reduce the probable sampling errors [24]. The contributions of both the subsystems for each other are evaluated.

1) Multirate interface for the slow subsystem

At the small time steps Δt within the large step ΔT, the fast subsystem will be solved for N steps:

$$\begin{cases} \boldsymbol{G}_{\mathrm{f}}\boldsymbol{v}_{\mathrm{f}}(t+k\Delta t) = \boldsymbol{i}_{\mathrm{f}}(t+k\Delta t) - \boldsymbol{I}_{\mathrm{h,f}}(t+(k-1)\Delta t) - \boldsymbol{I}_{\mathrm{f,f}}(t+k\Delta t - N\Delta t) \\ \qquad\qquad -\boldsymbol{I}_{\mathrm{f,s}}(t+k\Delta t - \Delta T),\ k=1,2,\dots N \end{cases} \tag{2-36}$$

In (2-36), $\boldsymbol{I}_{\mathrm{f,s}}(t+\Delta t-\Delta T)$, $\boldsymbol{I}_{\mathrm{f,s}}(t+2\Delta t-\Delta T)$,…, $\boldsymbol{I}_{\mathrm{f,s}}(t+N\Delta t-\Delta T)$ are unknown variables. With the assumption that the slow subsystem is varying slowly throughout the interval ΔT, a linear interpolation of $\boldsymbol{I}_{\mathrm{f,s}}(t)$ is used to calculate the unknown variables. The interpolation of $\boldsymbol{I}_{\mathrm{f,s}}$ is expressed as

$$\hat{\boldsymbol{I}}_{\mathrm{f,s}}\big((t+k\Delta t-\Delta T)\big) = \boldsymbol{I}_{\mathrm{f,s}}(t-\Delta T) + \frac{k}{N}\Big(\boldsymbol{I}_{\mathrm{f,s}}(t) - \boldsymbol{I}_{\mathrm{f,s}}(t-\Delta T)\Big),\ k=1,2,\dots N \tag{2-37}$$

After substituting $\boldsymbol{I}_{\mathrm{f,s}}$ by $\hat{\boldsymbol{I}}_{\mathrm{f,s}}$, it is possible to evaluate the history current source of the slow subsystem without having to run through the small integration steps. Polynomial extrapolation can also be used to obtain the unknown variables [25].

Fig. 2-21 shows how the interfacing for slow subsystem works, for example, $\Delta T = 4\Delta t$. In Fig. 2-21, "●" indicates the instants when both the slow and the fast subsystems are solved. "⊙"indicates the instants when only the fast subsystem is solved. "○" is the interpolation point.

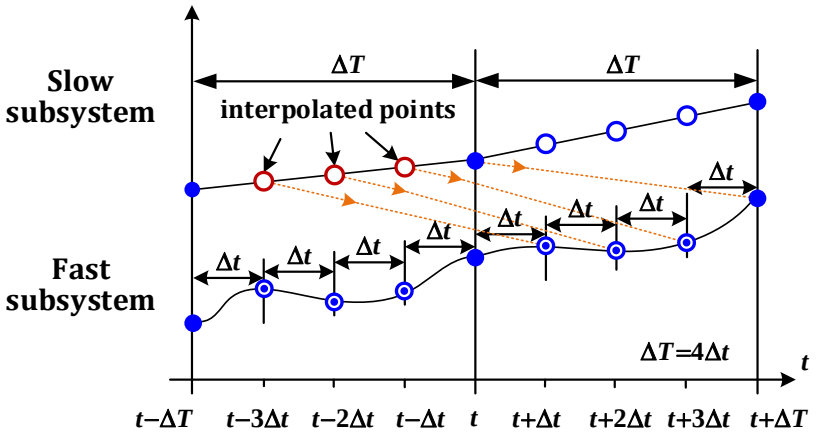

Fig.2-21 Multirate interfacing for the slow subsystem

The detailed interfacing procedure of the slow subsystem is as follows:

i) Determine the history current sources $\boldsymbol{I}_{\mathrm{f,s}}(t)$ of the slow subsystem at t;

ii) Calculate the interpolation values $\hat{\boldsymbol{I}}_{\mathrm{f,s}}(t-3\Delta t)$, $\hat{\boldsymbol{I}}_{\mathrm{f,s}}(t-2\Delta t)$ and $\hat{\boldsymbol{I}}_{\mathrm{f,s}}(t-\Delta t)$;

iii) Using the interpolation values together with $\boldsymbol{I}_{f,s}(t)$, the fast subsystem is solved for solutions at instant $t+\Delta t$, $t+2\Delta t$, $t+3\Delta t$ and $t+\Delta T$ shown in Fig.2-21.

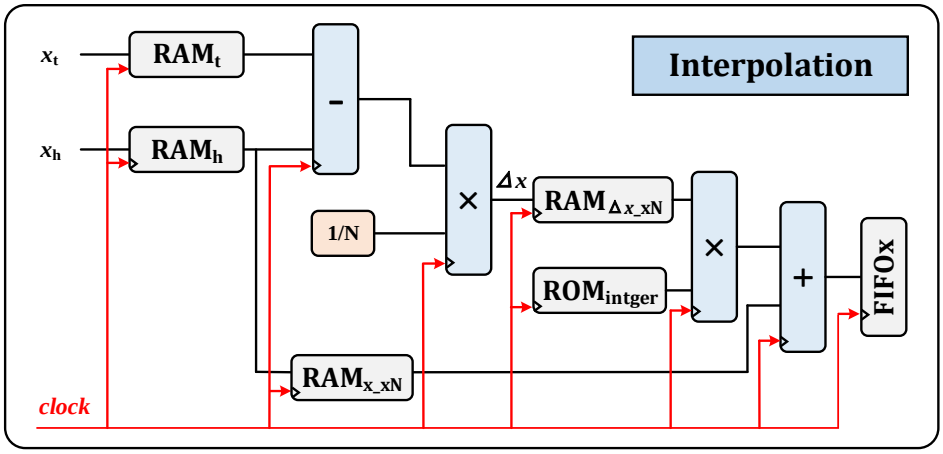

Fig. 2-22 Hardware design of the multirate interface for the slow subsystem

Hardware design of the multirate interface for the slow subsystem is shown in Fig. 2-22. It realizes the pipelined computation for the interpolated values. In the design, four random-access-memory (RAM) units, one read-only-memory (ROM) units and one first-in-first-out (FIFO) block are placed. $\mathrm{RAM_h}$ and $\mathrm{RAM_t}$ are used to store the values v_h and v_t to be interpolated. $\mathrm{RAM_{\Delta v\_xN}}$ and $\mathrm{RAM_{v\_xN}}$ are used to store the difference value Δv and v_t, that will be later read out for N times. N is the number of times of interpolation operations. The storage format of $\mathrm{ROM_{integer}}$ is $\{0,0,\ldots 0,1,1,\ldots 1,\ldots N\text{-}1,N\text{-}1,..N\text{-}1\}$. In the format, each element is repeated g times which is the number of the pipelined values.

2) Multirate interface for the fast subsystem

At the instant t when both the slow and fast subsystem are solved, the history current source of the fast subsystem is updated with the solution at $t-\Delta t$. It can't represent its variation through a complete ΔT from the viewpoint of the slow subsystem. An average of the history current sources of the fast subsystem through ΔT is more accurate [24].

Assuming $\Delta T = 4\Delta t$, the nodal equation of the slow subsystem can be expressed as

$$\boldsymbol{G}_{\mathrm{s}}\boldsymbol{v}_{\mathrm{s}}(t) = \boldsymbol{i}_{\mathrm{s}}(t) - \boldsymbol{I}_{\mathrm{h,s}}(t-\Delta T) - \boldsymbol{I}_{\mathrm{s,s}}(t-\Delta T) - \boldsymbol{I}_{\mathrm{s,f}}(t-4\Delta t) \tag{2-38}$$

At the instant when the solutions are resynchronized, the history current sources are both updated as Fig. 2-23. For the slow subsystem, $\boldsymbol{I}_{\mathrm{s,s}}(t-\Delta T)$ accommodate the variation from $t-2\Delta T$ to $t-\Delta T$. For the fast subsystem, it has been solved 4 times and $\boldsymbol{I}_{\mathrm{s,f}}(t-4\Delta t)$ accommodates the variation from instant $t-5\Delta t$ to $t-4\Delta t$. From the viewpoint of the slow subsystem, fast

subsystem's variation during Δt cannot represent the variation during ΔT. An average of values $\hat{\boldsymbol{I}}_{\mathrm{s,f}}$ during ΔT is used to substitute $\boldsymbol{I}_{\mathrm{s,f}}$. $\hat{\boldsymbol{I}}_{\mathrm{s,f}}$ is calculated as

$$\hat{\boldsymbol{I}}_{\mathrm{s,f}}(t - N\Delta t) = \frac{1}{N}\sum_{k=1}^{N} \boldsymbol{I}_{\mathrm{s,f}}(t - (k-1)\Delta t - N\Delta t) \tag{2-39}$$

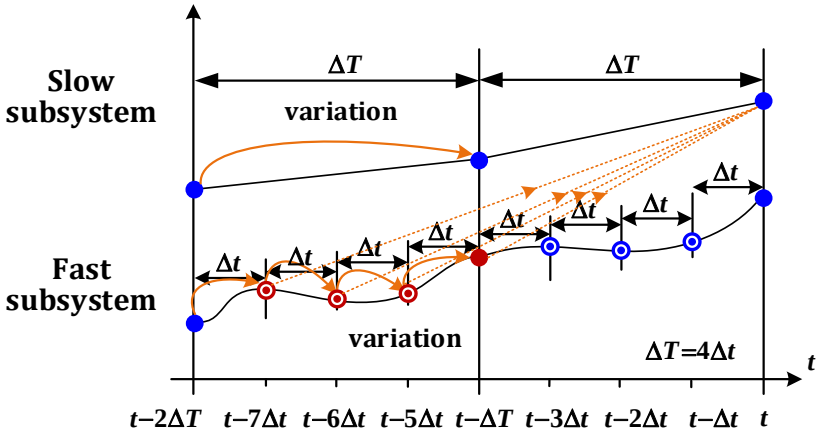

Fig.2-23 Multirate interfacing for the fast subsystem

The detailed interfacing procedure of the fast subsystem is as follows:

i) Determine the history current sources $\boldsymbol{I}_{\mathrm{s,f}}(t - 7\Delta t)$, $\boldsymbol{I}_{\mathrm{s,f}}(t - 6\Delta t)$, $\boldsymbol{I}_{\mathrm{s,f}}(t - 5\Delta t)$ and $\boldsymbol{I}_{\mathrm{s,f}}(t - 4\Delta t)$ of the fast subsystem;

ii) Calculate the average values $\hat{\boldsymbol{I}}_{\mathrm{s,f}}(t - 4\Delta t)$;

iii) Using the average value, the slow subsystem is solved for solutions at t shown in Fig.2-23.

In Fig. 2-24(a), the hardware design of the interface for the fast subsystem is realized with a pipelined computation scheme. In the design, input $\boldsymbol{x}$, in pipelined format, represents the history current sources of the fast subsystem throughout ΔT. The interface design consists of one floating-to-fixed point converter, one fixed-to-floating point converter, one accumulation unit, two FIFOs, one ROM and one RAM. $\mathrm{FIFO_x}$ is used to rearrange the input and insert zeros in the pipeline. The core of accumulation unit is a fixed point adder in which the addition operation is forced to finish in one clock cycle. $\mathrm{FIFO_{sum}}$ is used to select the required summation from the pipeline. The timing diagram of this operation is shown in Fig. 2-24(b).

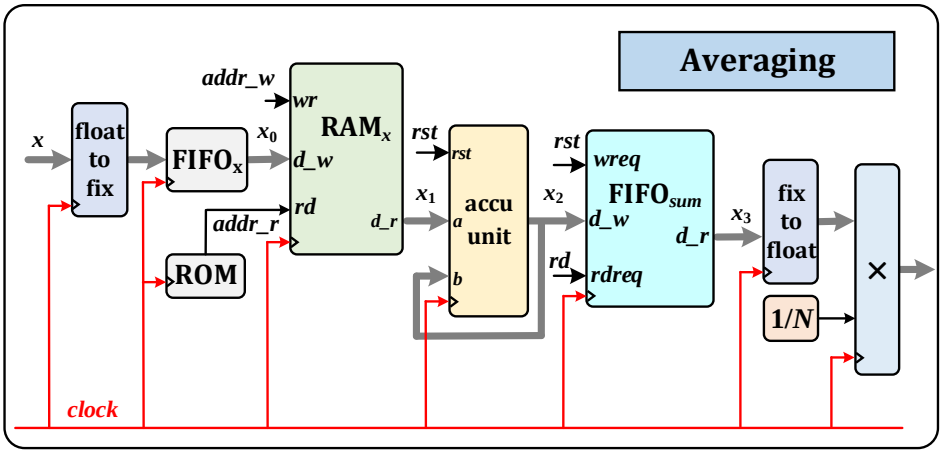

(a) Hardware design

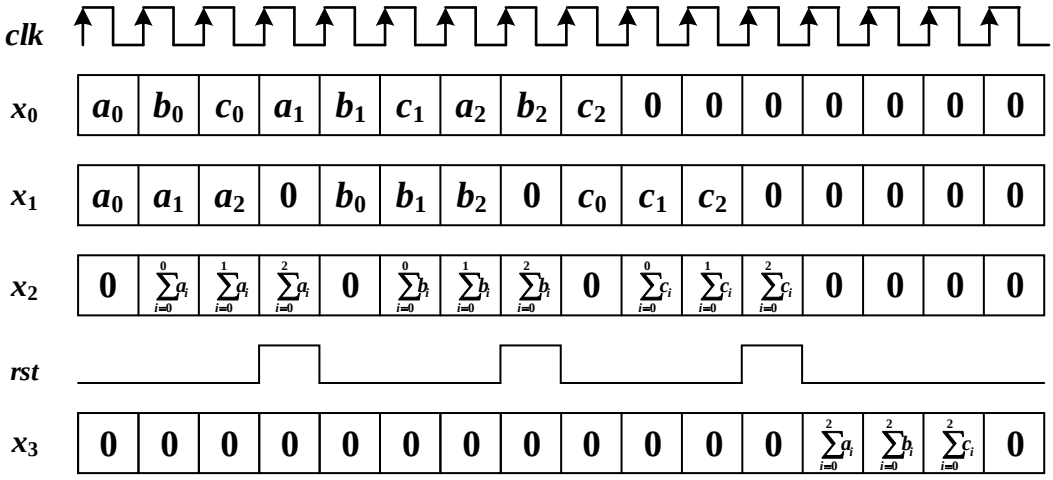

(b) Timing diagram

Fig.2-24 Hardware design and the timing diagram of the fast subsystem interface

(3) Hardware design of the multirate simulator

To ensure that each FPGA can be configured to simulate any subsystem whereas the time-scale, a universal hardware design is realized in Fig.2-25. It provides the full simulation functions for both network components and DG units. The multiplexer in Fig.2-25 is to decide whether the simulated subsystem is ‘fast’ or ‘slow’. The subscript ‘i’ indicates the interface variables of the inside subsystem and ‘o’ indicates the variables from outside.

The hardware design comprises five modules, including electrical system solving module, control system solving module, multirate interface module, data exchange module and global control module.

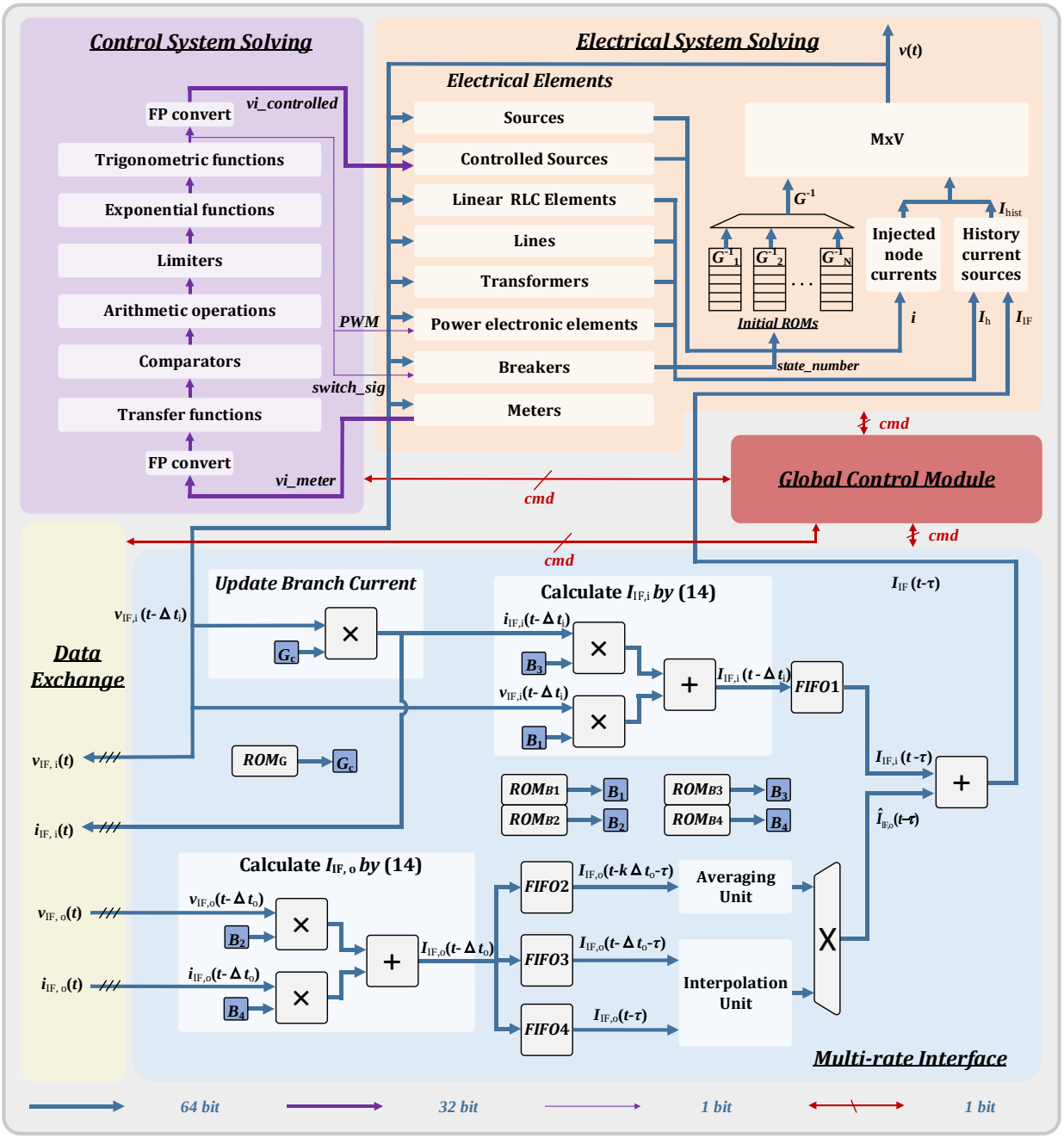

Fig.2-25 Hardware design of the FPGA-based extendable real-time simulator

1) In the electrical system solving module, different kinds of component models are established, such as lines, transformers, power electronic circuits, breakers and so on. The history term vector $\boldsymbol{I}_{\mathbf{hist}}$ is the summation of the Bergeron line model history term $\boldsymbol{I}_{\mathbf{IF}}$ and the other

network history term $\boldsymbol{I_h}$. After the right inverse admittance matrix $\boldsymbol{G^{-1}}$ is selected by the breaker state, the network solver is executed to obtain system nodal voltages.

2) Control system solving module covers the basic functioning bocks, such as transfer functions, trigonometric functions, comparators, limiters, exponential functions and so on. Generally, the resulting nonlinear equations should be solved by the iterative method to acquire the correct solution. For real-time simulation, it is not suitable since the numbers of iterations are uncertain [24]. We adopt the pseudo-nonlinearization method to solve the problem. The nonlinear equations, resulting from the relationships between the blocks, are transformed into linear equations by adding a time-step delay [26]. Considering that the control system is a relatively weak stiff system, the transition is appropriate.

3) In the multirate interface module, the inside history current sources of the interface $\boldsymbol{I}_{\mathrm{IF,i}}$ is calculated by (2-27). The outside history current sources $\boldsymbol{I}_{\mathrm{IF,o}}$ is calculated using the interface node voltage $\boldsymbol{v}_{\mathrm{IF,o}}$ and branch current $\boldsymbol{i}_{\mathrm{IF,o}}$. Both the interpolation and averaging operations are conducted for $\boldsymbol{I}_{\mathrm{IF,o}}$. A multiplexer is used to determine the required transformation of $\hat{\boldsymbol{I}}_{\mathrm{IF,o}}$. Then the summation of $\boldsymbol{I}_{\mathrm{IF,i}}$ and $\hat{\boldsymbol{I}}_{\mathrm{IF,o}}$ are sent to the electrical system solving module for system nodal voltages calculation. After obtaining the interface nodal voltage $\boldsymbol{v}_{\mathrm{IF,i}}$, it is sent back to the multirate interface module for next simulation step.

4) Data exchange module accomplishes the bidirectional data transmission between FPGAs by configuring their high-speed transceivers. The transmission data include the branch voltages and branch currents of the interface during each time-step.

5) Global control module sends resetting, initializing and starting signals to each module to enable it performing the designed function. It also receives the signals sent back from each module to judge if the required function has been executed properly. Especially, this module sets up a multirate synchronization mechanism to ensure that data transmission between FPGAs is in an orderly manner.

(4) Case studies and analysis

Fig. 2-26 shows the multi-FPGA-based real-time simulator. Four Stratix® V Edition DSP development boards from Altera® are used. Each FPGA development board provides four 2.5Gbps full-duplex optical fiber communication channels that enable the flexible connection between

FPGAs. FPGA1 is selected as the master FPGA and sends synchronization signals to the other three slave FPGAs. The slave FPGA starts simulation only if it receives the synchronization signal and the start time of the master FPGA is pushed back by the transmission delay of the signal. The maximum driven clock frequency for FPGAs is 125MHz, which severely determines the execution time of the hardware design. Real-time results can be captured either by the oscilloscope via DA converter or the host computer through JTAG bluster.

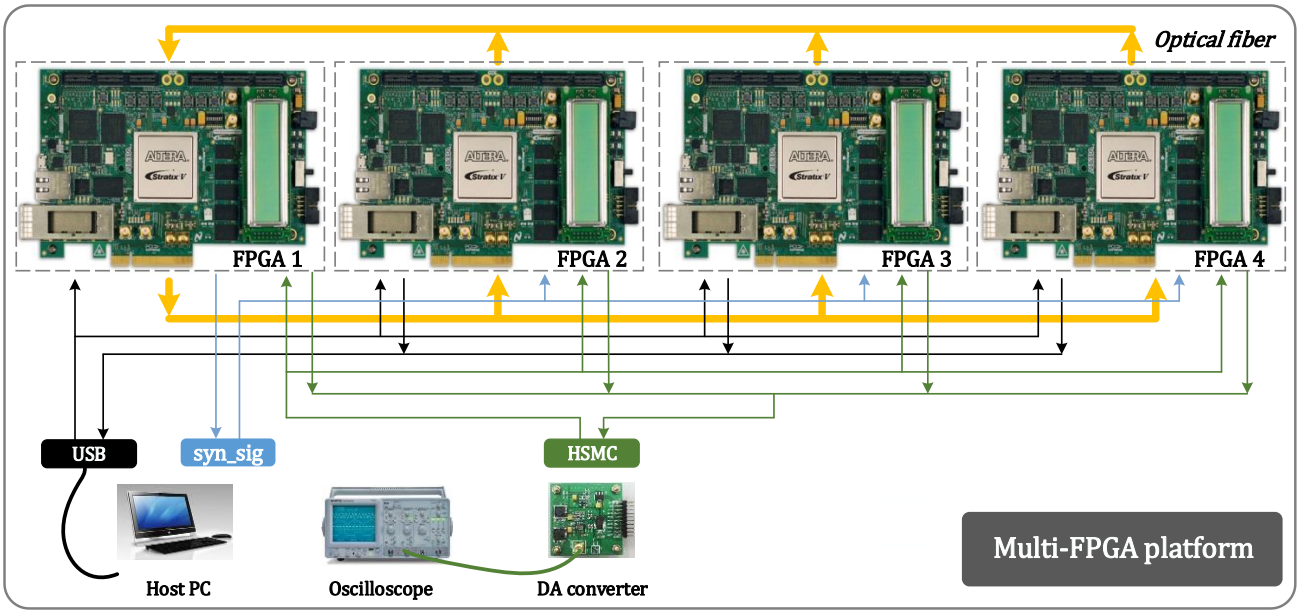

Fig. 2-26 The integrated simulation platform

The real-time simulation of a modified MG benchmark, including PVs and a battery, is implemented on the FPGA-based simulator. Fig. 2-27(a) shows the structure of the modified MG benchmark, which consists of a network with 12 three-phase nodes, a PV/battery unit and two PV units. The detailed structure of the PV/battery unit is shown in Fig. 2-27(b). Two transient events are simulated. The first transient event occurs at 2 s, over which the active load demand of the PV/battery unit increases from 3kW to 5kW. The second transient event occurs at 3s, in which a Phase-C ground fault occurs at the point of common coupling of PV unit 1 and is removed after 0.2s. The modified MG benchmark is portioned into four subsystems, including a network, a PV/battery unit, PV unit 1 and PV unit 2, and each subsystem is simulated on a single FPGA. The entire system contains 3 supply source elements, 7 controlled source elements, 70 RLC elements, 21 IGBTs, 22 diodes, 48 meters, 15 three-phase mutually coupled lines and 3 transformers. Each

end of the transformer belongs to a separate subsystem. The selected time-step is 3μs, which is the same with PSCAD/EMTDC.

Fig. 2-28(a) and Fig. 2-28(b) show the waveforms of the PV/battery unit during the first transient event. Fig. 2-28(a) shows the active power provided by PV, which is approximately 5.09 kW. The active power provided by battery is shown in Fig. 2-28(b). Before the transient occurs, battery is in charging state that absorbs 2 kW active power from PV. The total output active power of PV and battery is about 3.09 kW, which meets the active load demand 3 kW. The extra power is the losses of power electronic converters. During the transient, the active load demand increases from 3 kW to 5 kW. The output active power of battery is almost 0 kW. The required active power is provided entirely by PV. Fig. 2-28(c) and Fig. 2-28(d) show the simulation results during the second transient event. Fig. 2-28(c) shows the Phase-C voltage of PV unit 1. When the fault occurs, Phase-C voltage drops to 0 V. Fig. 2-28(d) shows the DC voltages of PV unit 2.

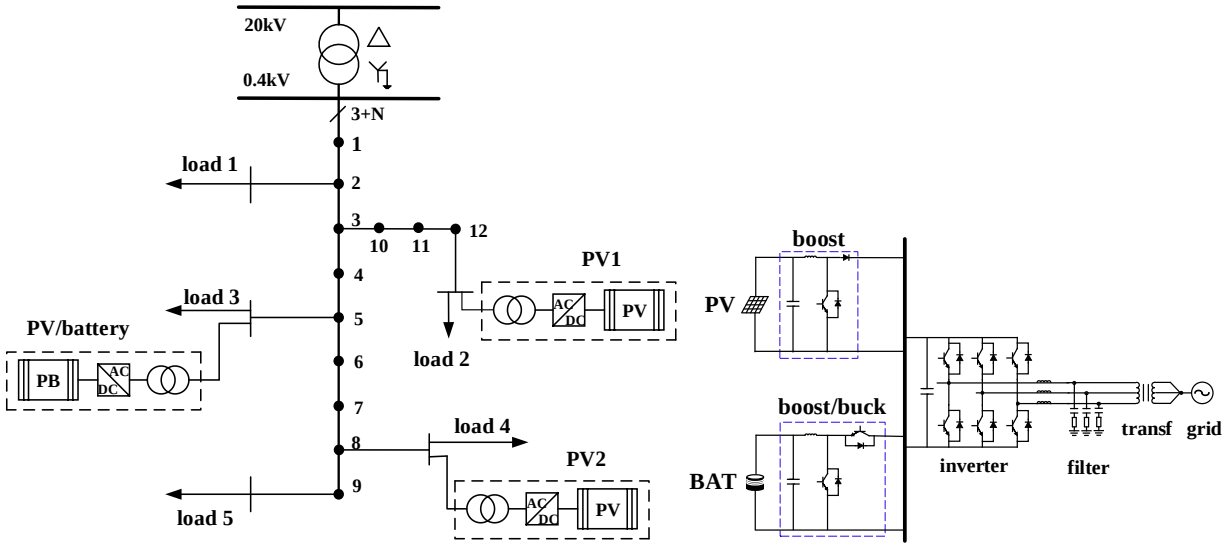

(a) The modified MG benchmark **(b) The detailed structure of the PV/battery unit**

Fig. 2-27 Test case

As can be seen from Fig. 2-28, the results of the two simulation tools are nearly the same. In contrast to PSCAD/EMTDC, the error of the FPGA incorporates four aspects. Firstly, the data format of control system in FPGA is 32-bit single precision floating point, which introduces inaccuracy. Secondly, the power electronic switches in the FPGA are modeled by constant impedances. In PSCAD/EMTDC, switches are modeled by a small/large resistance. Thirdly, the

irradiance in the FPGA is time-varying but is constant in PSCAD/EMTDC. Fourthly, transformers modeled by Bergeron's trans-mission line are introduced to decompose the MG, which further brings errors.

The proposed multi-FPGA based real-time simulator has been verified to reproduce the transients of MEMGs with acceptable fidelity. The major functional application for the simulator is testing the physical device under real time conditions which provides close reproduction of how the device will behave in the field. The simulator can also be used for fast developing models and rapid prototyping of novel device/concept in power and energy systems, which leads to a more efficient design process in industrial applications.

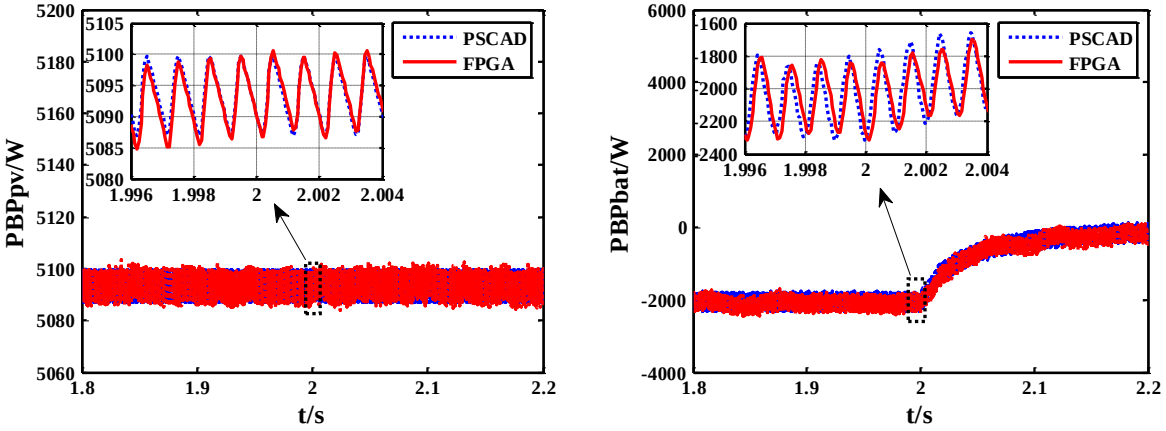

(a) Active power provided by PV

(b) Active power provided by battery

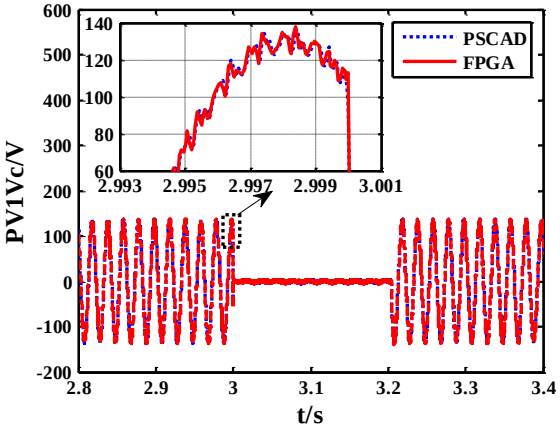

(c) Phase-C voltage of PV unit 1

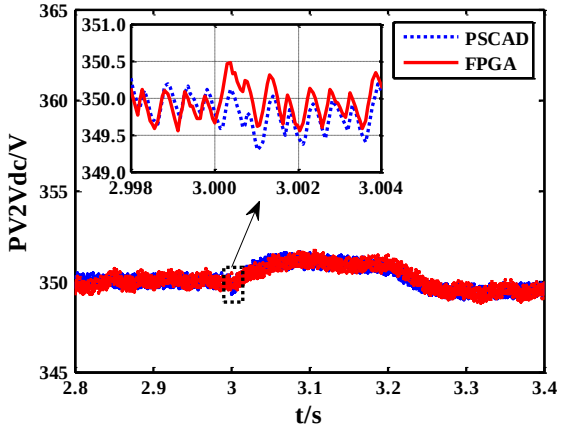

(d) DC voltage of PV unit 2

Fig. 2-28 Simulation results

2.3 Planning of MEMGs

The planning of MEMGs is intended to determine the optimal system configuration (i.e. equipment types, capacities, *etc*.) for the maximum economic/environmental benefits and energy efficiency. Different objectives and constraints are considered according to the load levels and DER conditions during the planning period. For a more complicated MEMG, i.e. integrated electricity and gas community energy system (IEGS), the cooling/heating/electric load demand and DG should be considered in the planning period as well as the equipment operation constraints, supply demand balance constraints and system standby capacity constraints in the event of a supply side failure.

2.3.1 Optimal Planning of MEMG

The MG design requires the equipment to be economically optimized in the whole life cycle, which makes the operation strategy determination become an important part of the design. Thus, it is essential to capture the effects of the strategies on the optimization results. For this reason, a two-stage optimal design model of MGs is established, which employs two modules to integrate optimizations of design and operation, respectively, as shown in Fig. 2-29. The first-stage optimization module determines the equipment types and capacities, and the optimization horizon is the whole life cycle. The second stage optimization module determines the optimal dispatch strategy by simulating the actual operations of MGs, and the optimization horizon is generally set to a typical day (in hours).

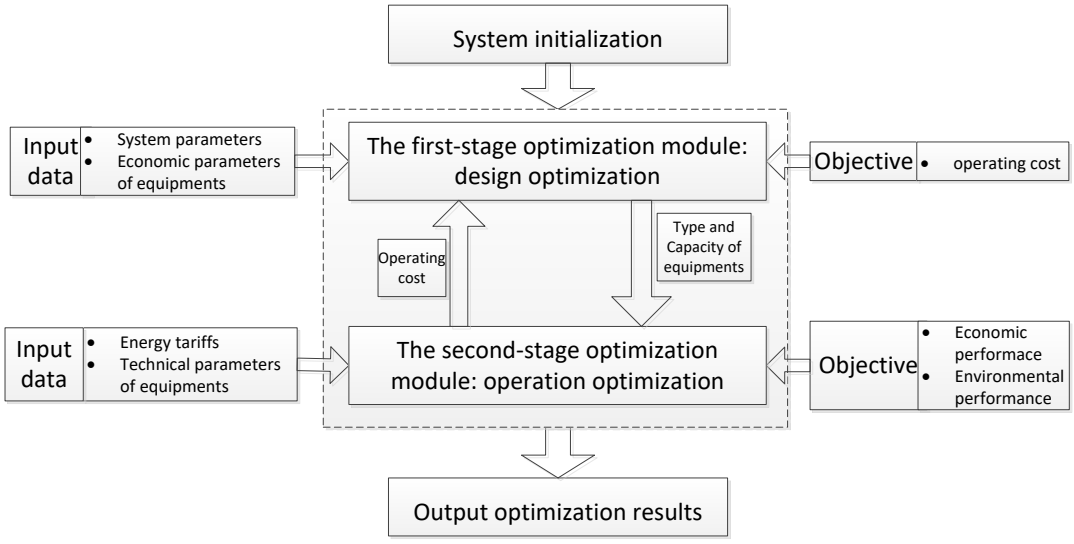

Fig. 2-29 The two-stage optimal design model for MG

(1) Analysis of investment and operation cost of MGs

1) Equipment investment and operation cost

The equipment investment and operation cost can be annualized to total annual equipment investment cost, which consists of the annual capital cost, the annual operation and maintenance cost, and the annual fuel cost:

$$C_{\mathrm{TEI}}^{\mathrm{ann}} = C_{\mathrm{C}}^{\mathrm{ann}} + C_{\mathrm{OM}}^{\mathrm{ann}} + C_{\mathrm{fuel}}^{\mathrm{ann}} \tag{2-39}$$

where $C_{\mathrm{TEI}}^{\mathrm{ann}}$ is the total annual equipment investment cost, $C_{\mathrm{C}}^{\mathrm{ann}}$ is the annual capital cost, $C_{\mathrm{OM}}^{\mathrm{ann}}$ is the annual operation and maintenance cost, and $C_{\mathrm{fuel}}^{\mathrm{ann}}$ is the annual fuel cost.

The annual capital cost $C_{\mathrm{C}}^{\mathrm{ann}}$ can be calculated by

$$C_{\mathrm{C}}^{\mathrm{ann}} = \sum_i C_{\mathrm{CR},i}\, r_{\mathrm{CR},i} = \sum_i C_{\mathrm{I},i} \frac{r(1+r)^{l_i}}{(1+r)^{l_i}-1} \tag{2-40}$$

where $C_{\mathrm{I},i}$ is the initial investment cost of equipment i, $r_{\mathrm{CR},i}$ is the capital recovery factor of equipment i, r is the discount rate, and l_i is the lifetime of equipment i.

The annual operation and maintenance cost $C_{\mathrm{OM}}^{\mathrm{ann}}$ can be expressed as

$$C_{\mathrm{OM}}^{\mathrm{ann}} = \sum_i C_{\mathrm{OM},i}^{\mathrm{ann}} \tag{2-41}$$

where $C_{\mathrm{OM},i}^{\mathrm{ann}}$ is the annual operation and maintenance cost of equipment i. For different applications, $C_{\mathrm{OM},i}^{\mathrm{ann}}$ is expressed in different forms, such as the fixed/variable cost for micro gas turbines, the fixed cost of unit power of PV arrays and wind turbines, and the fixed cost of unit capacity of lithium-ion batteries.

The annual fuel cost $C_{\mathrm{fuel}}^{\mathrm{ann}}$ refers to the cost that comes from the fuel consumption of distributed generators, which is closely related to annual electricity generation and can be expressed as

$$\begin{aligned} C_{\mathrm{fuel}}^{\mathrm{ann}} &= \sum_i C_{\mathrm{fuel},i}^{\mathrm{ann}} \\ C_{\mathrm{fuel},i}^{\mathrm{ann}} &= c_{\mathrm{fuel},i} F_i^{\mathrm{ann}} = c_{\mathrm{fuel},i} \frac{E_i^{\mathrm{ann}}}{\eta_i} \end{aligned} \tag{2-42}$$

where $C_{\mathrm{fuel},i}^{\mathrm{ann}}$ is the annual fuel cost of distributed generator i, $c_{\mathrm{fuel},i}$ is the price of unit fuel thermal value consumption of distributed generator i. F_i^{ann} is the total annual fuel consumption of distributed generator i and equals to the ratio of E_i^{ann} to η_i in value, where E_i^{ann} denotes the total annual electricity generation of distributed generator i, and η_i denotes the electric efficiency of

distributed generator *i*. Obviously, $C_{\text{fuel}}^{\text{ann}} = 0$ for the renewable energy generation system and the ESS that don't consume fossil fuel directly.

2) Electricity purchase cost

The electricity purchase cost is closely related to the tariff mechanism of different regions. Generally, the electricity purchase cost can be summarized as the annual fixed cost, the annual demand cost and the annual energy cost [27]:

$$C_{\text{elec}}^{\text{ann}} = C_{\text{f}}^{\text{ann}} + C_{\text{d}}^{\text{ann}} + C_{\text{e}}^{\text{ann}} \tag{2-43}$$

where $C_{\text{elec}}^{\text{ann}}$, C_{f}^{ann}, $C_{\text{d}}^{\text{ann}}$ and $C_{\text{e}}^{\text{ann}}$ are the total annual electricity charge, the annual fixed cost, the annual demand cost, and the annual energy cost, respectively.

The costs mentioned above may vary in charging practices in different countries or regions. For example, in China, the fixed cost is determined when the specific distribution transformer is selected. It must be paid monthly according to the capacity even if the transformer is not in use. The demand cost is proportional to the maximum power demand during a month, and the energy cost is the charge for the electricity supplied by the distribution network.

(2) Optimal design model of MGs

In the optimal design of MGs, the objective is to minimize the total annual cost, which consists of the total annual electricity charge and the total annual equipment investment cost. Thus, the objective function can be expressed as

$$\min C_{\text{total}}^{\text{ann}} = C_{\text{elec}}^{\text{ann}} + C_{\text{TEI}}^{\text{ann}} \tag{2-44}$$

where $C_{\text{total}}^{\text{ann}}$ stands for the total annual cost.

The constraints for the optimal design of MGs can be summarized as follows:

1) The power balance constraints;

2) The thermal energy balance constraints;

3) The equipment operation constraints on the capacity, the operation voltage and current, the running time, *etc*.

4) The regulation constraints on the minimum energy utilization efficiency, the maximum carbon emission, *etc*.

5) The capital constraints on the annual capital cost, the payback period, *etc*.

6) The available resource constraints on the installed area and capacity of PV arrays, the location and capacity of wind turbines, *etc*.

7) The operation performance constraints on the energy supply quality, the heat/cooling supply reliability, the power supply reliability, *etc*.

These constraints of MGs must be satisfied all the time throughout the planning period, which makes the optimization of MGs more complicated.

(3) Problem solving

In the optimal design model of MGs, various costs and operation variables are involved in the objective functions and constraints. These costs and variables are all obtained by calling the operation scheduler routine repeatedly. As shown in Fig. 2-29, the solving process is actually an iteration between the equipment selection and the dispatch optimization.

Several uncertainties during the planning period must be considered, such as the fluctuations of renewable energy systems (RESs) and loads, and the variations of electricity tariff and fuel price. These uncertainties bring heavy burden to the optimal design of MGs. Therefore, the operation scenarios must be simplified in the solving process. For example, the conditions of loads and DERs in each year can be replaced by the data of 36 typical days (i.e. one weekday, one weekend day and one peak day in each month). Thus the computational load is significantly reduced. There are various algorithms for optimization problems, including mathematical programming methods, and intelligent algorithms such as genetic algorithm (GA), particle swarm algorithm, *etc*. These algorithms are selected according to the specific problem type and scale. The proper algorithm is the one that provides the best compromise between the optimization speed and accuracy.

(4) Example

An islanded MG in the eastern coastal area of China is taken as a study case, which is shown in Fig. 2-30. Because of the abundant RESs like wind and solar energy in the site, wind turbines and PV arrays are intended to be installed in the system. Due to the intermittency of renewable energy generation, a diesel generator or ESS is needed to ensure power balance and stability. Here the task of design is to find an optimal combination of these equipment to meet the residential load and a seawater desalination system demand. In this MG, the residential peak load is about 100 kW, the rated power of seawater desalination system is 12 kW which has a production capability of

11.2 m^3/h, and the volume of the freshwater reservoir is 50 m^3. Here, the two-stage design method is used to optimize the system configuration.

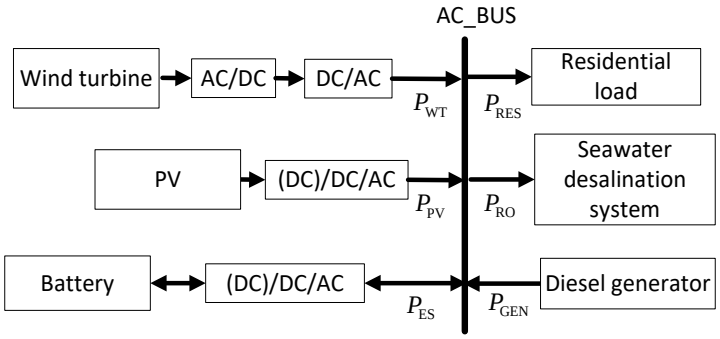

Fig. 2-30 The structure of an islanded MG

Since the system is an islanded MG, electricity purchase cost is not included in the objective function. The constraints mainly involve the range of variables, the balance equation of electrical bus, the equipment operational constraints. The revised hard cycle charge (RHCC) strategy is chosen for the system operation. The decision variables considered are the numbers of diesel generators and wind turbines with a given unit capacity, the capacity of the PV generation system and LA battery storage system. Some parameters of the equipment and the strategy are given in Table 2-1 and Table 2-2. Then, an optimization problem is formed and can be solved by GA.

Table 2-1 The economic and technology parameters

	Capacity (kW)	**Initial investment cost ($)**	**Operation and maintenance cost ($)**	**Lifetime**
PV array	----	983.3 /kWp	36.5 /year/kWp	20 years
Wind turbine	30 /unit	132,860.0 /unit	190.5 /year/unit	15 years
Diesel generator	100 /unit	8,730.0 /unit	0.159 /hour/unit	20,000 hours
Lead-acid battery	----	1.9 /Ah	0	1,064 cycles (50% DOD)
Converter	----	793.7 /kW	0	20 years
Control system	----	63,492.0	0	20 years

Table2-2 The RHCC strategy parameters

Parameters	S_{ES}^{min}	S_{ES}^{low}	S_{ES}^{up}	S_{ES}^{max}	$T_{WT,down}^{min}$	P_{PV}^{min}	P_{net}
Value	40%	50%	85%	100%	1 h	5 kW	0 kW
Parameters	P_{GEN}^{min}	P_{GEN}^{max}	$T_{GEN,up}^{min}$	P_{GEN}^{0}	H_{W}^{min}	P_{RO}	----
Value	30 kW	100 kW	1 h	30 kW	0 m3	12 kW	----

To illustrate the detailed dispatch process of RHCC, the system operation situation under the strategy is represented based on the data of load, wind speed and solar radiation during a typical week. The load profile is shown in Fig. 2-31, and the dispatch results of PV, wind turbine, ESS and diesel generator are described in Fig. 2-32 to Fig. 2-35. From Fig. 2-32, we can see that part of the PV power output is cut off during the periods from 105 h to 110 h. The reason is that the ESS isn't allowed to be charged by extra RESs in RHCC strategy when it works in the discharging state, and the power output of the PV arrays will be cut off first if needed.

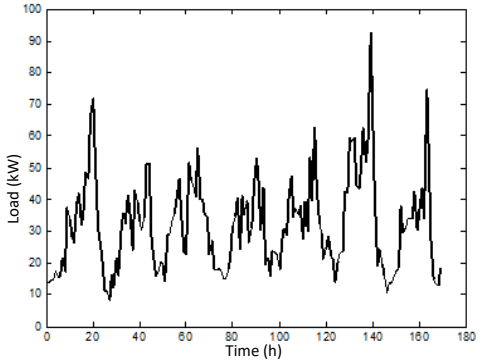

Fig. 2-31 Residential load curve

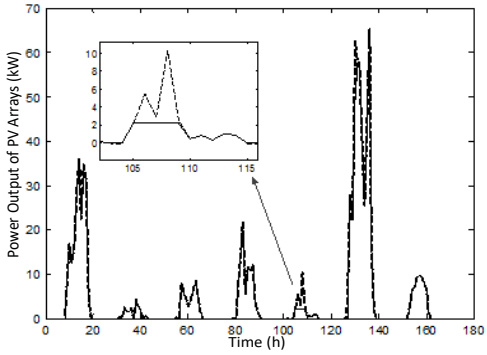

Fig. 2-32 Power output of the PV arrays

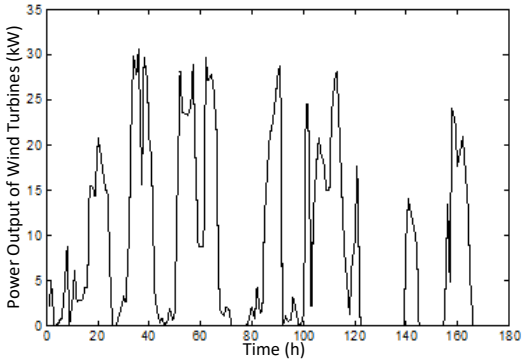

Fig. 2-33 Power output of the wind turbines

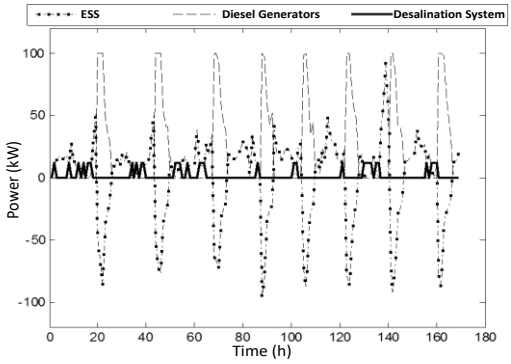

Fig. 2-34 Power output of other equipment

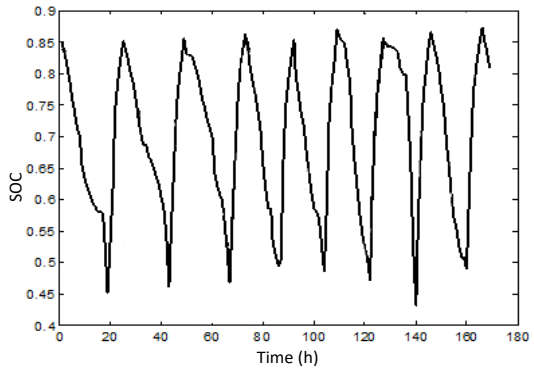

Fig. 2-35 SOC of the ESS

For the optimal design of MG, the project lifetime is taken as 20 years with a 5% capital discount rate and 1.168 $/L diesel price. In this case, the GA uses a population size of 100, a generation size of 200, a crossover rate of 0.8, and a mutation rate of 0.1. Based on the given parameters and the data of load, wind speed and solar radiation on the island, the most economical configuration obtained consists of 1×30 kW wind turbine, 90 kWp PV arrays, 1×100 kW diesel generator and 624 kWh ESS.

2.3.2 Planning of MEMG with Enhanced Operational Resilience

The coupling in MEMG provides alternative operation modes when unpredictable outages occur at energy supply sides. Reasonable operation strategies and system configuration can effectively improve the system's resilience, making reliable and continuous operation feasible. Considering the complementary characteristics and reserve capabilities of IEGS, a multi-stage scheduling strategy for resilience enhancement is adopted in which thermal storage serves as emergency response resources, including the following stages: 1) rolling optimization of the reserve for supply-side outages; 2) day-ahead economic scheduling with storage reserve; and 3) fault restoration in actual operation. A two-level planning model integrating the resilient operation strategy is formulated to better adapt to the source emergency. The upper level is to optimize the system configuration and the lower level is to run resilient operation strategy.

(1) Optimal planning mode

1) Objective function

The objective function of IEGS planning is to minimize the overall annual cost, including annual investment cost C_{inv} and annual operation cost C_{ope}:

$$\min F = C_{\text{inv}} + C_{\text{ope}} \tag{2-45}$$

i) Annual investment cost:

$$C_{\text{inv}} = \frac{r(1+r)^y}{(1+r)^y - 1} \sum_i C_{\text{inv}}^i \tag{2-46}$$

where r is discount rate, y is limited lifetime, and C_{inv}^i is initial investment cost of equipment i. The equipment can be divided into two categories: discrete equipment and continuous equipment. The initial investments of discrete equipment and continuous equipment can be calculated by:

$$\begin{aligned} C_{\text{inv}}^i &= C_u^i N^i, i \in \{\text{HP}, \text{WC}, \text{DC}, \text{EB}, \text{GT}, \text{AC}, \text{WT}\} \\ C_{\text{inv}}^i &= C_{\text{c}}^i M^i, i \in \{\text{IT}, \text{PV}\} \end{aligned} \tag{2-47}$$

where C_u^i is investment cost per unit of discrete device i and C_{c}^i is investment cost per-unit capacity of continuous device i; N^i and M^i refer to the installed number of discrete device i and the rated capacity of continuous device i, respectively.

ii) Annual operation cost: annual operation cost is the purchasing cost of IEGS. The cost is the sum of energy purchase cost for every day of the base year:

$$C_{\text{ope}} = 365 \sum_{s=1}^{N_S} p_s \sum_{t=1}^{N_{\text{T}}} (C_t^{\text{P}} P_{s,t}^{\text{TL}} + C_t^{\text{G}} F_{s,t}^{\text{GT}}) \Delta t \tag{2-48}$$

where N_{T} denotes the interval number of a scheduling cycle and N_{S} represents the number of typical scenarios. Moreover, p_s is the probability of scenario s, and $P_{s,t}^{\text{TL}}$ and $F_{s,t}^{\text{GT}}$ are the purchasing electricity power (tie-line power) and gas power at time t in scenario s, respectively.

2) Optimal variables

The numbers of GSHPs, conventional water-cooled chillers, double-duty chillers, electric boilers, water tanks, gas turbines and absorption chillers, as well as the capacities of ice-storage tank and PV system, are taken as the optimal variables, which can be expressed as:

$$X = [N^{\text{HP}}, N^{\text{WC}}, N^{\text{DC}}, N^{\text{EB}}, N^{\text{WT}}, N^{\text{GT}}, N^{\text{AC}}, M^{\text{IT}}, M^{\text{PV}}] \tag{2-49}$$

In this model, we optimize only the equipped number of water tanks rather than the numbers of cold water tanks and hot water tanks, which is in line with the actual planning situation. The water tanks can be used to store the cooling energy in summer and heating energy in winter; thus, the following constraint is added:

$$N^{\text{CT}} = N^{\text{HT}} = N^{\text{WT}} \tag{2-50}$$

3) Constraints

The constraints for the optimal planning of IEGS can be summarized as follows:

i) Operation constraints of energy supply equipment;

ii) System supply and demand balance constraints: the balance constraints of cold/heat/ electrical loads, and the power constraints of maximum electricity and gas purchase;

iii) System reserve capacity constraint: The system reserve capacity constraint is to ensure that the planning solution can meet the reserve requirement of the system during actual operation. In the event of a source-side supply failure, the supply of important loads can be met by means of gas and electricity complementation and energy reserve.

(2) Solving of the IEGS planning

A two-level solving method is adopted to address the optimal planning problem, where the upper level is to optimize the system configuration and the lower level is to run resilient operation strategy. GA is used for solving the optimization problem of upper level due to its high efficiency, parallelism and global searching [28]. After linearizing the nonlinear items by the method in [29], the optimization of lower level is transferred to a mixed-integer linear programming (MILP) problem and is solved by ILOG's CPLEX 12.8 solver [30]. The detailed solving procedure is illustrated as follows:

1) System initialization: to read the parameters of system, devices and GA.
2) Population initialization: a random set of N individuals is generated, which will act as the initial population P_1. Each individual of the population is a set of the optimal variables.
3) Fitness calculation of the population P_1 and ranking the population. Here, the variables of each individual in P_1 will be delivered to the operation model as a configuration scheme; and the multi-stage resilient scheduling strategy is called to obtain the annual operation cost. Then, the fitness value of each individual is evaluated with linear ranking according to the overall annual cost.
4) Selection, crossover, and mutation: population P_1 is updated by selection, crossover and mutation operators and the offspring population P_2 is generated.
5) Fitness calculation and ranking the population P_2. Similar to Step (iii), the fitness of population P_2 will be calculated and ranked.
6) Generating new population: a new population P_1 of N individuals will be obtained by reinsertion to P_1 and P_2 based on the individual fitness.

7) Stopping criterion: if the maximum evolution generation of GA reaches, the evolution terminates; otherwise, it returns to Step (iv) for next-generation evolution.

Note that the process of calling the resilient scheduling model (operation level) for the fitness calculation comprises only the first two stages, i.e., the rolling optimization stage for reserve and the day-ahead scheduling stage with storage reservation; and the operation cost will be delivered to the configuration level for the fitness calculation. The last stage (fault restoration stage) is to guarantee the supply of the critical loads in the event of supply-side outages in actual operation based on the reserves and operation conditions of the first two stages.

(3) Example

This section applies the two-level planning model described above to a community energy system with practical demands in north China. The cooling/heating demands of the system have seasonal characteristics: space cooling and electricity are needed in cooling period (May to September), space heating and electricity are needed in heating period (November to March), and only electricity is needed in the mid-period (April and October).

The operation data of typical scenarios during the cooling and heating periods, as well as mid-period, are selected as the basic data for system planning. According to the seasonal and hourly variations of loads and solar radiation, one typical scenario is introduced to represent the operation of each month; thus twelve typical scenarios can be obtained, as shown in Fig. 2-36. And the probability of each typical scenario is 1/12. As seen from the figure, there are significant differences between these scenarios: the load compositions are different in different supply periods; during the same supply period, the overall load levels, variation trends and peak values also differ significantly. Additionally, the overall cooling and heating demand levels are strongly correlated with the solar radiation, and the higher radiation corresponds to higher cooling demand and lower heating demand.

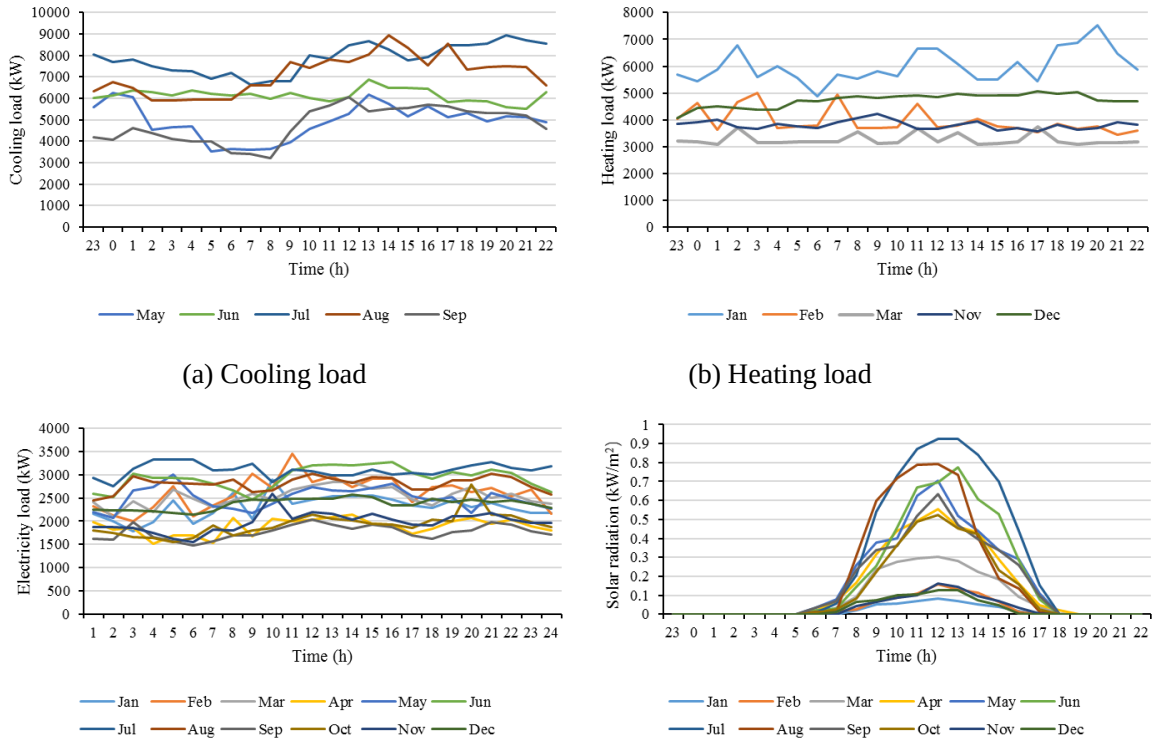

(a) Cooling load (b) Heating load

(c) Electricity load (d) Solar radiation

Fig. 2-36 Loads and solar radiation of the typical scenarios

The operation and investment parameters of candidate devices are listed in Table 2-3. The detailed performance parameters of the devices and their auxiliary devices can refer [29]. The time of use (TOU) tariff of electricity and the purchasing tariff of natural gas in the IEGS are presented in Table 2-4.

To verify the correctness and effectiveness of proposed planning method and resilient scheduling strategy, the analysis of planning and operation results with resilient scheduling strategy and the comparison with the traditional method are conducted. And the traditional method refers to the planning without considering resilient scheduling strategy.

1) Planning results

Based on the typical operation scenarios and the resilient scheduling strategy, the optimal configuration of the IEGS is obtained, as summarized in Table 2-5.

Table 2-5 shows that the system is equipped with both electricity-driven devices and gas-driven devices to take full advantage of the superiority of complementation and reservation of gas and electricity subsystems for reliability and economy. And the capacity of PV reaches the upper

limit to provide electricity using solar energy. Furthermore, the system is equipped with multi-type thermal storage devices, including one ice-storage tank and one water tank; the operation economy can be improved through energy storage/release under the TOU tariff mechanism, as well as the adaptation to source emergency. Meanwhile, GSHP has a higher COP and can work in cooling/cooling-storage mode in summer and heating mode in winter; thus the system is configured with several heat pumps. In order to play the role of ice-storage tank and water storage tank, a double-duty chiller and an electric boiler are also installed. In addition, the introduction of conventional water-cooled chiller can promote the complementation and coordination of energy supply/storage devices for economic improvement.

Table 2-3 Candidate equipment parameters for operation and investment [31][32]

Item		**Rated capacity (per unit)**	**Coefficient of performance/ efficiency**	**Investment cost /×10⁴ CNY**	**Comments**
Discrete equipment	GSHP	Cooling-1162 kW /Heating-1355 kW	Cooling-5.38 /Heating-4.14	300/unit	---
	Conventional water-cooled chiller	3164 kW	5.13	350/unit	---
	Double-duty chiller	Cooling-3164 kW /ice-making-2341 kW	Cooling-4.89 /ice-making-4.03	400/unit	---
	Water tank	Cooling storage-10000 kWh /Heating storage-22000 kWh	---	100/unit	Maximum power: cooling-1322 kW /heating-2933 kW
	Electric boiler	2050 kW	0.99	150/unit	---
	Gas turbine	1200 kW	Electricity-0.35 /heat-0.4	0.68/kW	---
	Absorption chiller	800 kW	1.2	0.12/kW	---
Continuous equipment	Ice-storage tank	---	---	0.007/kW	Maximum power: 7000 kW
	PV system	---	---	0.75/kW	---

Table 2-4 Electricity and natural gas purchasing tariffs of the IEGS

Item	Maximum power	Category	Period	Price/(CNY/kWh)
Electricity	10MW	Peak	8:00-11:00, 18:00-23:00	1.35
		Valley	00:00-7:00, 23:00-00:00	0.47
		Flat	7:00-8:00, 11:00-18:00	0.89
Natural gas	5MW	---	Whole day	0.4

Table 2-5 Optimal configuration incorporating the resilient scheduling

Category	Configuration	Investment cost /$\times 10^4$ CNY	Annual cost /$\times 10^4$ CNY
Overall annual cost	---	---	2,821.7
Annual investment cost	---	---	575.3
Annual operation cost	---	---	2,246.4
GSHP	3	900.0	---
Conventional water-cooled chiller	1	350.0	---
Double-duty chiller	1	400.0	---
Ice-storage tank	10009.0 kWh	70.1	---
Electric boiler	1	150.0	---
Water tank	1	100.0	---
Gas turbine	3	2,448.0	---
Absorption chiller	5	480.0	---
PV	1,000 kW	750	---

2) Performance comparison

The configuration without considering the resilience strategy is listed in Table 2-6. The configurations incorporating the resilient strategy or not are compared in Fig. 2-37. After considering the operation resilience, the system needs to be equipped with more flexible and controllable resources to meet the critical loads in case of source failure, as well as the reserve requirements in normal operation; hence, more gas turbines and absorption chillers, larger capacity of the ice storage tank are optimized. Although the reserves of thermal storage devices may restrict the improvement in the economy, the annual operation cost after considering the resilient strategy

is 553,000 CNY lower than before due to the increase of dispatching resources, which are 22,464,000 CNY and 23,017,000 CNY, respectively. The overall annual cost with the resilient strategy is 381,000 CNY (1.4%) higher than that without the resilient strategy; the proposed planning method can realize reliability improvement at a small economic cost.

Table 2-6 Optimal configuration without considering resilient scheduling

Category	**Configuration**	**Investment cost /×10⁴ CNY**	**Annual cost /×10⁴ CNY**
Overall annual cost	---	---	2,783.6
Annual investment cost	---	---	481.9
Annual operation cost	---	---	2,301.7
GSHP	3	900	---
Conventional water-cooled chiller	1	350	---
Double-duty chiller	1	400	---
Ice-storage tank	9,337.0 kWh	65.4	---
Electric boiler	1	150	---
Water tank	1	100	---
Gas turbine	2	1,632	---
Absorption chiller	4	384	---
PV	1,000 kW	750	---

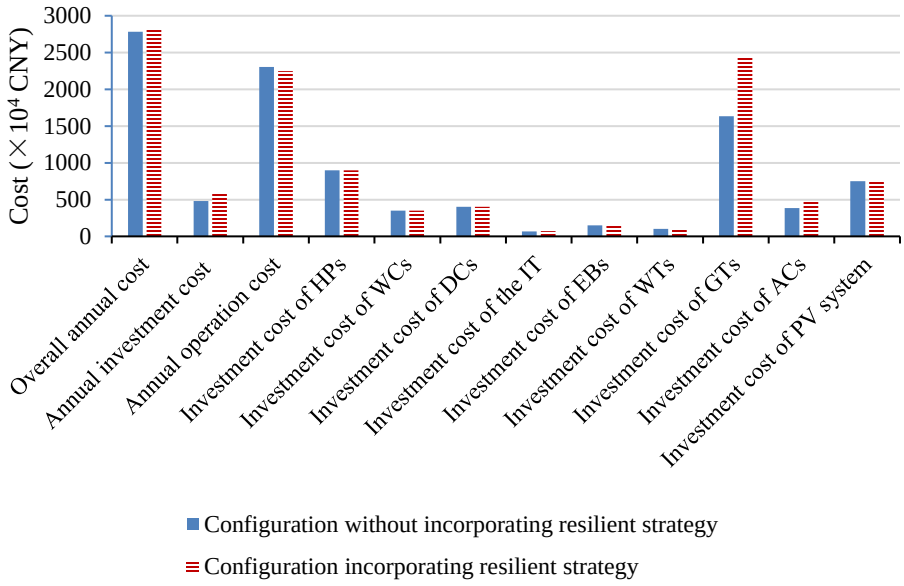

Fig. 2-37 Configuration comparisons incorporating resilience strategy or not

2.4 Operation of MEMGs

Operation of MEMG is aimed to realize optimized operation on the premise of the security and stability of the MGs. The objectives of MG operation include system operation cost, system RES utilization ratio, system energy efficiency, system carbon emission, or their combinations. MG operation strategies can be classified into two categories, the mathematical optimization based strategies and the fixed strategies. The former is obtained by solving the optimization problems of MG and is adaptable with different operation scenarios, while the latter is predefined according to the structure and typical operation conditions and is more suitable for simple MGs. We focus on the optimization-based strategies in this section.

2.4.1 Operation Modeling and Optimization of MEMGs

We first illustrate the basic concepts in the operation modeling of MEMG with a sample grid-connected MG. This MG is composed of WTGs, PV arrays, CCHP system, gas boilers, batteries and thermal storage devices to satisfy the cooling, heat and electrical demand simultaneously. The energy flow of the MG is shown in Fig. 2-38.

A bus based structure can be established to represent the power balance of different energy forms, which is shown in Fig. 2-39. It is then straightforward to read off energy balance equations from Fig. 2-39 as: 1) The balance equation of the electrical bus:

$$P_{grid} + P_{\mathrm{GEN}} + P_{\mathrm{PV}} + P_{\mathrm{WT}} + P_{\mathrm{ES,D}} = P_{\mathrm{load}} + P_{\mathrm{EC}}^{\mathrm{in}} + P_{\mathrm{CS,C}} + P_{\mathrm{ES,C}} \tag{2-51}$$

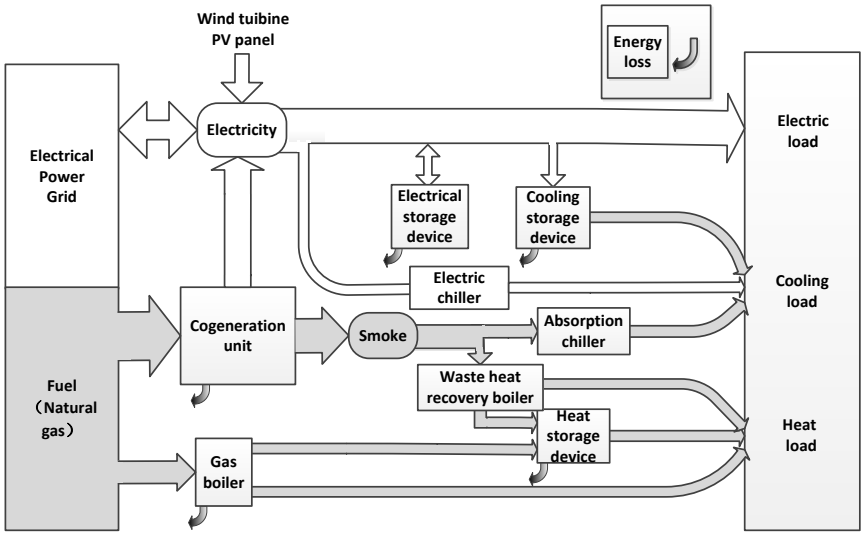

Fig. 2-38 Energy flow of a CCHP system

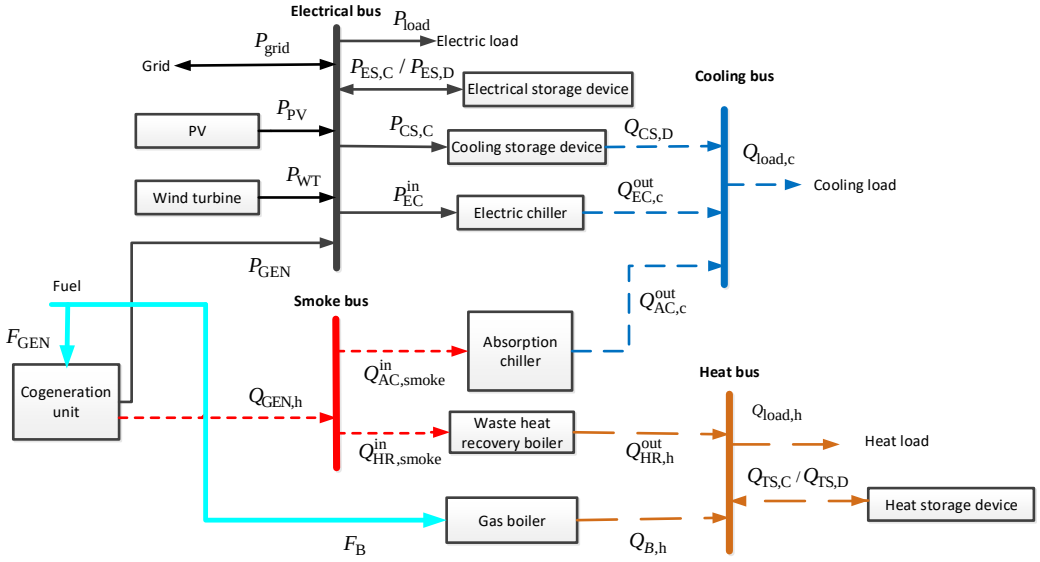

Fig. 2-39 Bus-based structure for a MG

where P_{grid} is the electric power purchased from the grid, P_{load} is the electric load, and $P_{\mathrm{CS,C}}$ is the charging electric power of cooling storage devices; 2) The balance equation of the smoke bus:

$$Q_{\mathrm{GEN,h}} = Q_{\mathrm{AC,smoke}}^{\mathrm{in}} + Q_{\mathrm{HR,smoke}}^{\mathrm{in}} \tag{2-52}$$

where $Q_{\mathrm{AC,smoke}}^{\mathrm{in}}$ is the thermal power of smoke input of the absorption chiller; 3) The balance equation of the heat bus:

$$Q_{\mathrm{HR,h}}^{\mathrm{out}} + Q_{\mathrm{B,h}} + Q_{\mathrm{TS,D}} = Q_{\mathrm{load,h}} + Q_{\mathrm{TS,C}} \tag{2-53}$$

where $Q_{\mathrm{load,h}}$ is the heat load; 4) The balance equation of the cooling bus:

$$Q_{\mathrm{EC,c}}^{\mathrm{out}} + Q_{\mathrm{CS,D}} + Q_{\mathrm{AC,c}}^{\mathrm{out}} = Q_{\mathrm{load,c}} \tag{2-54}$$

where $Q_{\mathrm{CS,D}}$ is the discharging cooling power of cooling storage devices, and $Q_{\mathrm{load,c}}$ is the cooling load. In addition to the energy bus balance constraints, constraints from the device models are another important part of the operation model and will be presented in more detail with some typical devices of the MEMG.

A variety of objective functions exist for the operation optimization of MGs. As an example, the objective function of the minimum operation cost can be chosen:

$$\min C = C_{\mathrm{elec}} + C_{\mathrm{fuel}} \tag{2-55}$$

where C is the total operation cost, C_{elec} is the total electricity charge, and C_{fuel} is the total fuel cost. The total electricity charge C_{elec} is given by:

$$C_{\mathrm{elec}} = \sum_{n=1}^{m} C_{\mathrm{elec}}^{n} P_{\mathrm{grid}}^{n} \Delta t \tag{2-56}$$

where m is the total number of the time steps in the dispatch horizon, P_{grid}^{n} is the electric power purchased from the grid at time step *n*, and C_{elec}^{n} is the electricity price at time step *n*. Meanwhile, the total fuel cost C_{fuel} can be obtained by:

$$\begin{aligned} C_{\mathrm{fuel}} &= c_{\mathrm{fuel}} \sum_{n=1}^{m} (F_{\mathrm{GEN}}^{n} + F_{\mathrm{B}}^{n}) \\ &= c_{\mathrm{fuel}} \sum_{n=1}^{m} \left(\frac{P_{\mathrm{GEN}}^{n}}{\eta_{\mathrm{GEN}}} + \frac{Q_{\mathrm{B}}^{n}}{\eta_{\mathrm{B}}} \right) \Delta t \end{aligned} \tag{2-57}$$

where F_{GEN}^{n} and F_{B}^{n} are the fuel consumption of the generator and the gas boiler at time step *n* respectively, P_{GEN}^{n} and Q_{B}^{n} are the electric power output of the generator and the heat power output of the boiler at time step *n*, and c_{fuel} is the price of unit fuel thermal value.

At each time step of the dispatch horizon, the bus balance equations and device constraints should be satisfied. Besides, the stored energy of the ESS at the start and end of the dispatch horizon should be equal. Taking batteries as an example, there should be:

$$S_{\mathrm{ES}}^{\mathrm{end}} = S_{\mathrm{ES}}^{\mathrm{start}} \tag{2-58}$$

where $S_{\mathrm{ES}}^{\mathrm{end}}$ and $S_{\mathrm{ES}}^{\mathrm{start}}$are the SOC of the electrical ESS at the end and start of the dispatch horizon, respectively. Other types of ESSs have the similar constraints.

We then present the operation model of typical MEMG devices.

(1) GSHP system model

The GSHP is a device that realizes the transfer of low-grade thermal energy to high-grade thermal energy by inputting a small amount of high-grade energy (electric energy), which can be used for space cooling and heating. When used for space cooling, the GSHP can be equipped with cold water tanks to store cooling energy, and the cooling energy of the tanks can be released when required. In this report, the CWPs of the cold water tanks refer to the discharge and charge circulating CWPs installed on both sides of the plate heat exchanger. The pumps of both sides work in a chain.

The constraints on the GSHPs' cooling and cooling-storage power are explained as follows. According to the proportional relation of the cooling sources' power to the flow of the corresponding primary CWPs, the cooling power of each GSHP is calculated based on its cooling mode, the rated flow of its CWP, the total flow of the system's air conditioning chilled water and the cooling demand, as shown in

$$Q_{t,i}^{\mathrm{HP,C}} = U_{t,i}^{\mathrm{HP,C}} F^{\mathrm{HP}} L_t^{\mathrm{C}} / F_t^{\mathrm{C}}, \forall i \in \Omega_{\mathrm{HP}} \tag{2-59}$$

Here, we suppose that the cooling power of the GSHPs in cooling mode is equivalent. L_t^{C} is the cooling demand of the community integrated energy system (CIES) at time *t*. The constraint of the GSHP's cooling-storage power is

$$Q_{t,i}^{\mathrm{HP,S}} \sum_{j=1}^{N^{\mathrm{HP}}} U_{t,j}^{\mathrm{HP,S}} = U_{t,i}^{\mathrm{HP,S}} \sum_{j=1}^{N^{\mathrm{HP}}} Q_{t,j}^{\mathrm{HP,S}}, \forall i \in \Omega_{\mathrm{HP}} \tag{2-60}$$

which guarantees that the balance of the cooling-storage power of the GSHPs in cooling-storage mode is maintained. The lower/upper limits of the cooling and cooling-storage power of the GSHP units in cooling and cooling-storage mode is described in the following equations.

$$U_{t,i}^{\mathrm{HP,C}} \underline{Q}_i^{\mathrm{HP}} \le Q_{t,i}^{\mathrm{HP,C}} \le U_{t,i}^{\mathrm{HP,C}} \overline{Q}_i^{\mathrm{HP}}, \forall i \in \Omega_{\mathrm{HP}} \tag{2-61}$$

$$U_{t,i}^{\mathrm{HP,S}} \underline{Q}_i^{\mathrm{HP}} \le Q_{t,i}^{\mathrm{HP,S}} \le U_{t,i}^{\mathrm{HP,S}} \overline{Q}_i^{\mathrm{HP}}, \forall i \in \Omega_{\mathrm{HP}} \tag{2-62}$$

The cooling mode and cooling-storage mode of the GSHPs at time *t* are distinguished by

$$U_{t,1}^{\mathrm{HP,C}} + U_{t,1}^{\mathrm{HP,S}} \le 1 \tag{2-63}$$

The startup/shutdown orders of the GSHPs restrictions are

$$U_{t,i}^{\mathrm{HP,C}} \geq U_{t,i+1}^{\mathrm{HP,C}}, \forall i = 1, 2, \cdots, N^{\mathrm{HP}} - 1 \tag{2-64}$$

$$U_{t,i}^{\mathrm{HP,S}} \geq U_{t,i+1}^{\mathrm{HP,S}}, \forall i = 1, 2, \cdots, N^{\mathrm{HP}} - 1 \tag{2-65}$$

The number of GSHPs in the cooling-storage mode is less than the number of CWPs collateral to the cold water tanks,

$$\sum_{i=1}^{N^{\mathrm{HP}}} U_{t,i}^{\mathrm{HP,S}} \leq N^{\mathrm{WT,CWP}} \tag{2-66}$$

The relationship between the cooling/cooling-storage mode and ON/OFF state of the GSHPs is described in the following equations.

$$U_{t,i}^{\mathrm{HP}} \geq U_{t,i}^{\mathrm{HP,C}}, \forall i \in \Omega_{\mathrm{HP}} \tag{2-67}$$

$$U_{t,i}^{\mathrm{HP}} \geq U_{t,i}^{\mathrm{HP,S}}, \forall i \in \Omega_{\mathrm{HP}} \tag{2-68}$$

$$U_{t,i}^{\mathrm{HP}} \leq U_{t,i}^{\mathrm{HP,S}} + U_{t,i}^{\mathrm{HP,C}}, \forall i \in \Omega_{\mathrm{HP}} \tag{2-69}$$

The GSHP is on when operating in cooling or cooling-storage modee and off otherwise.

The following equations describes the power consumption of the GSHPs, where COP_i^{HP} is the COP of the *i*th GSHP; $P^{\mathrm{HP,CWP}}$ and $P^{\mathrm{HP,CP}}$ are the rated powers of the CWP and the cooling water pump (CP) interlocked with the GSHP, respectively; and $P^{\mathrm{WT,CWP,1}}$ and $P^{\mathrm{WT,CWP,2}}$ are the rated powers of the interlocked discharge and charge circulating pumps on both sides of the plate heat exchanger, respectively.

$$P_t^{\mathrm{HP}} = \sum_{i=1}^{N^{\mathrm{HP}}} \begin{bmatrix} (Q_{t,i}^{\mathrm{HP,C}} + Q_{t,i}^{\mathrm{HP,S}})/\mathrm{COP}_i^{\mathrm{HP}} + \\ U_{t,i}^{\mathrm{HP,C}}(P^{\mathrm{HP,CP}} + P^{\mathrm{HP,CWP}}) + \\ U_{t,i}^{\mathrm{HP,S}}(P^{\mathrm{WT,CWP,1}} + P^{\mathrm{WT,CWP,2}} + P^{\mathrm{HP,CP}}) \end{bmatrix} \tag{2-70}$$

(2) Conventional water-cooled chiller system model

When the conventional water-cooled chiller is in operation, the refrigerant evaporates to absorb heat from the high temperature chilled return water and then condenses to release heat into the supply water of the cooling tower (CT). The above cycle is repeated for refrigeration.

The cooling power of each conventional water-cooled chiller according to the flow ratio based on its operating state, the rated flow of the CWP, the total flow of the primary CWPs and the cooling demand is calculated as

$$Q_{t,i}^{\mathrm{WC}} = U_{t,i}^{\mathrm{WC}} F^{\mathrm{WC}} L_t^{\mathrm{C}} / F_t^{\mathrm{C}}, \forall i \in \Omega_{\mathrm{WC}} \tag{2-71}$$

This equation ensures that the cooling power of the units in operation remains consistent.

The upper/lower power limits of the conventional water-cooled chillers in operation and the units' startup/shutdown order, respectively.

$$U_{t,i}^{\mathrm{WC}} \underline{Q}_i^{\mathrm{WC}} \le Q_{t,\mathrm{i}}^{\mathrm{WC}} \le U_{t,i}^{\mathrm{WC}} \overline{Q}_i^{\mathrm{WC}}, \forall i \in \Omega_{\mathrm{WC}} \tag{2-72}$$

$$U_{t,i}^{\mathrm{WC}} \ge U_{t,i+1}^{\mathrm{WC}}, \forall i = 1, 2, \cdots, N^{\mathrm{WC}} - 1 \tag{2-73}$$

The power consumption of the conventional water-cooled chillers is depicted in

$$P_t^{\mathrm{WC}} = \sum_{i=1}^{N^{\mathrm{WC}}} \begin{bmatrix} Q_{t,i}^{\mathrm{WC}} / \mathrm{COP}_i^{\mathrm{WC}} + \\ U_{t,i}^{\mathrm{WC}} (P^{\mathrm{WC,CWP}} + P^{\mathrm{WC,CP}} + P^{\mathrm{WC,CT}}) \end{bmatrix} \tag{2-74}$$

where $\mathrm{COP}_i^{\mathrm{WC}}$ is the COP of the *i*th conventional water-cooled chiller and $P^{\mathrm{WC,CWP}}$, $P^{\mathrm{WC,CP}}$ and $P^{\mathrm{WC,CT}}$ are the rated powers of the CWP, CP and CT interlocked with conventional water-cooled chiller, respectively.

(3) The ice storage system model

The ice storage system consists of two double duty chillers and one ice-storage tank. The double-duty chiller includes two main operating modes. In cooling mode, the ethylene glycol solution exchanges heat with chilled water to realize refrigeration. In ice making mode, the ethylene glycol solution at low temperature freezes the water of the ice storage tank to ice. The ice storage tank makes use of the water/ice phase change to achieve the charge and discharge of cooling energy.

The sum of the cooling power of the double-duty chillers and the ice-storage tank is equal to that of the ice storage system, which is depicted in

$$\sum_{i=1}^{N^{\mathrm{DC}}} Q_{t,i}^{\mathrm{DC,C}} + Q_t^{\mathrm{IT}} = Q_t^{\mathrm{IS}} \tag{2-75}$$

where N^{DC} is the number of double-duty chillers. Similar to other subsystems, the following equation calculates the cooling power of the ice storage system according to the ON/OFF state, the rated flow of its CWPs, the total flow of the primary CWPs and the cooling demand.

$$Q_t^{\mathrm{IS}} = F^{\mathrm{IS,CWP}} \sum_{i=1}^{N^{\mathrm{IS,CWP}}} U_{t,i}^{\mathrm{IS,CWP}} L_t^{\mathrm{C}} / F_t^{\mathrm{C}} \tag{2-76}$$

To ensure that the power outputs of the double duty chillers in cooling mode and ice-making mode are the same, we have

$$Q_{t,i}^{\mathrm{DC,C}} \sum_{j=1}^{N^{\mathrm{DC}}} U_{t,j}^{\mathrm{DC,C}} = U_{t,i}^{\mathrm{DC,C}} \sum_{j=1}^{N^{\mathrm{DC}}} Q_{t,j}^{\mathrm{DC,C}}, \forall i \in \Omega_{\mathrm{DC}} \tag{2-77}$$

$$Q_{t,i}^{\mathrm{DC,I}} \sum_{j=1}^{N^{\mathrm{DC}}} U_{t,j}^{\mathrm{DC,I}} = U_{t,i}^{\mathrm{DC,I}} \sum_{j=1}^{N^{\mathrm{DC}}} Q_{t,j}^{\mathrm{DC,I}}, \forall i \in \Omega_{\mathrm{DC}} \tag{2-78}$$

The following two equations restrain $Q_{t,i}^{\mathrm{DC,C}}/Q_{t,i}^{\mathrm{DC,I}}$ within their lower and upper bounds when operating in cooling/ice making mode.

$$U_{t,i}^{\mathrm{DC,C}} \underline{Q}_i^{\mathrm{DC,C}} \leq Q_{t,i}^{\mathrm{DC,C}} \leq U_{t,i}^{\mathrm{DC,C}} \overline{Q}_i^{\mathrm{DC,C}}, \forall i \in \Omega_{\mathrm{DC}} \tag{2-79}$$

$$U_{t,i}^{\mathrm{DC,I}} \underline{Q}_i^{\mathrm{DC,I}} \leq Q_{t,i}^{\mathrm{DC,I}} \leq U_{t,i}^{\mathrm{DC,I}} \overline{Q}_i^{\mathrm{DC,I}}, \forall i \in \Omega_{\mathrm{DC}} \tag{2-80}$$

The cooling mode and ice-making mode of the double duty chillers cannot operate simultaneously, as depicted in

$$U_{t,1}^{\mathrm{DC,C}} + U_{t,1}^{\mathrm{DC,I}} \leq 1 \tag{2-81}$$

The startup/shutdown orders of the double duty chillers constraints are

$$U_{t,i}^{\mathrm{DC,C}} \geq U_{t,i+1}^{\mathrm{DC,C}}, \forall i = 1,2,\cdots,N^{\mathrm{DC}} - 1 \tag{2-82}$$

$$U_{t,i}^{\mathrm{DC,I}} \geq U_{t,i+1}^{\mathrm{DC,I}}, \forall i = 1,2,\cdots,N^{\mathrm{DC}} - 1 \tag{2-83}$$

The relationship between the ON/OFF state of each double-duty chiller and its cooling/ice making mode is:

$$U_{t,i}^{\mathrm{DC}} \geq U_{t,i}^{\mathrm{DC,C}}, \forall i \in \Omega_{\mathrm{DC}} \tag{2-84}$$

$$U_{t,i}^{\mathrm{DC}} \geq U_{t,i}^{\mathrm{DC,I}}, \forall i \in \Omega_{\mathrm{DC}} \tag{2-85}$$

$$U_{t,i}^{\mathrm{DC}} \leq U_{t,i}^{\mathrm{DC,C}} + U_{t,i}^{\mathrm{DC,I}}, \forall i \in \Omega_{\mathrm{DC}} \tag{2-86}$$

A double duty chiller is on when operating in cooling or ice making mode and off otherwise.

The relationship between the stored cooling energy and charge/discharge power of the ice-storage tank is described as

$$W_t^{\mathrm{IT}} = (1 - \varepsilon^{\mathrm{IT}}) W_{t-1}^{\mathrm{IT}} + \sum_{i=1}^{N^{\mathrm{DC}}} Q_{t,i}^{\mathrm{DC,I}} \Delta t - Q_t^{\mathrm{IT}} \Delta t \tag{2-87}$$

$$0 \leq W_t^{\mathrm{IT}} \leq \overline{W}^{\mathrm{IT}} \tag{2-88}$$

and restrict the total cooling energy stored in the ice storage tank within its limit. The cooling power of the ice storage tank should be lower than its upper limit and that the ice-storage tank cannot release cooling when the double duty chillers are operating in ice making mode.

$$0 \leq Q_t^{\mathrm{IT}} \leq \left(1 - U_{t,1}^{\mathrm{DC,I}}\right) \overline{Q}^{\mathrm{IT}} \tag{2-89}$$

The running number of CWPs in the ice-storage system according to the principle of "one chiller-one pump", i.e.

$$\sum_{i=1}^{N^{\mathrm{IS,CWP}}} U_{t,i}^{\mathrm{IS,CWP}} \geq \sum_{i=1}^{N^{\mathrm{DC}}} U_{t,i}^{\mathrm{DC,C}} \tag{2-90}$$

and the CWPs in operation can satisfy the cooling supply requirement of the ice storage system.

$$\sum_{i=1}^{N^{\mathrm{IS,CWP}}} U_{t,i}^{\mathrm{IS,CWP}} \overline{Q}^{\mathrm{IS,CWP}} \geq Q_t^{\mathrm{IS}} \tag{2-91}$$

The power consumption of the ice storage system is described as

$$P_t^{\mathrm{IS}} = \sum_{i=1}^{N^{\mathrm{DC}}} \begin{bmatrix} \frac{Q_{t,i}^{\mathrm{DC,C}}}{\mathrm{COP}_i^{\mathrm{DC,C}}} + \frac{Q_{t,i}^{\mathrm{DC,I}}}{\mathrm{COP}_i^{\mathrm{DC,I}}} + \\ U_{t,i}^{\mathrm{DC,C}}(P^{\mathrm{DC,CP}} + P^{\mathrm{DC,CT}}) + \\ U_{t,i}^{\mathrm{DC,I}}(P^{\mathrm{DC,CP}} + P^{\mathrm{DC,CT}} + P^{\mathrm{EP}}) \end{bmatrix} + \frac{P^{\mathrm{EP}} Q_t^{\mathrm{IS}}}{\overline{Q}^{\mathrm{EP}}} + \sum_{i=1}^{N^{\mathrm{IS,CWP}}} U_{t,i}^{\mathrm{IS,CWP}} P^{\mathrm{IS,CWP}} \tag{2-92}$$

where $\mathrm{COP}_i^{\mathrm{DC,C}}$ and $\mathrm{COP}_i^{\mathrm{DC,I}}$ are the COP of the *i*th double duty chiller in cooling mode and ice-making mode, respectively, and $P^{\mathrm{DC,CP}}$, $P^{\mathrm{DC,CT}}$, P^{EP} and $P^{\mathrm{IS,CWP}}$ are the rated powers of the CP, opening CT, ethylene glycol pump (EP) and CWP in the ice-storage system, respectively.

(4) Optimal operation model of the MEMG

The goal of the operation model is to formulate the day-ahead scheduling plan at the hourly scale (23:00-22:00 tomorrow) based on the forecast results of electricity and cooling demands and the PV system's output with minimizing the overall operation cost. The day-ahead scheduling plan for multi-hours contains the ON/OFF states, operation modes, and supply power of each chiller, and the operation modes and power of the thermal storage devices. The plan is then assigned to each subsystem to coordinate the operation of various energy supply/storage devices.

1) Problem formulation

The optimization objective is to minimize the overall operation cost and the startup penalty of each cooling unit in a scheduling cycle:

$$\min F = \sum_{t=1}^{N_T} C_t^{\mathrm{P}} P_t^{\mathrm{TL}} + \sum_{i \in \mathrm{S}} \sum_{j \in \Omega_i} \sum_{t=2}^{N_T} U_{t,j}^{i} (1 - U_{t-1,j}^{i}) E_i \tag{2-93}$$

where C_t^{P} denotes the purchase price of electricity at time *t*, P_t^{TL} denotes the tie-line power (purchasing power from the external grid) at time *t*, E_i denotes the startup penalty of different types of units, and N_T represents the total hours of a scheduling period (24 in day-ahead scheduling).

Because all devices in the system are electrically driven, the operation cost is the cost of purchasing electricity from the external grid. The startup cost is the total penalty of each unit in each subsystem, where S is the set of HP, WC, and DC. The purpose of considering the startup penalty of each unit in the objective is to avoid frequent equipment start/stop.

The economic scheduling model of the CIES can be described as follows:

$$\begin{cases} \min F \\ \text{s. t. all energy bus balance and device constraints are satisfied} \end{cases} \tag{2-94}$$

2) Linearization of the optimization model

In the above optimization model, a number of constraints contain product terms of a binary variable and a continuous variable, and the objective function contains the product terms of two binary variables when expanded. To reduce the difficulty of solving this problem, we linearize the nonlinear terms by introducing auxiliary variables. The linearization process can be described as follows.

For the nonlinear terms $U * r$, where U is a binary variable, r is a continuous positive variable, and the upper limit of r is $\overline{r}$, the auxiliary variable R is introduced to replace the nonlinear terms and is subject to the following constraints.

$$\begin{cases} 0 \le R \le U\overline{r} \\ r - \overline{r}(1-U) \le R \\ R \le r \end{cases} \tag{2-95}$$

For the nonlinear terms $U_1 U_2$, where U_1 and U_2 are binary variables, the auxiliary binary variable Z is introduced to replace the nonlinear terms and is subject to the following constraints.

$$\begin{cases} 0 \le Z \le U_1 \\ 0 \le Z \le U_2 \\ Z \ge U_1 + U_2 - 1 \end{cases} \tag{2-96}$$

Through the above linearization process, the above scheduling problem is converted to a mixed-integer linear programming problem.

After linearization, the compact form of the optimization problem is given as follows:

$$\min_{\boldsymbol{x},\boldsymbol{y},\boldsymbol{r},\boldsymbol{z}} \boldsymbol{c}^{\mathrm{T}}\boldsymbol{x} + \boldsymbol{d}^{\mathrm{T}}\boldsymbol{z}$$

$$\text{s.t.} \begin{cases} \boldsymbol{Fx + Gy \geq f} \\ \boldsymbol{Hy \geq h} \\ \boldsymbol{Kx + Ly = k} \\ \boldsymbol{Mx \geq m} \\ \boldsymbol{Nx = n} \\ \boldsymbol{Oy + Pr = p} \\ \boldsymbol{Sr = s} \\ \boldsymbol{Ty + Wz \geq w} \end{cases} \tag{2-97}$$

where ***x, y*** are the vectors of the continuous variables and binary variables before the linearization process, respectively; ***r*** is the vector of the auxiliary continuous variables related to the product terms of a binary variable and a continuous variable; ***z*** is the vector of the auxiliary binary variables related to the product terms of two binary variables; and ***c***, ***d*** are the coefficient vectors of the linearized form of objective function; ***F, G, H, K, L, M, N, O, P, S, T*** and ***W*** are the coefficient matrixes; and ***f, h, k, m, n, p, s*** and ***w*** are constant column vectors.

2.4.2 MEMG Robust Scheduling with MPC

MEMG couples multiple energy forms and links, it is important to cope with the inadequacy of flexibility for realizing efficient utilization and reliable supply. A model predictive control (MPC) based robust scheduling strategy is desirable to maintain and utilize MEMG flexibility for enhancing the uncertainty adaptability. The scheduling framework consists of rolling optimization and robust constraint generation. Additionally, the MPC based optimization can well adapt to the rolling forecasting uncertainties, and the schedule generated by advance reserving means has stronger robustness for real-time errors.

(1) MPC based rolling optimization

In the stage of rolling optimization, the energy management system first updates the predictive data of outdoor temperature, solar radiation and loads based on the weather and history information. Then, multi-interval equipment scheduling and demand management plans are generated based on the predicted values, including the ON/OFF states, operating conditions, supply power of chillers, operation conditions and power of the thermal storage devices, supply water temperature of the CES and the injected powers of buildings. However, the system only executes the schedule of the first interval.

In each rolling period, multiple devices are coordinated to minimize the operation cost and unit startup/shutdown penalty.

$$\min F = \sum_{t=t_S}^{N_T} C_t^P P_t^{TL} \Delta t + \sum_{i \in S} \sum_{j \in \Omega_i} \sum_{t=t_S}^{N_T} U_{t,j}^i (1 - U_{t-1,j}^i) E_i \quad (2\text{-}98)$$

where t_S is the first interval of the rolling optimal scheduling; C_t^P denotes the purchase price of electricity at time *t*; P_t^{TL} denotes the tie-line power (purchasing power from the external grid) at time *t*; E_i denotes the startup penalty of different types of units; and N_T represents the total interval of the rolling period. Because all devices in the system are electrically driven, the operation cost is the cost of purchasing electricity from the external grid. The startup/shutdown cost is the total penalty of each unit in each subsystem, where S is {HP, WC, DC}. The purpose of considering the startup penalty of each unit in the objective function is to avoid frequent equipment start/stop. Here, we ignore the shutdown cost due to its lower value.

For better adaption to the cyclical changes of TOU tariff, the rolling method with prediction horizon reducing and control horizon unchanged is selected to minimize the cost of each scheduling day. The scheduling plan has the optimality throughout the whole scheduling day. And the overall economy for long-time operation can be realized through the reasonable consideration of different scheduling days. The schematic of the rolling optimization based on MPC is shown in Fig. 2-40. At the time $t_0 + m\Delta t$, the system scheduling plan of the prediction domain is obtained by the optimization solution based on the prediction domain information ($t_0 + m\Delta t$ to $t_0 + n\Delta t$), and only the scheduling plan in the control domain is executed. Then the prediction domain is compressed to the last scheduling interval, and the control domain is continuously moved backward. This rolling process repeats until the execution scheduling is generated for all scheduling intervals.

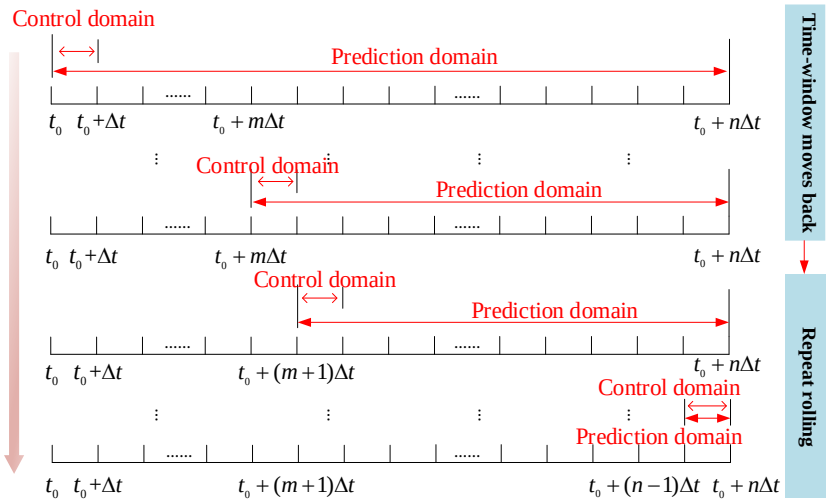

Fig. 2-40 Rolling optimization based on MPC

(2) Robust scheduling of the control domain

In the actual operation process, due to the existence of prediction error, the outdoor temperature, solar radiation, and electrical load will change in every scheduling interval. For electricity, the system can automatically balance the fluctuations of solar radiation and electrical load. However, deviation of the outdoor temperature will directly affect the indoor temperature of buildings, causing problems that seriously affect the energy supply quality, such as too high/low temperatures, and large temperature fluctuations between adjacent times.

Incorporating the rolling optimization method, we formulate the robust scheduling plan for adapting to the outdoor temperature uncertainty, through adjustments of the lower/upper limits and the ramping rates of the indoor temperature on the basis of uncertain information in the control domain.

Each rolling optimization should determine not only the predictive data of the prediction domain, but also the outdoor temperature deviation amplitude of the control domain relative to the rolling prediction value. The deviation amplitude of the outdoor temperature in the control domain can be denoted as $M_{t_S}^{\text{out}}$. Therefore, the indoor temperature's deviation amplitude of building i can be calculated by:

$$M_{i,t_S} = \frac{M_{t_S}^{\text{out}} K_i F_i \Delta t}{C_{\text{air}} \rho_{\text{air}} V_i} \tag{2-99}$$

The indoor temperature upper and lower limits of building i in the control domain can be modified as follows:

$$\overline{T}_{i,t_S} = \overline{T} - M_{i,t_S} \tag{2-100}$$

$$\underline{T}_{i,t_S} = \underline{T} + M_{i,t_S} \tag{2-101}$$

Similarly, the indoor temperature ramping limits of building i in the control domain can be modified as follows:

$$\Delta T_{i,t_S,\text{upper}} = \Delta T - M_{i,t_S} \tag{2-102}$$

$$\Delta T_{i,t_S,\text{lower}} = \Delta T - M_{i,t_S} \tag{2-103}$$

The adjustment schematics of the lower/upper and the ramping limits of the indoor temperature are presented in Fig. 2-41.

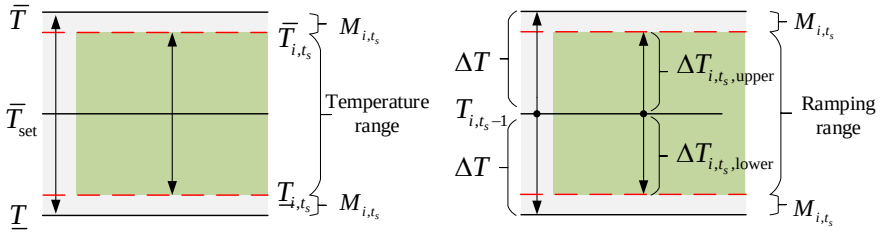

(a) Lower and upper limits (b) Ramping limits

Fig. 2-41 Adjustment of lower/upper ramping limits of indoor temperature

In engineering practice, the application and coordination of the proposed scheduling strategy are depicted in Fig. 2-42. Based on the statues and forecasting data of CIES, energy management system delivers the corresponding schedules of control domain to each device for execution. After responsing to the actual RES, loads and environment information, the operation statuses of the physical system will be acquired for the next rolling optimization, which plays a role in feedback correction. The proposed scheduling framework provides a novel operation flexibility of CIES by unified source-network-load scheduling and feedback strategy. Based on rolling optimization and advance reserving means, the strategy regulates multiple flexible and controllable links to facilitate the system operation, including the economic performance and adaptability to the uncertainties.

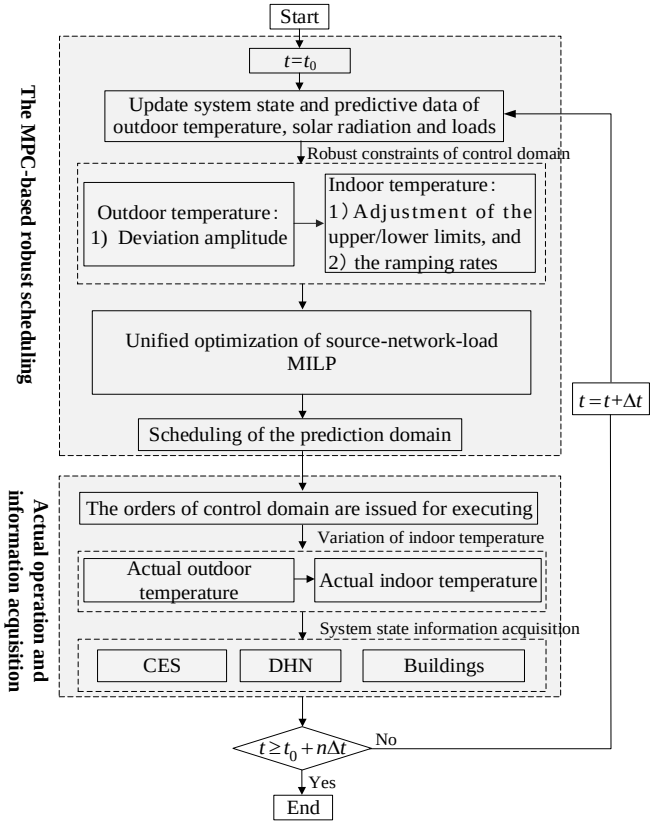

Fig. 2-42 Coordinated control process of the MPC-based robust scheduling

(3) Linearization of the optimization model

In the above optimization model, a number of constraints contain product terms of a binary variable and a continuous variable, and the objective function contains the product terms of two binary variables when expanded. To reduce the solving difficulty, we linearize the nonlinear terms.

(4) Case study

This section applies the proposed method to a practical MEMG in typical day in the cooling period. The scheduling period is from 23:00 to 22:00 of next day, and the scheduling interval is 30 min, i.e., a whole scheduling cycle contains 48 scheduling intervals. Table 2-7 shows the TOU tariff of the relevant region. The TOU tariff presents the “peak-valley-flat” characteristics and the first 16 intervals are in the valley period of the electricity price.

The structure of the system’s heating network is shown in Fig. 2-43. The control modes of heating networks can be quality regulation (the mass flow rates are constant; the water temperatures are variables) or quality-quantity regulation (the mass flow rates and the water

temperatures are both variables), and quality regulation is widely used in northern China. Likewise, the CIES adopts the quality regulation mode.

Table 2-7 TOU tariff of the CIES

Category	Period	Electricity price /(CNY/kWh)
Peak	8:00-11:00, 18:00-23:00	1.35
Valley	00:00-7:00, 23:00-00:00	0.47
Flat	7:00-8:00, 11:00-18:00	0.89

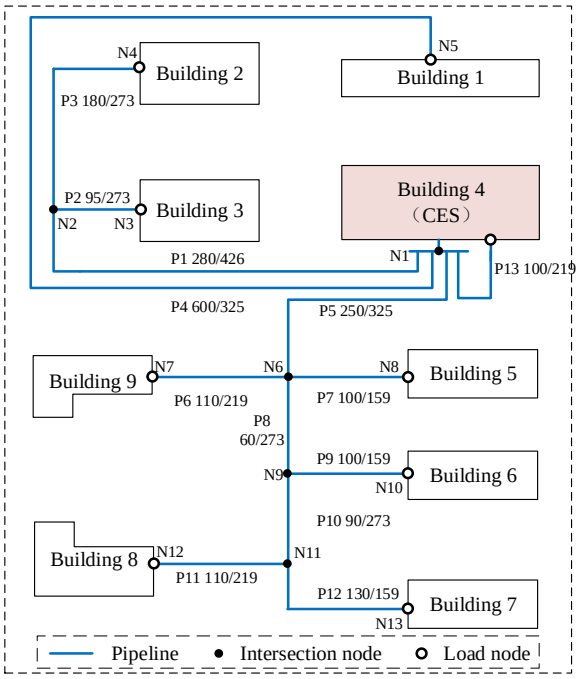

Fig. 2-43 Structure of the heating network in the CIES (P denotes pipeline; N denotes node. The numbers attached to the pipelines are lengths (m) and diameters (mm))

In this scenario, it is assumed that the rolling forecasting information is accurate, so there is no need to perform robust scheduling of the execution interval. Fig. 2-44 shows the cooling power allocation of the CIES. In the valley period (23:00-07:00), the cooling demand is mainly supplied by the GSHPs (double duty chillers are in ice-making mode). In the non-valley period, the ice-storage tank and GSHPs are the main cooling suppliers, and the conventional water-cooled chillers serve as the complementary suppliers due to the lower COP. Throughout the whole period, the electricity demand of the CIES is satisfied by the PV and the external grid. When the PV output is fully absorbed, the insufficient electricity demand will be balanced by the external grid.

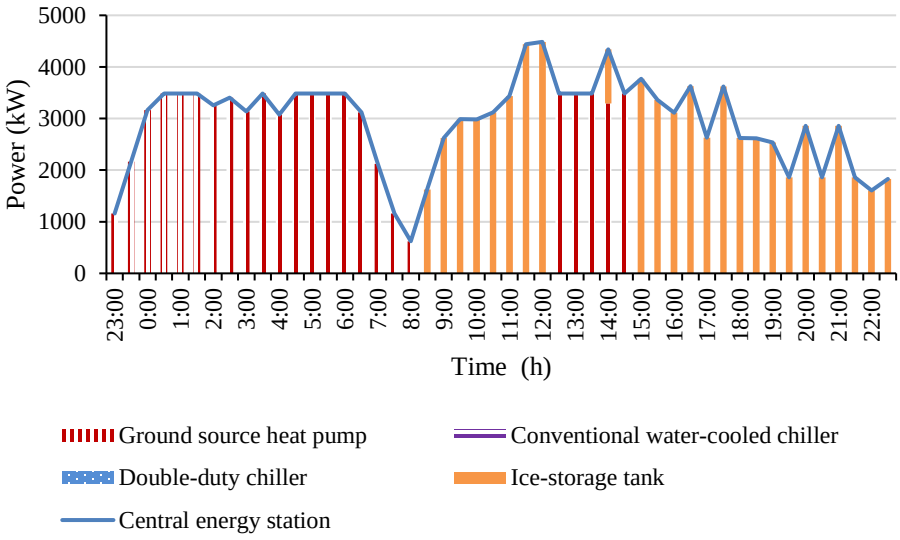

Fig. 2-44 Cooling power allocation of the CIES

Fig. 2-45 shows the curve of the cooling energy stored in the ice-storage tank. The double-duty chillers are in ice making mode during most of the valley period. During this period, the energy stored in the cooling storage equipment increases gradually. In the non-valley period, the energy stored in the ice-storage tank is discharged completely to meet the cooling demand and there is no energy redundancy. The charge-discharge characteristics of the thermal storage device and the "peak-valley-flat" characteristic of the TOU tariff are well incorporated by the scheduling strategy for the goal of less operation cost.

The supply/return water temperature of the CIES is shown in Fig. 2-46. The supply water temperature varies between 5-8℃ according to the schedule, and the return water temperature rises due to the heat exchange of the pipelines with ambient soil and the power consumption of buildings on the demand side. Meanwhile, due to the influence of the pipeline transfer delay, the return temperature curve has an overall rightward trend relative to the supply curve. Combining Fig. 2-45 with Fig. 2-46, it can be seen that the cooling power of the CIES is directly proportional to the difference between the supply and return water temperatures.

Fig. 2-47 depicts the variation of the indoor temperature in each building. The temperature change trends of multiple buildings are similar overall, and there are slight shifts on the time axis duo to delay differences. In the valley period, the overall building temperatures are relatively low, and plenty of cooling energy is stored in the building storage system. In the non-valley period, the

indoor temperatures are higher than those in the valley period. The cooling energy stored during the valley period is released and the overall stored cooling energy decreases. The DR method with the cooling energy transfer between the different periods adjusts the indoor temperature in the comfort range (19-25℃) rather than remaining it at the standard temperature (22℃) and can obtain a better economy incorporating the TOU tariff.

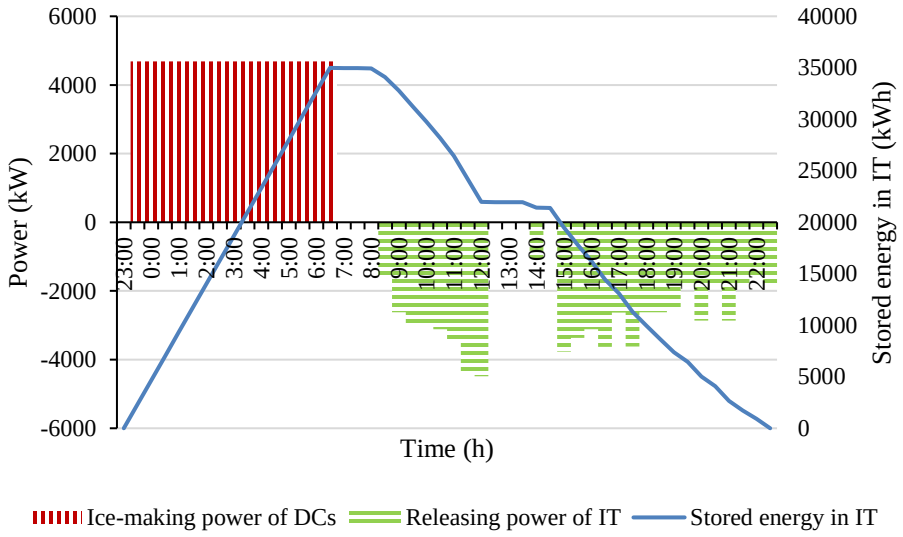

Fig. 2-45 Curve of the cooling energy stored in the ice-storage tank

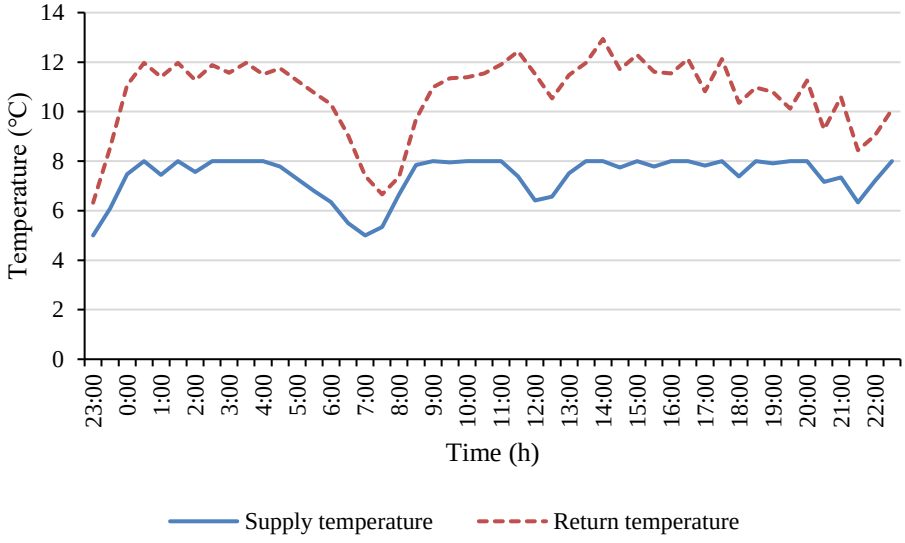

Fig. 2-46 Supply/return water temperature curve of the CIES

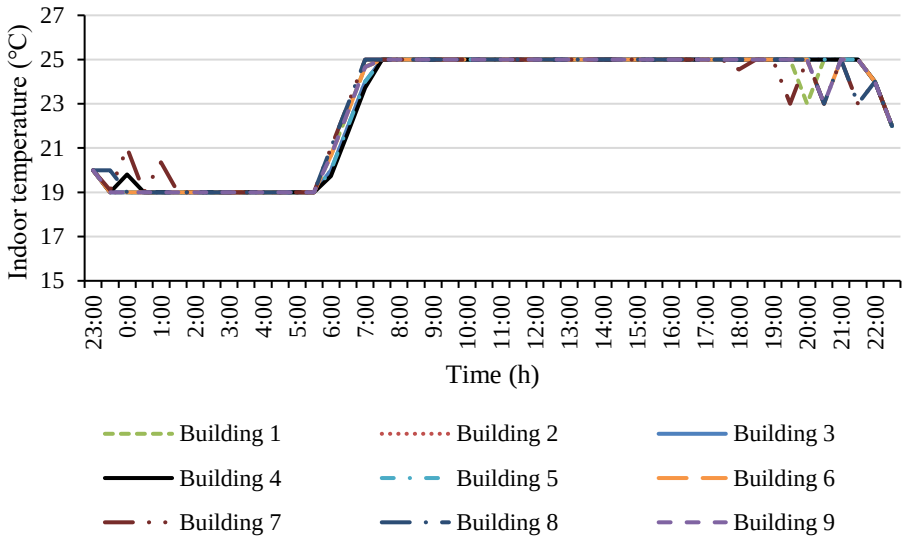

Fig. 2-47 Indoor temperature curves of the buildings

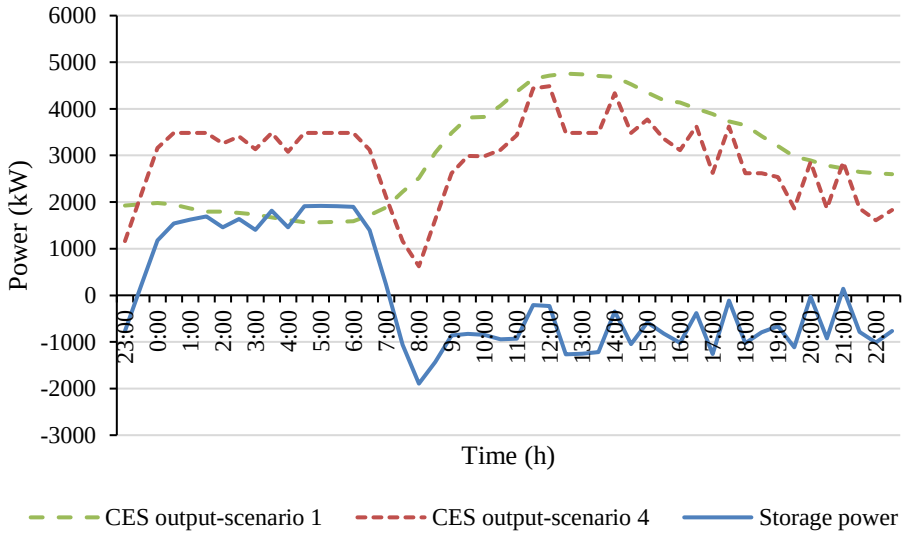

Fig. 2-48 Storage curves of the pipelines and buildings

The power stored in the pipelines and buildings can be calculated by the output power difference of the CIES between scenario 4 and scenario 1(the scenario adopting the proposed scheduling strategy and the scenario adopting the conventional economy scheduling strategy, respectively), as shown in Fig. 2-48. It can be seen that the pipelines and buildings are in the charge/discharge state in the valley/non-valley period. Combined with the TOU tariff, the

operation cost can be significantly reduced by utilizing the characteristics of “valley to charge and non-valley to discharge” in the pipelines and buildings.

Chapter 3 Case Studies of MEMG Demonstration Projects

3.1 Santa Rita Jail MEMG in the US

3.1.1 Project Overview

The Santa Rita Jail, located in Dubin CA, about 65 km east of San Francisco, is a 4,500 inmate facility opened in 1989 and considered one of the most energy efficient jails in the US Over the past decade, Alameda County, which operates the Jail, has installed a series of DERs and undergone a series of efficiency improvements to reduce energy consumption at the site, transforming the Santa Rita Jail into a "green prison" with multiple energy resources. Up to now, Santa Rita Jail Microgrid is still one of the representative MG demonstration project in the world.

Fig. 3-1 Top view of Santa Rita Jail

Under the terms of the US DOE grant, the Jail must contract with the local utility, PG&E, to reduce the peak load on the local feeder by 15%. The peak load of the Jail in summer is close to 3 MW, therefore, 1.5 MW roof PV power generation system, 1 MW molten carbonate fuel cell with CHP system, two 1.2 MW diesel generator sets and a 2 MW/4 MWh lithium-ion battery and associate power conversion system (PCS) are installed to provide electricity and heat to the Jail. Moreover, a static disconnect switch (SDS) was installed between the utility and the MG to allow fast islanding and autonomous operation of the MG in case of failure. As the Jail has high reactive power demand due to large rotating loads, reactive power compensation with 990 kVar capacitor bank is also considered to avoid low power factor penalties on utility billing and provide enough

reactive power support during the islanding process. The equipment capacities are summarized in Table 3-1, the structure diagram of the MG is demonstrated in Fig. 3-2 [1].

Table 3-1 Equipment capacities of Santa Rita Jail MG

Equipment	Rating	MG function
Roof PV	1.2 MW	Supply power in grid-connected and island operation
Fuel cell	1 MW	Supply power in grid-connected and island operation
Diesel generator	2*1.2 MW	Backup source in island operation when battery is at low state-of-charge
Battery and PCS	Battery：2 MW/4 MWh PCS: 2 MW/2.5 MVA	Support island operation; Realize peak load shifting
Capacitor bank	12.47 kV, 900 kVar	Supply reactive power in grid-connected and island operation
SDS	12.47 kV, 300 A	Separate from grid upon disturbance

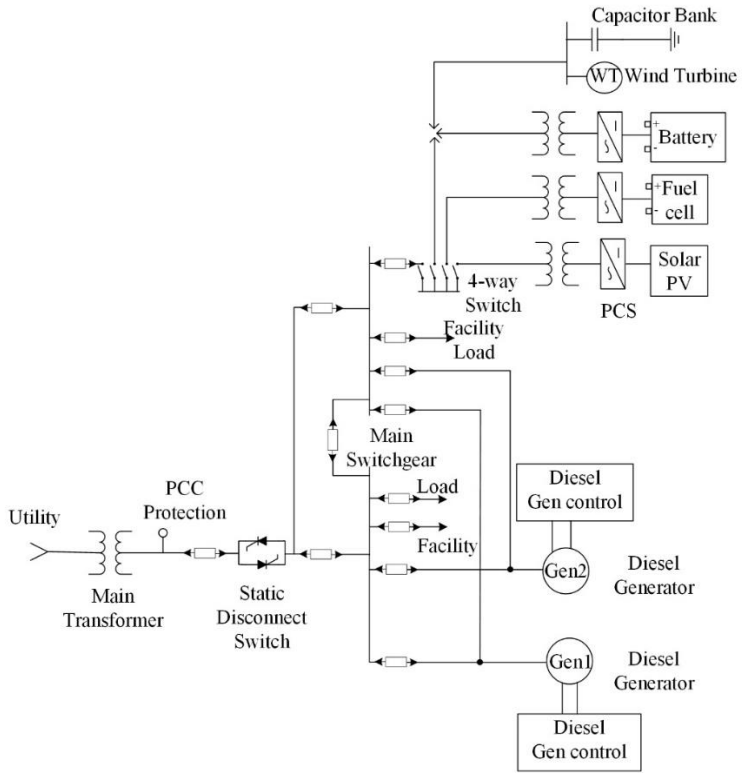

Fig. 3-2 Structure diagram of Santa Rita Microgrid

3.1.2 Key Technologies

The Santa Rita Jail Microgrid project is a demonstration of CERTS Microgrid concepts. The CERTS based DG can regulate the voltage and frequency both in grid connected and islanded mode, thus can realize automatically islanding without communications during utility faults, and

resynchronizing with the grid once the disturbance has dissipated. This concept relies on the following key technologies:

(1) Plug-and-play

One of the objectives of the CERTS Microgrid concept was to reduce MG system cost and increase reliability, requiring for flexible integration of DGs and simplified control of the whole system. Therefore, CERTS based DG (battery and diesel generator) seamlessly balances the power on the islanded MG using an active power vs. frequency droop controller, and ensure a reasonable voltage range using a voltage vs. reactive power droop controller. Under the droop characteristic, the battery storage system increases the output power and reduce the frequency along with the increase of load in the island operation. The maximum allowable frequency drop of the system is set to be less than 1%. The non-critical loads will be cut to avoid the frequency from falling below the lower limit if necessary.

The CERTS MG protocol gives the battery storage system and diesel generator the ability to interconnect with each other without any additional communication or customized supervisory generator control system, this “plug-and-play” nature reduces the engineering cost and enhance the flexibility for application of the MG.

(2) Seamless switching

The key equipment to realize seamless switching of MG is SDS, which connects the MG with the utility grid. The voltage and frequency of both the utility grid and MG are monitored real time through the voltage and current transformers on the line and load sides of the SDS, assisting the SDS in decision making of the automatic islanding and synchronization. The SDS operates within a quarter cycle on the order of 4 to 10 ms, which ensures the seamless switching that the inverter sources in the MG cannot detect any utility events during the switching process. Islanding operations are triggered by overvoltage, undervoltage, overfrequency, and underfrequency, as listed in Table 3-2.

Table 3-2 Protection setting for SDS

Event	Device design range	Implemented value
overvoltage	105%-115%	115%, 10ms 120%, 2ms
undervoltage	95%-80%	80%, 10ms 50%, 3ms

overfrequency	60.1Hz-63Hz	60.5Hz, 0.5ms
underfrequency	59.9Hz-57Hz	59.5Hz, 0.5ms

3.1.3 Social and Economic Benefits

The Santa Rita Jail Microgrid demonstration is one of nine supported by the US DOE, which achieves good demonstration benefits in the application of several key technologies [2]. Prior to the MG project, the Santa Rita Jail facility was susceptible to momentary utility outages and power quality events. The CERTS Microgrid technology, including the "plug-and-play" characteristic of the DG and the SDS and battery storage based seamless switching, enable the system with the ability of islanding during the grid blackouts. The power supply reliability, power quality and operation economy are thus significantly enhanced. The fuel cell with CHP, PV generation system, and the battery storage system provide a reliable and economic power and heat to the officers, staff and inmates, saving nearly 0.1 million USD per year for the Alameda County on the cost of energy consumption [3].

3.2 The Sendai MEMG Project in Japan

3.2.1 Project Overview

In March 2011, the Great East Japan Earthquake (GEJE) and the accompanying tsunami caused devastating damage to the energy supply system of Northeast Japan. Damage to power stations, including Fukushima Daiichi Nuclear Power Station, caused a long term, nationwide power shortage, 8.5 million power customers were affected. Despite the extreme devastation, the Sendai Microgrid continued supplying power and heat to the critical loads within its service scope, proving its effectiveness on improving the power supply elasticity and reliability, thus enjoyed a high reputation all over the world.

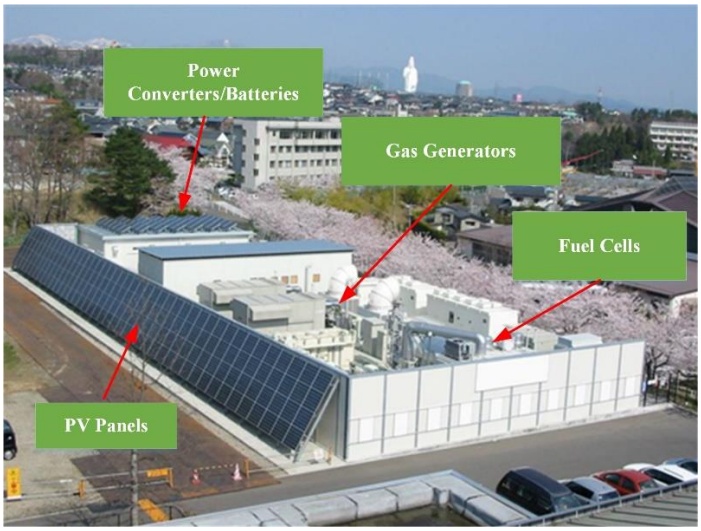

Fig. 3-3 Top view of the energy center of Sendai Microgrid

As part of the "experimental study of multi power quality supply system" demonstration project supported by the NEDO under the Ministry of economy, trade and industry (METI) from 2004 to 2008, Sendai Microgrid was built by Nippon Telegraph and Telephone Corporation (NTT). The goal of the project was to build a MG system that could supply multiple power quality levels of AC power as well as DC power to various consumer loads at the same time. Fig. 3-3 illustrates the overhead view of the energy center of Sendai Microgrid. The major DERs are two 350 kW gas gensets, a 250 kW molten carbonate fuel cell (replaced by phosphoric acid fuel cell after earthquake), a 50 kW rooftop solar PV, and a 600 Ah LA battery [4]. After completion of the NEDO demonstration phase, the MG system continued in operation under the management of NTT. Then, the heating system of the MG was reformed to enable it as a multi-energy system utilizing thermal energy from the waste heat produced by the gas engines and fuel cell to supply heat, hot water, and chilled water, cooled by absorption chillers.

3.2.2 Key Technologies

(1) Integrated multi power quality service

The notable feature of this project are the integration of multi-levels power quality supplied on various circuits. The loads served during the NEDO phase mainly include municipal facilities, a water treatment facility, a high school and the hospital, buildings, laboratories on campus. As demonstrated in Table 3-3, electricity supplied by the Sendai Microgrid is divided into six classes

according to the level of power quality. The magnetic resonance imaging (MRI) machine of the clinic and the server of the laboratory are supplied by A-Class power source, indicate that the power interruption is forbidden. The DC power of the energy center shall not be interrupted as well. B-Class service is supplied at three qualities, the differences based on backup during utility grid outages. B1 and B2 are backed up by battery storage and a genset, respectively, while B3 is not backed up. The switch-over time for B-Class and C-Class is less than 15 ms when the grid has a momentary voltage sag or outage. The hospital, which serves patients with psychiatric illnesses and internal diseases is supported by C-Class power [5].

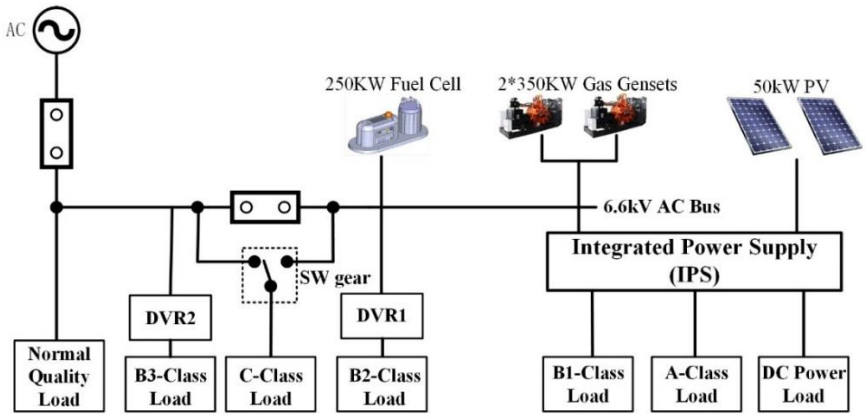

Fig. 3-4 Structure diagram of the Sendai Microgrid

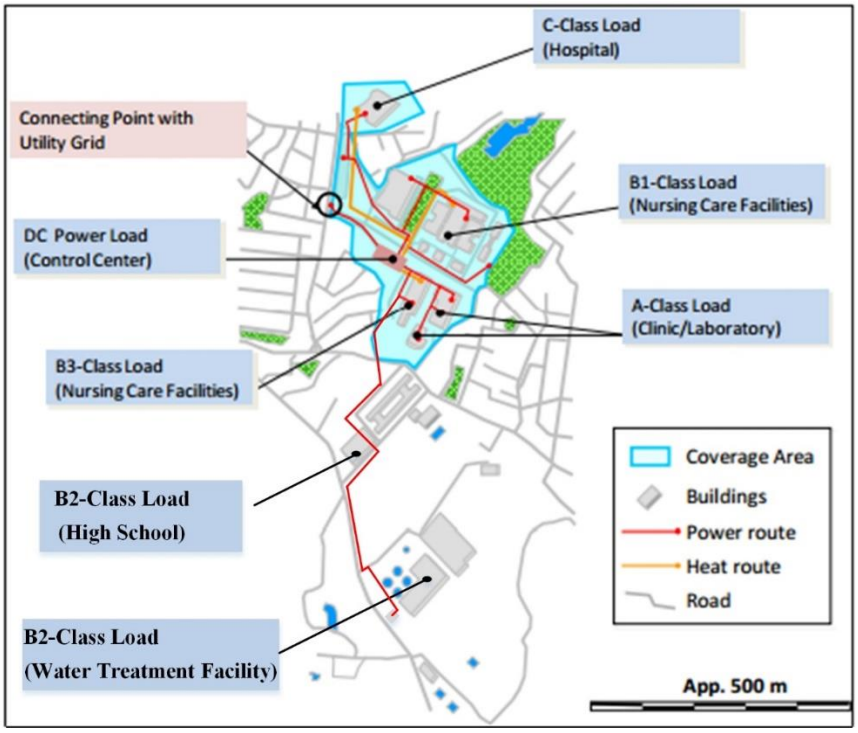

Fig. 3-5 Supply area of the Sendai Microgrid

Table 3-3 Power Quality Classes

Class	Service object
DC Power	Energy center
A	MRI of clinic， Server of the laboratory
B2	High school and water treatment facility
B1、B3	Nursing care facilities
C	Hospital

* Power supply to B2-Class was suspended after completion of the demonstration project

(2) Integrated power supply system

In Fig. 3-4, DC power and the loads of A and B1 classes are supplied via an Integrated Power Supply (IPS), configured with four types of bidirectional converters: high-quality inverter, DC-DC converter, PV connected converter, and a valve-regulated LA battery as an emergency backup, enabling the supply of high quality power. Fig. 3-6 illustrates the internal structure of IPS, the LA battery can offer 30 minutes of backup power and restrain voltage and frequency fluctuations resulting from loads changes and PV output through active and reactive power control of the bidirectional converter. Moreover, the MG also includes a “back-to-back” system to ensure that

any voltage dips are of small depth and short duration. Most voltage dips last less than 100 ms during normal system operation [6].

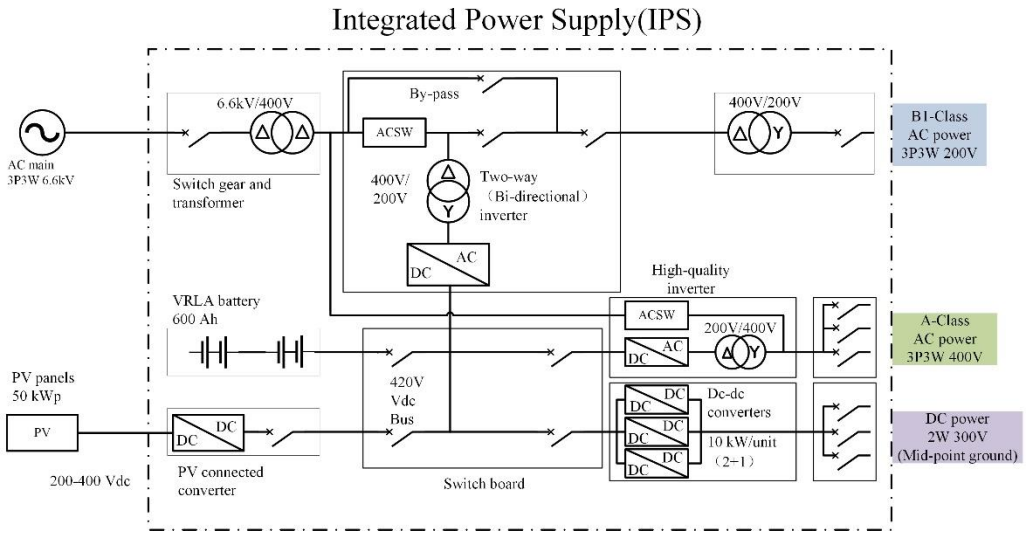

Fig. 3-6 IPS structure [5]

3.2.3 Social and Economic Benefits

The Sendai Microgrid successfully realized the islanding and provided continuing power and heat supply for the critical loads of the hospital during the two days of regional power grid blackout caused by GEJE, showing that the MG not only has application value in improving the utilization rate of renewable energy and creating new business models for power generation and distribution, but also has incomparable advantages in terms of reliable power supply for critical loads in case of disaster. The experience learned from the Sendai Microgrid has many implications for the future design, siting, and construction of MGs.

Moreover, Sendai Microgrid also proves the importance for multi-energy integration. Equipped with various forms of energy, such as gas turbine, PV, battery storage, fuel cell, *etc*., the MG is able to support the critical loads by the backup battery and PV when the gas turbine is out of operation due to abnormal voltage at the early stage of the earthquake, and then restore the power supply for other loads through the gas turbine when the state-of-charge of the battery is low.

Furthermore, a long-term operation data shows that the Sendai Microgrid could reduce energy costs by 14-30%, reduce equipment space by 23-42%, and reduce the CO_2 emission by 12% when

compared with a baseline of 15 years of cost and performance data, and the electrical loss is close to or slightly decreased compared to the pre-existing system [6].

3.3 “Solar-Diesel-Energy Storage” Integrated MEMGs in Maldives.

3.3.1 Project Overview

The Maldives consists of 1,192 coral islands grouped in a double chain of 26 atolls, along the north-south direction, spread over roughly 90,000 square km (35,000 sq mi), making this one of the world's most dispersed countries. Among the numerous islands, nearly 200 of them are inhabited. Due to the limited geographical conditions and economic development level, it is hard for the Republican Government to establish a unified power grid for power supply. As a result, most islands are basically powered by diesel generators, facing with high pressure of fuel cost. It is estimated that the average cost of diesel power generation in Maldives has reached about $0.3/kWh. Although the government of Maldives has repeatedly raised the electricity price for residents, it still cannot make up for the high generation cost. The average daily loss of state power company of Maldives is about $25,000 USD. Moreover, serious CO_2 emissions brought by the diesel power generation increases the risks of global warming and sea level rise, which is a huge disaster for Maldives, the country with lowest altitude in the world. Therefore, developing the renewable based power generation becomes the inevitable choice of Maldives government, who has jointed the project of "assisting low income countries to upgrade new energy" led by the United Nations. With the support of the World Bank and the Asian Development Bank, Maldives has invested approximately $138 million USD in the five years from 2013 to 2017 for the development of renewable energy.

Maldives has a good potential for solar resources development with an annual average of 5-5.5 kWh/m^2 of horizontal irradiation energy. However, the capacities of the diesel generators that were already installed in most islands are relative small due to low load level (Besides the capital, Male and some islands), thus the system frequency may fluctuate violently and even lose its stability with the severe fluctuations of PV generation due to low inertia. To this end, integrating the ESS with solar PV and diesel generators as MEMG becomes a feasible power supply solution for Maldives.

In cooperation with the Ministry of energy of the Republic of Maldives, Tianjin University and TrinaSolar, an equipment supplier in China, assisted the Maldives government to establish 14 “Solar-Diesel-Energy Storage” integrated MEMG in islands. The Solar PV was installed on the roof of the school and power house of each islands, the diesel generators as well as the EMS was assigned inside the power house, and the energy storage was integrated within a container outdoors. Fig. 3-7 gives the system structure of the MG. Each MG is equipped with a number of diesel generators with different capacities. The customized EMS is able to optimize the unit commitment scheme according to the real time monitoring of load consumption and PV generation, and reduce the fuel consumption. Table 3-4 summarizes the load and sources configuration in each island. Fig. 3-8 shows the project picture of some islands. Up to now, 10 MG projects have been put into operation.

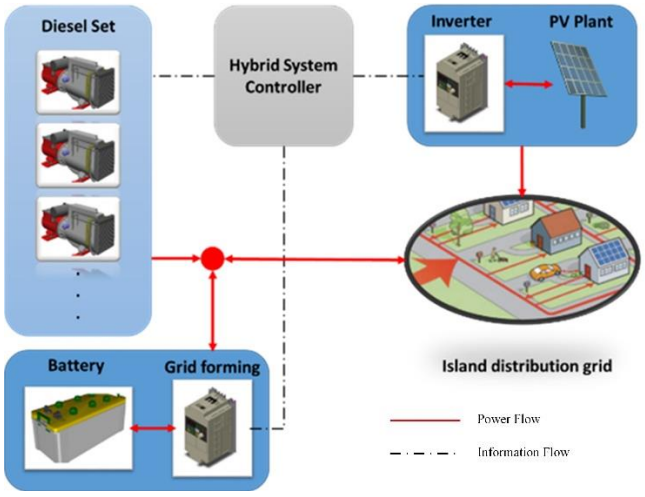

Fig. 3-7 “Solar-Diesel-Energy Storage” integrated MEMG structure

Fig. 3-8 “Solar-Diesel-Energy Storage” integrated MEMG in Maldives

Table 3-4 load and sources configuration of the project

Island	Measured load in 2016/kW (peak, average)	Forecast load in 2022 /kW (peak, average)	Solar PV / kWp (STC)	Energy storage (capacity, rated power)	Diesel generators /kW
Thuraakunu	80,70	100,87	100	60kWh,100 kW	50,128,160
Uligamu	79,60	98,75	126	240 kWh,100 kW	80,128,165
Molhadhoo	48,29	57,35	60	120 kWh,100 kW	50,48,60
Hoarafushi	400,340	540,459	330	150 kWh,300 kW	350,250,600
Ihavandhoo	383,331	513,443	320	150 kWh,300 kW	250,450,350
Kelaa	260,165	338,215	200	100 kWh,200 kW	120,200,236
Vashafaru	70,52	81,43	120	240 kWh,100 kW	60,80,80
Dhidhdhoo	712,540	960,729	246	150 kWh,300 kW	500,800,600
Filladhoo	90,71	112,88	140	280 kWh,100 kW	70,80,160

Island	Measured load in 2016/kW (peak, average)	Forecast load in 2022 /kW (peak, average)	Solar PV / kWp (STC)	Energy storage (capacity, rated power)	Diesel generators /kW
Maarandhoo	85,66	95,75	142	280 kWh,100 kW	60,90,160
Thakandhoo	56,36	64,41	91	180 kWh,100 kW	60,70,58
Utheemu	115,82	132,94	150	280 kWh,120 kW	100,80,160
Muraidhoo	90,53	100,60	139	240 kWh,100 kW	60,80,150
Baarah	140,128	180,160	162	70 kWh,120 kW	90,60,120

3.3.2 Key Technologies

(1) Customized energy management system

The goal of building MEMGs is to maximize the utilization rate of renewable energy on the basic of ensuring superior power quality and power supply reliability to the residents of the islands, so as to reduce the high power generation cost of the state power company of Maldives. However, it comes to a contradiction that the economic benefit from PV generation is accompanied by the increasing risk of operational reliability due to the intermittent nature of PV. This means a real-time monitoring and control system are therefore required to effectively dispatch and coordinate the PV, ESS, and diesel generators.

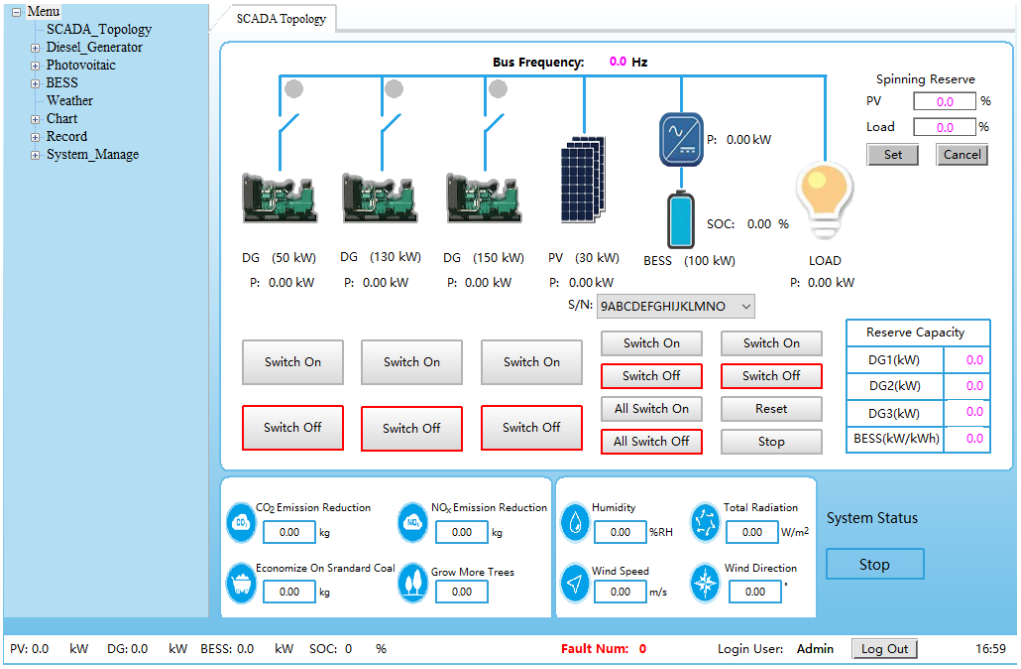

Fig. 3-9 HMI of *i*-MEMS

For part of the islands listed in Table 3-4, such as Uligamu, Molhadhoo, Vashafaru, Filladhoo, Maarandhoo, Thakandhoo, Utheemu, Muraidhoo, and Baarah, the load level is relatively low. From the perspective of economy, the electrical demand can be mostly supplied by PV generation with the coordination of ESS with high storage capacity (compared with the load). For these islands (defined as Type C), the ESS can store the surplus PV generation and discharge it to meet the load demand when the PV generation is insufficient, so as to avoid turning on the diesel generators and achieve the goal of minimizing diesel consumption. For the other islands (defined as Type B), as the load is relatively large, it is uneconomical to allocate large capacity energy storage. The primary goal of energy storage in these islands is to provide instantaneous and fast power support and suppress the impact of PV fluctuations on diesel generators, thus Type B islands are equipped with PCS with higher rated power, which allows the energy storage battery to operate at a higher charging and discharging rate.

Tianjin University assisted in the completion of the EMS for the island MGs (*i*-MEMS), which integrates the functions of operation control and energy management, real-time monitoring and data storage, and human machine interface (HMI), *etc*. *i*-MEMS can provide customized energy management strategy according to the capacity of DERs and load level. Fig. 3-9 presents the HMI of *i*-MEMS.

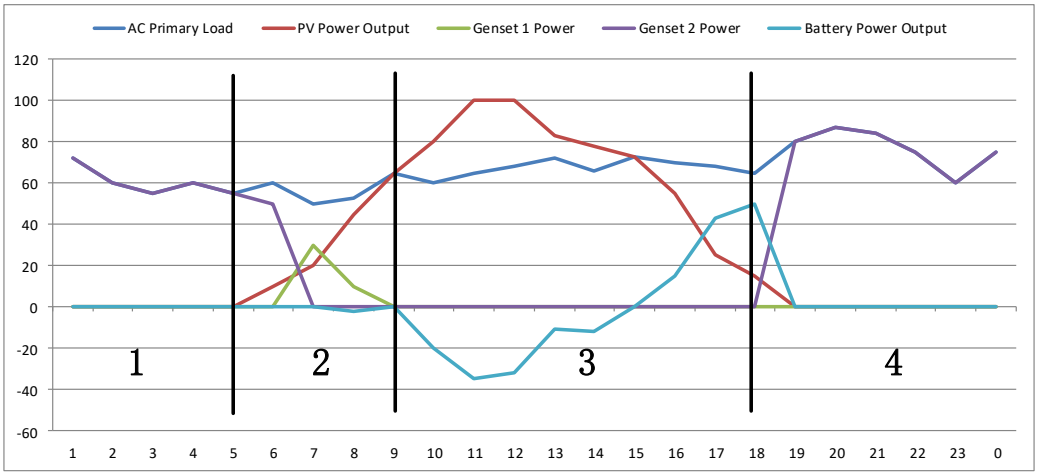

Fig. 3-10 Typical operation strategy for Type C islands

The typical operation strategy for Type C islands can be seen in Fig. 3-10, with the following scenarios:

- Region 1: the loads are supplied by #2 diesel generator at night;
- Region 2: the output of #2 diesel generator reduces along with the increase of PV generation and is replaced by #1 diesel generator with a smaller capacity when the output is lower than its minimum load rate. Then the output of #1 diesel generator reaches to its lower limit as well and the system is transferred to "Solar-Energy storage" mode seamlessly without any diesel generators by *i*-MEMS;
- Region 3: the MG is operating in a most economic manner with the ESS as the main source to support the voltage and frequency. The surplus PV power is absorbed by energy storage automatically. Then, the stored energy is released to supply the loads after the PV generation is less than the load demands;
- Region 4: the #2 diesel generator is restarted when the state-of-charge of the battery is lower than a preset threshold, e.g. 20%. It is uneconomical to charge the battery by diesel generator unless the state-of-charge is further reduced to a certain degree, e.g. 10%.

Fig. 3-11 demonstrates the typical operation strategy for Type B islands, including:

- Region 1: the loads are supplied by #1 diesel generator at night;
- Region 2: the output of #1 diesel generator reduces along with the increase of PV generation, and the battery is charged to stabilize the output power of the #1 diesel generator at the minimum load rate. The PV power may be curtailed if the state-of-charge of the battery exceeds the upper limit, e.g. 90%. With the gradual reduction of PV output, the battery storage is discharged to reduce the fuel consumption until the state-of-charge is reduced to the lower limit;
- Region 4: The #2 diesel generator is turned on to take over the loads as the peak load at night is higher than the rated power of #1 diesel generator.

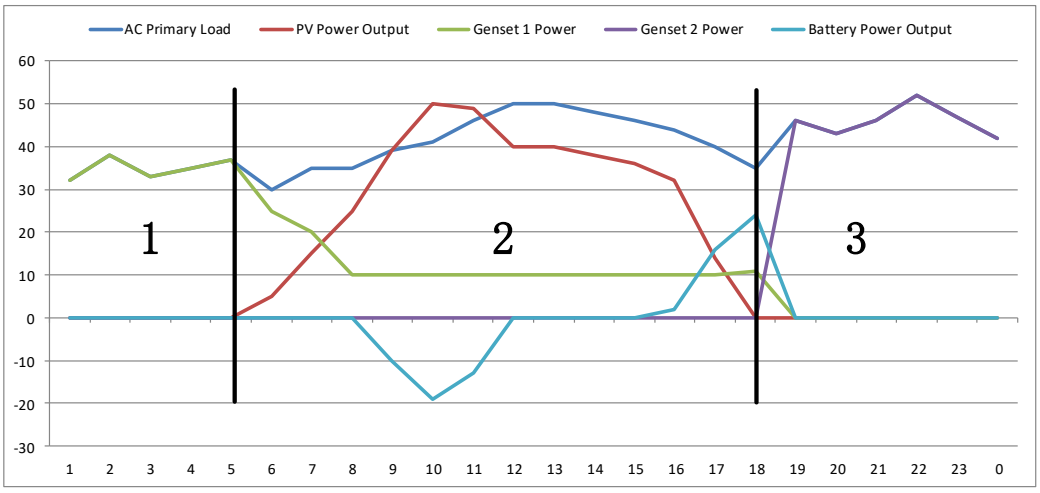

Fig. 3-11 Typical operation strategy for Type B islands

(2) Fast power tracking technology

To provide the power supply with high power quality and reliability for the islanded MG, energy storage must be able to quickly track the fluctuation of PV power. A frequency vs power droop controller is integrated into the PCS of the ESS to realize this objective, which is able to response to the frequency fluctuation within 200 ms based on local measurement.

3.3.3 Social and Economic Benefits

Since the project was put into operation, the power generation cost and fuel consumption of the islands have been greatly reduced according to the long term operation monitoring data. Compared with the “diesel-only” system, the fuel consumption of Type C islands is reduced by nearly 50%, and about 28% for Type B islands. The average power generation cost is reduced from $0.3/kWh USD to $0.2/kWh USD, and is close to $0.1/kWh USD under the “Solar-Energy storage” mode.

As a country with tourism as its pillar industry of national economy, developing low-carbon tourism is of great significance to Maldives. The clean and low-carbon energy system constructed by this project is benefit to help Maldives to realize the goal of becoming a "carbon neutral" country by 2020. The experience and achievements of the project can be further extended to other islands in Maldives and even more standalone MG projects of other countries in the world, so as to promote the development of MG.

3.4 Smart Integrated Energy Microgrid in Customer Service Center of State Grid Corporation of China

3.4.1 Project Overview

This project winned APEC ESCI Best Practices Awards: 2019 Silver Award of Smart Grid [7].

Customer Service Center (CSC) is responsible for providing online customer services for the service area of State Grid Corporation of China (SGCC), which covers 26 provinces and affects over 1.1 billion people. It provides a 24-hour all year service for individual and enterprise users including blackout notice, customer information inquiries, business consultation, and business processing. CSC has two parks, the Northern Customer Service Center (NCSC) and Southern Customer Service Center (SCSC). NCSC, located in Tianjin, was completed and put into use in 2015, which includes one monitoring building, two call buildings, two public service buildings and five staff dormitory buildings and can accommodate 3,000 staff to provide business consultation, failure reporting and suggestion services for users in 13 provinces. SCSC, located in Nanjing, has a total construction area of 136,000 square meters, and can accommodate 2,200 employees' working and living. As a result of high population density and working schedule, the variety and high level of energy demands pose new challenges for energy supply solutions of electricity, heat, cooling, and hot water. Thus, a Smart Integrated Energy Microgrid (SIEM) is built in CSC. The energy facilities of SIEM include GSHP, ice-storage system, electric boiler with HS, solar water heating system, PV system, and electric distribution networks. The capacities of energy subsystems are given in Table 3-5.

Moreover, a control and energy management platform is developed to realize the intelligent coordinated dispatching of SIEM. The various demand of the park could be met with a lower operation cost and more environment-friendly way. Fig. 3-12 demonstrate the SIEM as well as the corresponding control and energy management platforms of NSCS and SCSC.

The pilot project, SIEM in NCSC of Tianjin, has received the title of "the First APSEC International Training Base". The project is open to the public and receives 4,000 visitors per year from government, enterprises, and academics. It has played an outstanding publicity role in promoting the concept of energy consumption and the new technology of energy utilization. As a

representative of the smart energy project, SIEM was exhibited in the “Great Change” exhibition held at the National Museum and was well received by the public.

(a) Overview of NCSC (b) Control and energy management platform of NCSC

(c) Overview of SCSC (d) Control and energy management platform of SCSC

Fig. 3-12 SIEM in CSC

Table 3-5 Capacities of energy subsystems

Energy subsystem	SCSC	NCSC
PV system	1,009 kWp	823 kWp
GSHP	Cooling: 4,900 kW Heating: 4,922 kW	Cooling: 3,690 kW Heating: 4,065 kW
Solar water heating system	1,411 kW	1007 kW
Solar air conditioning system	/	Cooling: 350 kW Heating: 210 kW
Wind power generation system	80kW	/
Air source heat pump	1,932 kW	216 kW
Ice storage system	Icing: 7,737 kW Cooling: 5,416 kW	Icing: 6,328 kW Cooling: 4,680 kW
Electric boiler with heat storage	6,568 kW	8,200 kW
MG with ESS	50 kW*4 h	50 kW*4 h
Electric cooling system	2,461 kW	6,328 kW

3.4.2 Key Technologies

The innovative ideas and technologies of SIEM are that each kind of energy is coupled with electricity, the latter is the core of the energy production, conversion, storage, and consumption.

A series of novel methods, including the modeling, planning, energy management, evaluation of the multi-energy system, are proposed.

(1) Energy bus

The concept of "energy bus" on system modeling is proposed (as shown in Fig. 3-13). The energy relationship among all equipment in SIEM can be accurately expressed and calculated, which facilitates the standardization and scalability of energy system modeling and analysis. The relationship of energy transfer can be accurately expressed and the dimension of the system model is lower and solving efficiency can be improved via the energy bus-based modeling technology.

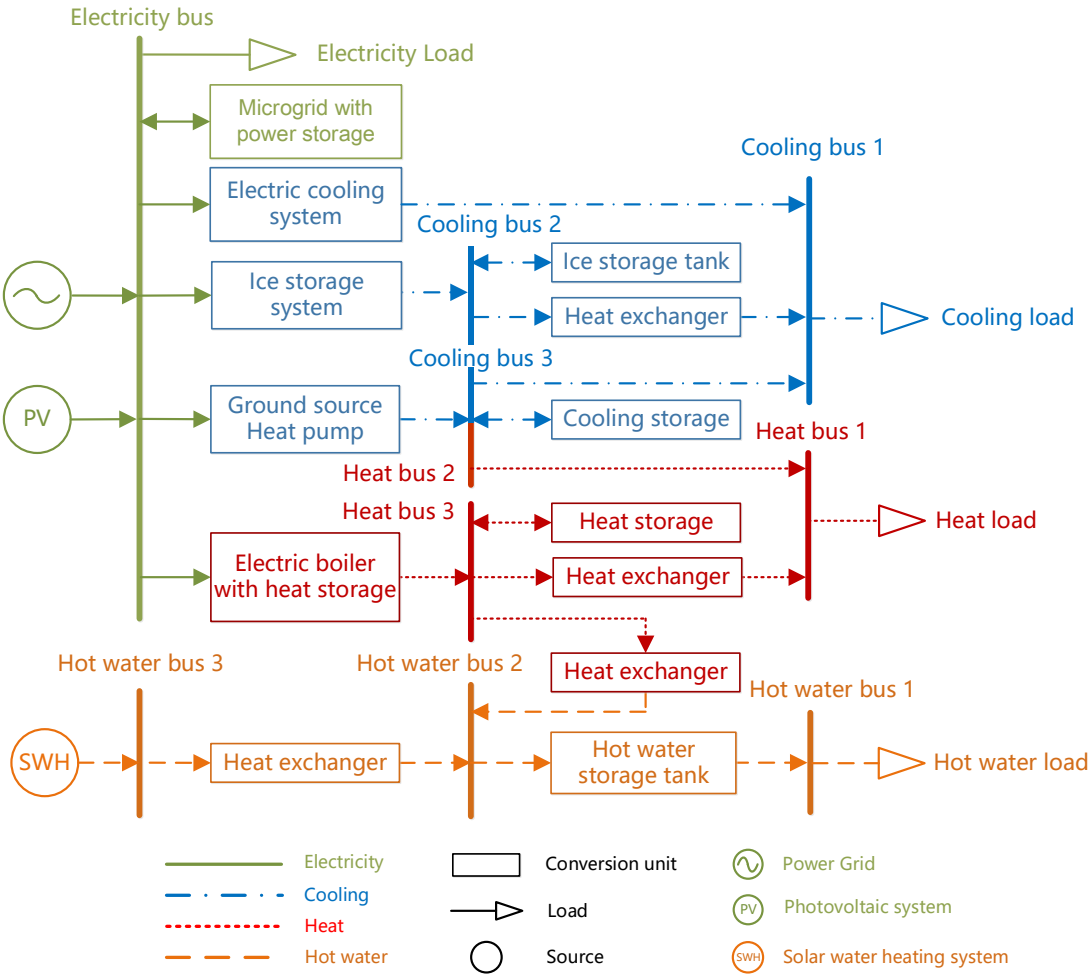

Fig. 3-13 Energy Bus Structure of SIEM

(2) Planning tool for SIEM

A planning tool for SIEM is developed to realize the standardized modeling and optimal siting and sizing of the energy equipment in SIEM. It can provide optimized energy supply solutions for various situations with multi-energy demand.

(3) Coordinated operation of SIEM

The brain of SIEM, a control and energy management platform, is proposed and constructed to realize the intelligent coordinated dispatching of SIEM. The control and energy management platform can effectively coordinate and optimize the production, transmission, distribution, storage, and consumption of the involved energies. The physical structure of the platform is shown in Fig. 3-14.

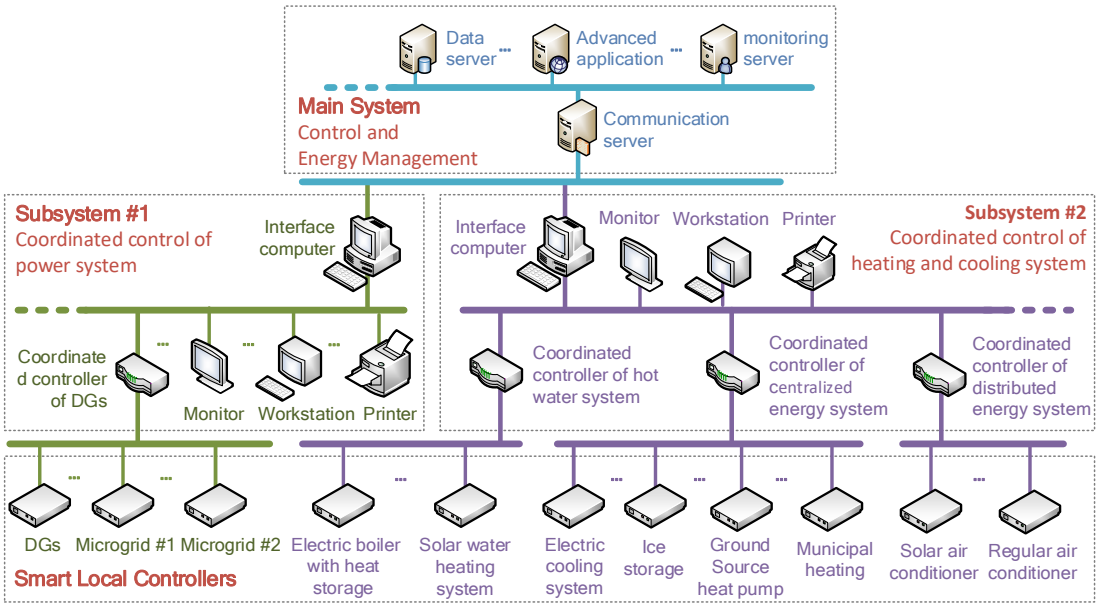

Fig. 3-14 Structure of control and energy management platform of SIEM

This work has been applied and tested in CSC. The pilot project shows that the new concept and technologies can effectively increase the penetration of renewable energy in customer side energy consumption and the energy efficiency through coordination and optimization.

(4) Evaluation for SIEM

To evaluate the performance of SIEM, evaluation indexes and method are proposed. Regional indexes are macro-indexes used to access the performance in system level, the detailed indexes are shown in Table 3-6. The other indexes including subsystem, equipment, and environment are used

as micro-indexes to compare different aspects of the system. With these indexes, the comprehensive and objective evaluation of energy system can be realized.

Table 3-6 Regional Indexes of SIEM

Indexes	Abbreviation	Description	Formula
Rate of integration	ROI	The level of integration and utilization of multi-energy resources.	ROI=(number of integrated energy subsystem/ total number of energy subsystem)*100%
Ratio of self-sufficiency	ROS	The balance of the energy supply and consumption in the system.	ROS=(1-purchased energy/ total energy consumption)*100%
Coefficient of performance	COP	The efficiency of energy conversion of cooling and heat.	COP=average power output/ average electric power consumption
Penetration of renewable energy	POR	The usage level of renewable energy in the system.	POR=(renewable energy utilization/ total energy consumption)*100%
Ratio of peak-valley difference	ROP	The ability of peak load shifting of the energy system.	ROP=energy used in peak power / energy used in valley power
Ratio of electric power alternative	ROE	The proportion of electric power in total energy.	ROE=(energy used in electric power /total energy consumption)*100%

3.4.3 Social and Economic Benefits

(1) Investment benefit analysis

- **Construction investment**

The energy facilities of this project include GSHP, ice storage system, electric boiler with HS, solar water heating system, PV system, and electric distribution networks. The total construction investment is 187.02 million CNY. If conventional energy supply scheme is adopted, the construction investment of municipal heating, chiller units, electric heating system and electric distribution networks is 126.64 million CNY. Therefore, the construction investment of SIEM is 60.38 million higher than conventional energy supply scheme.

- **The benefit of control and energy management platform**

The control and energy management platform can achieve realize precise control of the balance of energy supply and consumption, which is more accurate and efficient than the manual scheduling strategy. In the cooling season, the operating cost is 4.21 million CNY, which is 0.39 million CNY lower than the manual scheduling strategy of 4.6 million CNY, a decrease of 8.4%. In the heating season, the operation cost is 6.98 million CNY, which is 0.9 million CNY lower than the manual scheduling strategy of 7.88 million CNY, a decrease of 11.4%. In summary, the control and energy management platform can reduce the operating cost by 1.28 million CNY per year, with a decrease of 10.4%.

- **Operation cost**

The cost of annual energy purchase of SIEM is 10.07 million CNY, which is only the cost of electricity supply, as a result of the heating is completely covered by the system. The operation and maintenance cost is 2.4 million CNY. The annual income of PV system is 2.24 million CNY. The annual benefit of the control and energy management platform is 1.28 million CNY. Thus, the total operation cost of SIEM is 8.95 million CNY per year. If conventional energy supply scheme is adopted, the annual energy purchase cost (including electricity and heating supply costs) is about 18.47 million CNY and the annual operation cost is 1.2 million CNY. The total operation cost is 19.67 million CNY per year. Therefore, the operation cost of SIEM is 10.72 million CNY lower than the conventional scheme every year.

In summary, comparing with the conventional energy supply scheme, the construction investment of SIEM is 60.38 million CNY higher, but the operation cost is 10.72 million CNY lower. As a result, the payback period for the increased construction investment is about 60.38/10.72=5.63 years.

(2) Environmental benefit analysis

This project realizes 100% electric power alternative in the park, using electricity as the core of energy conversation form to meet the multiple energy demands. Thus the emission reduction of GHG and air pollutants can be calculated by the amount of fossil fuel saved and renewable energy used.

From January 2016 to December 2018, the average penetration of renewable energy was higher than 32%, and the highest level was 64.17%. More than 80% of the cooling and heating was provided by renewable energy. PV power generation accounts for more than 5% of the total power consumption. The alternative power consumption of the project is 28,766.8 MWh, reducing about 7,824.6 tons of carbon dust, 28,680.5 tons of CO_2, 863 tons of SO_2 and 431.5 tons of NOx. The results show that the project is very environmental friendly and has a convincing illustration of energy saving and emission reduction.

(3) Application prospect analysis

The integrated energy solution proposed in this project is highly scalable and replicable. It can be applied in many scenarios such as towns, industrial parks, business districts, public facilities, and islands. Especially in APEC economies with rapid development of economic and social, the demand for clean, low-cost and high-efficiency energy systems is increasing. Thus, the related technologies of this project will have promising applications and can provide systematic solutions and technical support for the construction of other projects. For distance, the ideas and technologies proposed in this project have been applied in the energy system construction of Beijing-Tianjin Zhongguancun tech city, Beichen demonstration area, *etc*.

3.5 Hybrid AC/DC MG in Shangyu, Zhejiang Province, China

3.5.1 Project Overview

Shangyu Hybrid AC/DC MG demonstration project is the first project of commercial operation of AC/DC MG on the user side in China, which was completed and put into use in August 2017 with the support of "key technologies for high-density distributed energy access to AC-DC hybrid MG" project of China National High Tech Research and development plan (863). The project is led by State Grid Zhejiang Electric Power Co., Ltd, and jointly constructed by the Electric Power Research Institute of Zhejiang, Zhejiang University, Tianjin University, Beijing Sifang Automation Co., Ltd, and XJ Group Corporation, *etc*, with a total investment of 24.85 million CNY [8].

The implementation place of the project, Century Huatong Automobile Co., Ltd, is located in Shangyu economic development zone, Shaoxing city, which is one of the 14 industrial clusters in Zhejiang Province with multiple emerging industries. The production load is mainly plastic

injection moulding machine, which is a kind of high power motor with pre-stage AC-DC-AC variable frequency device. In addition, the plant has already installed 2.35 MW roof solar PV. Prior to the construction of the project, the plastic injection moulding machine needs to be connected to the AC system through the pre-stage AC-DC rectifier, and the PV generation is used by the user through an inverter, step up transformer and step-down transformer. To reduce the power conversion link and improve the energy utilization efficiency, the project adopts a hybrid AC/DC structure, as shown in Fig. 3-15. The AC side is divided into two sections of bus I and II, with rated voltage of 10 kV, which are connected by switch KG1; The DC side also contains two sections of bus I and II, connected by switch KG2, and the rated voltage is 560V. AC and DC grid are connected and controlled by three 250 kVA Power Flow Controllers (PFC) and a 250 kVA Power Electronic Transformer (PET). The plastic injection moulding machine (7*50 kW), the LED lamps (50 kW), and DC charging spots of electric vehicle (4*60 kW) are connected as DC loads. Besides that, the existing solar PV of 850 kW, two permanent magnet direct drive wind turbines of 5 kW, and a lead-carbon battery of 250 kW *4h are connected to DC bus. AC loads are connected to 400 V AC bus. The hybrid AC/DC MG can realize friendly interaction with the utility grid by controlling the power flow of PCC under normal circumstances, and is able to islanding in case of grid failure to provide continuous power supply to the critical loads.

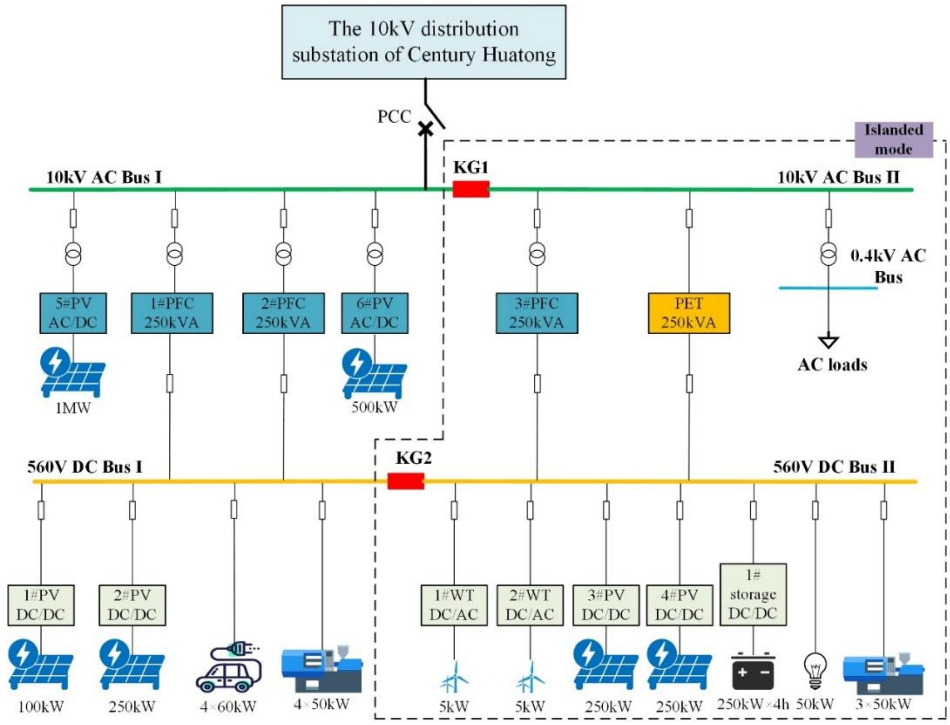

Fig. 3-15 Shangyu hybrid AC/DC MG configuration

Fig. 3-16 Part of the Shangyu hybrid AC/DC MG project

3.5.2 Key Technologies

(1) Flexible control with multiple operation modes

To fully display flexibility of operation mode of the hybrid AC/DC MG, and ensure continuous and highly reliable power supply in case of failures, the hybrid AC/DC MG is designed with four operation mode: “grid connection operation”, “DC bus II islanded”, “AC bus II islanded” and “islanding operation”. The operation mode switching between different modes is fast, reliable and smooth, and the relationship between the KG1 and KG1 states and the operation mode is illustrated in Fig. 3-17. In the first three operation modes, the system is connected with external distribution power network and the economic interest is the priority issue, but, in islanding operation mode, the system takes the high reliability of power supply as the main control target. To enhance the reliability and simplify the control logic for the hybrid AC/DC MG, DC voltage droop control is adopted for #1, #2 PFC and DC-DC converter of energy storage, and the #3 PFC works in a virtual synchronous machine control manner in this project, guaranteeing the “plug and play” nature for these key devices. The DC bus voltage is regulated both by #1, #2 PFC and DC-DC converter of ESS in grid connected operation mode, greatly enhanced the impact resistance of the system. In AC bus II islanded mode, automatic voltage and frequency stabilization is realized via the AC droop characteristics of #3 PFC. When KG1 and KG2 are both open, the DC bus II and AC bus II transfer to islanding operation to provide stable power supply for the critical loads. The PEC is used to dispatch the active and reactive power flow through AC and DC bus. Meanwhile, an appropriate algorithm is adopted to realize current sharing between three PFC and PEC.

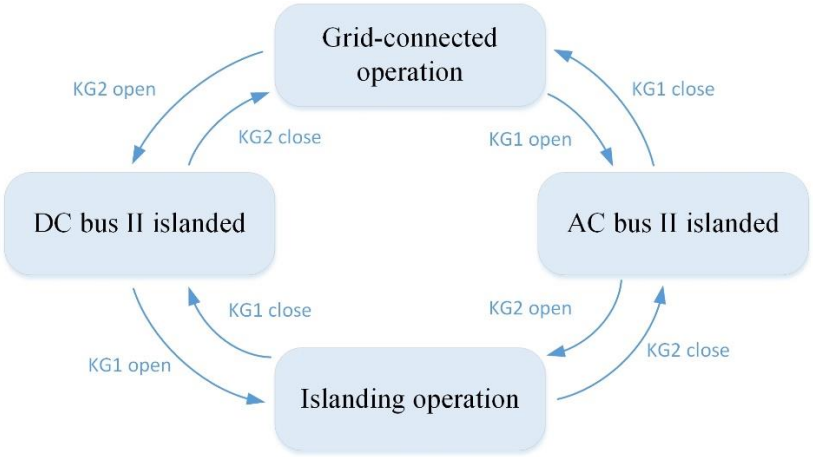

Fig. 3-17 Mode switching logic of hybrid AC/DC MG

(2) Power quality optimization

One of the objectives of the hybrid AC/DC MG is to provide superior power quality service under high penetration of wind turbines and solar PV. This project firstly created a robust autonomous control technology for DC bus voltage, the DC bus voltage sag is limited less than 5% via a nonlinear disturbance observer based DC bus voltage control method with feedforward compensation. The response speed for disturbance is greatly improved so that can provide superior power quality for the DC loads. Meanwhile, a unified power quality coordination controller has been developed with a hierarchical structure to realize the cooperative governance of the hybrid AC/DC MG, the DC voltage high frequency resonance, ripple disturbance, and AC harmonic can be effectively suppressed by the coordination controller.

3.5.3 Social and Economic Benefits

Shangyu hybrid AC/DC MG demonstration project provides a complete set of solution for AC/DC hybrid MG construction with high density access of distributed renewable energy, such as planning design, protection plan, operation control, and fault ride through (FRT) realization, *etc*. It has achieved great breakthroughs in the development and manufacturing of the core equipment of AC/DC hybrid MG and laid technical foundation and engineering experience of AC/DC MG development in China.

According to the on-site operation data from August 2017 to February 2019, the power supply reliability has increased from 99.9% to 99.99%. The comprehensive operation cost of the facilities has reduced by 6%. The project successfully improved the power quality for a certain degree, the THD, DC ripple, and DC voltage fluctuation rate were limited within 2%, 1%, and 2%, respectively.

3.6 Daxing Airport MEMG, Beijing, China

3.6.1 Project Overview

Daxing Airport, hailed as the first of the "new seven wonders of the world", was officially put into operation on September 25, 2019. The airport is constructed between Daxing District of Beijing and Langfang city of Hebei Province, and is famous for its grand scale and ingenious design. The total investment of the airport is up to 80 billion CNY, with a designed annual passenger throughput of 100 million people, and take-off and landing of 0.8 million aircrafts in the future.

Fig. 3-18 Top view of Daxing Airport

Fig. 3-19 DERs and charging station in Daxing Airport

As a key project, Daxing International Airport has been committed to the green construction concept of "resource conservation, environmental friendly, efficient operation and humanized service". To achieve this goal, a renewable energy-based multi-energy service system has been built, which utilizes the solar PV, shallow geothermal, sewage source heat, flue gas waste heat, and ESS *etc*. to provide about 12% of the total annual comprehensive energy consumption of the airport. The solar PV is installed mainly on the roof of parking building, freight area, and energy center with a rated capacity of 5.61 MWp (4 MWp in phase I), expected to generate 6.1 million

kWh per year. In addition, large scale PV collectors are considered to support the hot water demand of the airport. The GSHP project is located in the detention basin of Yongding River, and can extract 563,600 GJ of shallow geothermal energy every year, which is the largest GSHP project with multi-energy in China so far. The #1 energy station is equipped with two 7.9 MW GSHP units and five 6.9 MW flue gas recovery heat pumps. Four 435 kW sewage source heat pumps are installed in the sewage treatment plant of the airport to provide the cool and heat energy. Moreover, the airport plans to increase the proportion of clean energy vehicles in service vehicles, and a 129.5 kWh Lithium-ion battery system has been put into use for the charging stations.

3.6.2 Key Technologies

The core of MEMG of Daxing airport lies in a comprehensive application for different kind of energies, and fully considers their distinct features to integrate them into the system while coordinating and optimizing several kinds of energies. The subsystems of the MEMG include the PV power generation system, solar water heating system and GSHP system, all of which are coordinated organically to realize the goals of energy saving and emission reduction.

(1) **PV power generation system**: the PV power generation undertakes 1% of total energy consumption of the airport, and mainly takes advantage of office building roof to install PV panels. It is worth mentioning that the PV power generation system is also laid on the runway in the flight area, which is the first PV system around the runway of civil aviation system in China;

(2) **Solar water heating system:** it is estimated that the basic living and working hot water demand for nearly 20,000 staff at Daxing Airport exceeds 1,000 tons per day. Considering the huge traffic in the future, great energy consumption and pollution will occur under the conventional energy supply mode. Therefore, ensuring the hot water supply in a cleaner and energy saving way is also an important goal of the project. To this end, the project will create a total collector area of 13,152 square meters, and adopt innovative U-tube solar collectors and all glass vacuum tube solar collectors, so as to solve the large scale and highly concentrated hot water demand;

(3) **GSHP system:** the project integrates various technologies such as GSHP, boiler flue gas waste heat recovery, sewage source heat pump, *etc*., giving full play to the important role of

renewable energy recovery and energy conservation and emission reduction, and maximizing the energy supply area of the whole GSHP.

3.6.3 Social and Economic Benefits

The multi-energy system effectively unifies the social benefits of environmental protection and energy conservation with the economic benefits of reducing energy cost, and is benefit to making the Daxing airport as a global benchmark for green airports. It is estimated that the energy consumption of Beijing Daxing International Airport terminal is 20% lower than that of the airport terminal of the same scale, and the annual CO_2 emission can be reduced by 22,000 tons and save 8,850 tons of standard coal every year.

3.7 "Net-zero energy houses" MEMG in Canada

3.7.1 Project Overview

The EQuilibrium™ Housing Demonstration Initiative was launched by Canada Mortgage and Housing Corporation (CMHC) in 2006， which is aimed to design, construct and showcase healthy, resource efficient, affordable, net-zero energy houses (NZEH), defined as a house that consumes as much energy as it produces over a year.

The EQuilibrium™ projects have been demonstrated in Quebec, Ontario, Manitoba, Saskatchewan and Alberta. As the first NZEH, the ÉcoTerra™ house, shown in Fig. 3-20 is located on a 1.1 ha (2.7 acre) rural lot in Eastman, Quebec. The ÉcoTerra house is a two-story detached home with 234 $m^2$of heated floor area including the full basement, and a volume of 671 m^3. The house has a sophisticated home automation system with real-time graphic display and touch screen user interface that displays current indoor and outdoor conditions, and the operation of the various systems (PV electrical generation and supply to or from the grid, PV/T heat, and GSHP).

Fig. 3-20 ÉcoTerra™ house [9]

The building integrated PV system of the ÉcoTerra™ house includes 21 PV film sheets laminated to a standing-seam metal roof, with peak electrical output 3 kW. Moreover, a 10.6 kW (3 ton) two stage GSHP is used for both space heat and hot water. There is also a drain water heat recovery device for preheating hot water.

Residential energy consumption in cold climate areas, such as Quebec is primarily for space and domestic hot water (DHW) heating. In addition, the annual electrical loads include interior lighting, appliances and exterior use electrical equipment (e.g. exterior lighting and dryer). Table 3-7 shows data of this house's energy performance [10]: energy consumption (e.g. space heating, water heating, lighting, cooling, appliances and equipment) and carbon emission. Data of this building's energy performance were collected from December 2009 to December 2010. During this occupied year, the house had the net electricity use of 40.9 kWh/m^2/year. The overall net carbon emissions were estimated to be 818 gCO_2/m^2/year.

Table 3-7 Measured end-use energy and estimated carbon emissions of EcoTerra

End-use energy	Energy use data (kWh/m^2/year)	Source of energy	Carbon emission data (gCO_2/m^2/year)
Space heating	14.3	electricity	286
Water heating	6.6	electricity	132
Lighting	4.6	electricity	92
Cooling	0.5	electricity	10
Appliance	15.2	electricity	304
Other equipment	12.9	electricity	258

Solar electricity	-10.8	electricity	-216
Solar thermal	-2.4	electricity	-48
Total	40.9	electricity	818

3.7.2 Key Technologies

(1) Building-integrated PV System/Thermal System

The building-integrated PV system is combined with thermal recovery (BIPV/T) on the roof of the ÉcoTerra™ house (as shown in Fig. 3-21). The BIPV/T system is an on-grid application accompanied with an inverter for the AC/DC conversion, which allows to sell the locally generated electricity surpluses to the grid. Compared to the stand-alone PV arrays or solar thermal collectors, the BIPV/T system can generate both thermal and electrical energy simultaneously on one complete surface.

The BIPV/T system uses an air drawn beneath the metal roof to cool the PV sheets for increasing the PV efficiency. The solar-heated air from the BIPV/T roof is brought via an insulated duct with a variable speed fan to the mechanical room in the basement where it is used for the following three applications in order of priority: for clothes drying (running the dryer in fan mode), DHW heating through an air water heat exchanger, or heating a hollow core floor slab. The airflow rate in the BIPV/T system can be controlled to achieve the desired temperature. The BIPV/T system installed in the ÉcoTerra house has the capacity to produce up to 12 kW of heat at 14 m^3/min of air flow.

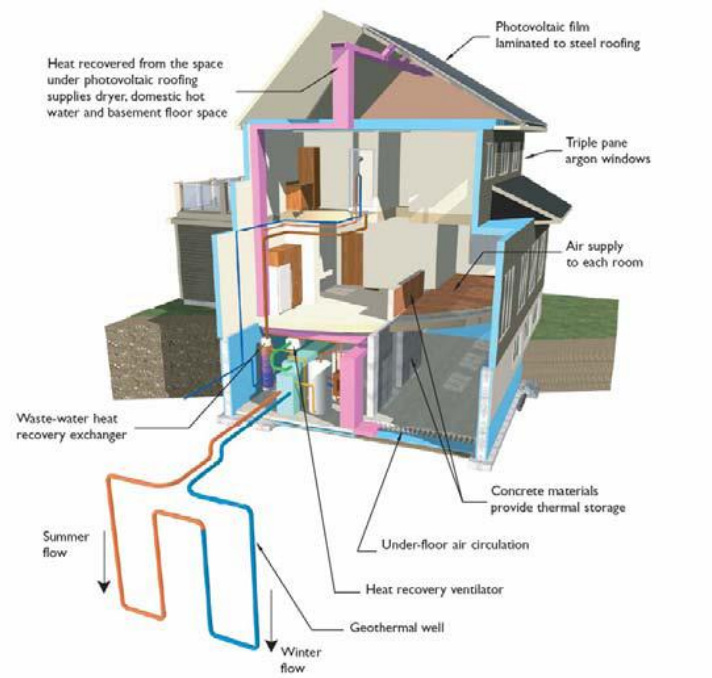

Fig. 3-21 The BIPV/T system of ÉcoTerra™ house [11]

(2) Two Stage Geothermal Heat Pump

The ÉcoTerra house is heated or cooled by a two-stage geothermal heat pump with environmentally-friendly refrigerant. The geothermal heat pump can assist both space heating with a ducted forced air system, and watering heating with a desuperheater. It is expected to reduce the energy consumption related to water heating by approximately 700 kWh/yr. In addition, the system lifespan is over 20 years [12].

In the basement of ÉcoTerra house, there is a multifunctional space and machine room with all mechanical equipment, including the geothermal heat pump, BIPV/T fan, electricity distribution panel, heat recovery system and heat exchanger. The house is also designed to use the heat released from the machines to supplement space heating by letting the warm air circulate through the open staircase driven by stack effect.

3.7.3 Social and Economic Benefits

The EcoTerra home was commissioned in early 2009 and occupied in August 2009. The house combines energy efficient construction techniques and RES to achieve Canada's energy efficient guide for house rating in excess of 98 points. As a successful net zero-energy healthy house project, the ÉcoTerra house won the Canadian federal government's Equilibrium sustainable

housing competition. The BIPV/T system achieved a thermal efficiency of 20%. Although EcoTerra did not realize net-zero energy consumption, it was reported to have consumed only 12.4% of the energy of a typical Canadian home.

Chapter 4 Establishment of Cloud-based Sharing Platform of MEMGs

4.1 Background and Activities

As mentioned in the previous sections, worldwide has significant concern regarding the GHG reduction, and in general energy de-carbonization, as well as the contribution to the rollout of renewables without compromising on the reliability, flexibility as well as resilience of the grid. MEMGs can satisfy all the energy requirements in a most effective way for coupling integrated supply of energy, even for rural areas or places with extreme weather conditions.

Therefore, MEMGs have been considered as an effective approach to mitigate the potentially impacts brought by the various types of intermittent renewables, in particular to provide clean, reliable and affordable energy to remote, rural and developing areas. However, the planning, operation and control of such a system with the integration of multiple energy resources including non-dispatchable renewable energy is a challenging task due to the fluctuations in demand and coupling effects between multiple energy sources while maintaining economic optimization goals and achieving carbon footprint minimization. The emerging technologies in MEMGs also constitute a major societal challenge, one that will encourage technology, data and standard sharing opportunities among scholars, practitioners as well as policy makers.

The MG research team in Tianjin University has motivated by the challenges and consequently established a Microgrid Cloud based Sharing Platform (M-CSP) to grow the research community and enhance the capability in the planning, operation and management of MGs worldwide, in particular for APEC economies, which can facilitate the goal of doubling the share of renewables in the APEC energy mix from 2010 level by 2030. The following activities have been taken.

(1) Develop a cloud based sharing platform of MGs enabling data sharing, case demonstration, technical exchange, personnel training, and academic collaborations among APEC economies.

The project team of Tianjin University developed the cloud based sharing platform of MGs and built the website for partners access, the website address is http://www.cm2energy.com/. The platform provides 5-dimensional cloud based information sharing among partners, including raw

data; formatted cases for research; real-time energy management system for multi-energy MGs; fundamental and advanced optimization and control tools, consequently support the research community and enhance the capability in planning, operation and management of MGs for APEC economies. The raw data obtained by the platform is processed to form typical case study systems of MEMGs and to provide formatted data sets (e.g. DG data, energy demand), which can be used directly for research purpose. Useful tools such as planning, energy management are provided for a better MG design, monitoring, operation and visualization. The visualization of the system operation and performance are shared among partners. Partners are voluntarily sharing their own fundamental tools and source codes, as well as the optimization and control tools on the cloud platform. Currently, the connected partners are around the world include universities, research institutes and utilities, for instance, Tohoku Gakuin University in Japan, Qatar Environment and Energy Research Institute, State Grid Tianjin Electric Power Co. in China and Warwick University in the UK *etc*.

(2) Develop MG technologies and policy recommendations on eliminating gaps in ability of promoting MGs among APEC economies, and building closer partnership between developed and developing economies on MGs.

With the support of the cloud based MEMG platform, as well as the DG and MG lab facilities in Tianjin University, research has been carried out to develop MG related technologies. For MG planning, a two-stage optimal design model of MGs was established, which employs two modules to integrate optimizations of design and operation, respectively[1]; a multi-stage scheduling strategy for resilience enhancement was adopted in which thermal storage serves as emergency response resources[2]; an energy storage capacity optimization algorithm was presented for MEMGs[3]; an electric vehicle fast charging station planning with associate charging pricing schemes are determined considering the stations' income and the users' response to the pricing signal[4]; a reliability assessment approach for MEMGs using hierarchical decoupling optimization framework and impact increment based state enumeration method *etc*[5]. For MG operation and control, a MPC based robust scheduling strategy was utilized to maintain the flexibility for enhancing the uncertainty adaptability[6]; an optimal DERs scheduling strategy for a smart building MG was developed considering uncertainties[7]; a two-stage multi-objective

scheduling method for multi-energy system was proposed with multi-attribute characteristics of scheduling schemes and the uncertainties of decision makers[8]; an operation and planning method integrating renewable energy generation and thermal load control for MG was developed considering not only comfort levels but also fairness of customers *etc* [9]. For MG economics, game theory-based smart energy trading approach between DNO and multi-MGs was proposed under different market pricing scheme [10]; an optimal charging scheme for aggregated electric vehicles is delivered [11]; techno-economic evaluation for AC/DC hybrid system is given to achieve economic benefit maximization [12].

The project team of Tianjin University has been highly involved in the standard and policy recommendations in multi-energy MGs. For instance, the 'IEEE 2030.9-2019 IEEE Recommended Practice for the Planning and Design of the Microgrids'; 'GB/T51341-2018 Technical Requirements for Connecting Microgrid to Power System'; 'GB/T 36274-2018 Technical Specification for Energy Management System of Microgrids'; 'T/CEC 147-2018 Operation and Control Specification for Microgrids Connected to Distribution Network'; *etc*. The standards and recommendations delivered have considered various types of MGs with different operation modes,

(3) To increase members' general knowledge in new opportunities and challenges of MG technology applications and innovations by building a cloud based sharing platform.

The project team of Tianjin University utilizes the extensive research and demonstration experiences to bridge the gap of MG associate technologies in planning, operation, and management in a collaborative and sustainable way. During the project, a workshop regarding the MG planning and energy management tools was organized, several speeches were given on a numbers of international symposiums to promote innovative and creative capabilities related to the cloud based multi-energy platform. Researchers for this project also have attended the workshop on "Promoting Resilience in Energy Sector" organized by the EWG09 2017A project. Taking the hands on experiences and suggestions from other APEC economies, relevant research on resilience of MEMGs have been conducted to against the disasters and severe attacks on energy systems. Joint research projects with US, Japan, Sweden, Australia, Canada and UK have been

carried out in this area, and more than 100 scientific papers, 3 international patents, as well as 8 books have been published.

Direct beneficiaries of this project are government policy makers, industrial partners, and technical practitioners, particularly in all APEC developing member economies, are primary target beneficiaries of the platform. These beneficiaries can participate the cloud based sharing platform of MGs, where data sharing, case demonstration, technical exchange, personnel training, and academic collaborations will be carried out in a collaborative way. The beneficiaries can directly get access to these resources online 24/7 to improve jointly innovative and creative capability on MEMGs.

4.2 Integration and Analysis

Currently, the entire M-CSP has been built, more than 10 MGs from universities, research institutes, and industrial parks with multi-energy resources have been connected as planned, including Qatar Environment and Energy Research Institute PV-storage Microgrid; Mälardalen University Microgrid Test Bench in Sweden; Northeast Electric Power University Microgrid in China; Tianjin-Singapore Eco-city Microgrid in China; Active distribution grid simulation system in China; Main energy center and Cryfield energy center in the UK; Hybrid PV-wind-Hydro-Battery Microgrid in Japan; and Tianjin Binhai Multi-Energy Microgrid in China, *etc*. The project team has provided technical support during the connection for all partners, and shared all the necessary tools with them as promised. On the other hand, with the project partner involvement, the platform has been fully tested, valuable data has been gathered for further research, therefore scientific papers, technical specifications and recommendations for policy have been achieved. And all tools, data, research outcomes can be used as training tools for helping APEC economies to promote technological progress of renewable energy and energy policy making, cultivating professional researchers, engineers and policy makers in the field of MEMG as well.

4.2.1 Requirements of Integration

The general requirement for connection to the platform is fairly simple, including the following aspects:

- Partner has a team to carry out the related R&D in MGs and integrated multi-energy systems, and allocates own funding (reserved for own funding, not transferring to other partner) for the research linked to the platform.
- Connects the MG to the M-CSP (desirable but not compulsory), shares data and R&D results, and be willing to collaborate to other partners.
- Actively involves the joint research and publications.
- Be willing to organize or takes part in organizing session(s) in conference and symposium, Special Issue in Journals.

The technical specification for connection to the platform are identified as follows:

(1) Provide MG Information

- Provide basic information of the MG, including equipment list, contact information *etc*.
- Provide main wiring graph of the MG, with the capacity of each facility labeled on the plate.
- Provide the list of monitoring (remote sign data and remote measure data) of each facility.

(2) Provide Data Transmitting Computer

- Provide a computer or an industrial computer on site.
- The operating system should be windows7 or later version.
- Minimum hardware configuration: CPU: 2.2Hz; memory: 2G; hard disk: 20G, network interface card: 100M.

(3) Provide Serial Device Server

- Partners are required to provide serial device server if their MGs need to transmit data through serial ports. Those customers whose MG data are transmitted by net interface are not required to provide the server.

(4) Network

- Connect data transmitting computer to the router (or provide wireless interface), which should be connected to the Internet, with an internet speed of 4M/s or above.
- Connect data transmitting computer to MG backstage.
- Connect serial device server to the MG through serial lines if needed.

(5) Cooperate in Joint Commissioning

- Cooperate in network commissioning.
- Cooperate in consistency check of data from the platform and the local MGs.

4.2.2 Analysis

Numbers of MEMGs have been fully connected on the M-CSP, as shown in Fig. 4-1, the scales of the connected MEMG varies from small scale lab testing facility to university size electricity/heating distribution MEMG. Real time monitoring data can be transmitted and saved remotely to carry out further case analysis, the instantaneous statistical analysis results are shown on the user interface. With the permission of the partners, the state estimation and energy management strategy recommendations are delivered to the operators, comprehensive assessments are given upon requests.

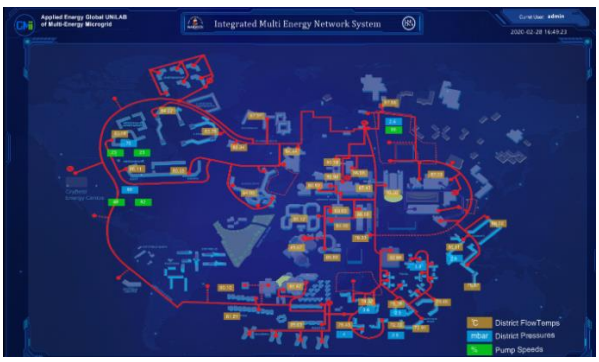

(a)

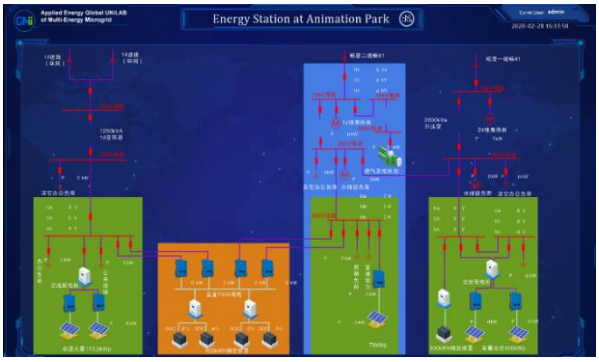

(b)

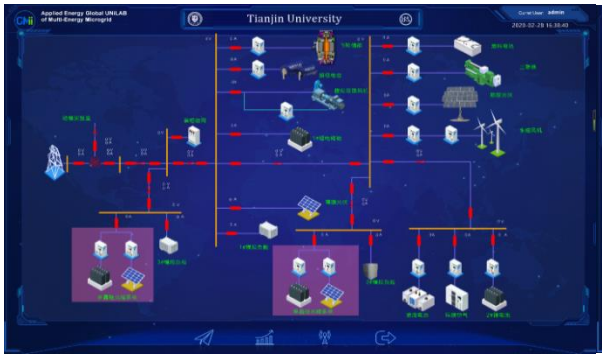

(c)

(d)

Fig. 4-1 Various types of MEMGs connected on M-CSP

(a) Monitoring of the heating distribution system of a university MEMG; (b) System topology with real-time data of the energy station of an industry park;(c) Medium scale lab MEMG with flexible topology; (d) Monitoring of a small scale lab MEMG

Taking Tianjin Binhai MEMG as an example, it is an industry park MEMG with PV: 600 kWp; CCHP: 120kW; battery: 450 kWh; GSHP: 135kW; HS tank: 875 kWh. The overall area of this MEMG is approximate 300,000 m^2, the physical layout and configuration of the system are shown in Fig. 4-2 and Fig. 4-3 for details. The user interface of the M-CSP is shown in Fig. 4-4. The feature of this MEMG is the utilization of the CCHP which can provide electricity, cooling and heating demand simultaneously, and the heat storage tank is employed to improve the overall economics of operation.

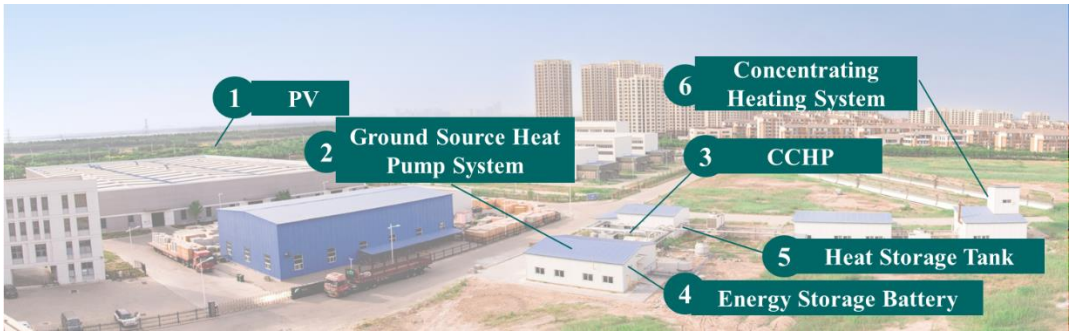

Fig. 4-2 The layout of Tianjin Binhai Multi-Energy Microgrid

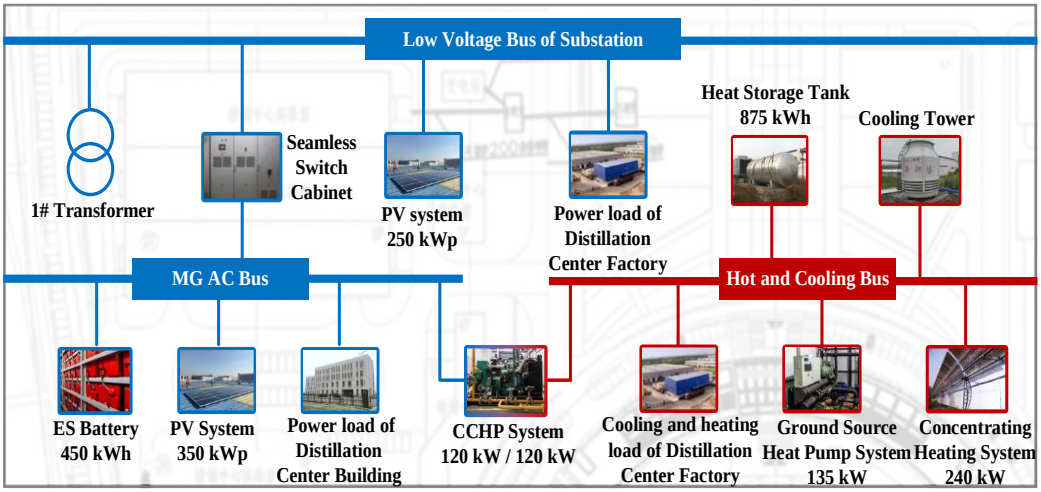

Fig. 4-3 The topology and configuration of Tianjin Binhai MEMG

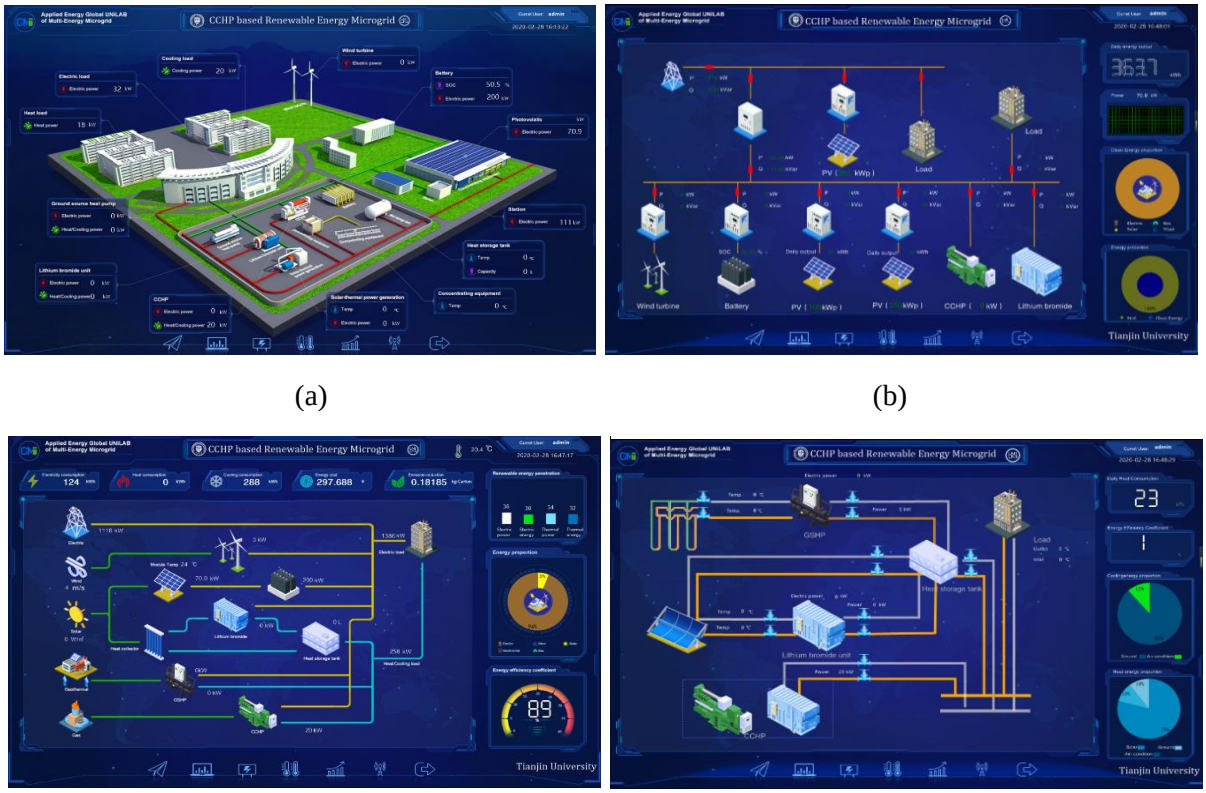

(a) (b)

(c) (d)

Fig. 4-4 Integration of Tianjin Binhai Multi-Energy Microgrid

(a) Overview of the MEMG; (b) System topology of the MEMG;(c) CCHP system of the MEMG; (d) Thermal distribution system topology of the MEMG

The owner of the MEMG has gained extensive knowledge and experiences on economic dispatching with target on overall cost minimization. According to the historical operation data gathered by the M-CSP, the overall penetration of the renewables within the MEMG has approached 65.17%.

4.3 Further Development

The M-CSP will continue to serve as not only a data sharing platform but a knowledge exchange center to help partners, as well as worldwide practitioners in the field of MEMGs to establish collaborations online and offline. The following activities will be arranged in the near future:

i. The research team of Tianjin University will continue to provide technical support and possible solutions for all potential partners to strengthen the connectivity of innovative

technologies, policy making and standard mutual recognition for APEC economies on MGs. The team will open for joint research opportunities for universities, industry and policy makers to promote key technologies and performance of MEMGs.

ii. With the existing connected MGs, the platform will work closely with all the partners to maximize the benefits, including the data analysis utilizing machine learning technologies, the tools improvement considering uncertainties, and to provide skilled workforce for the current global energy revolution.

iii. Further research will be carried out on technologies and policies in relevant fields, consequently promote technological progress of renewable energy and energy policy making in APEC region.

Chapter 5 Summary and Prospects

5.1 Summary

MEMG is a novel energy system that has multiple terminal resources and multiple distributed components for energy production, conversion, and storage within clearly defined boundaries. The autonomous system consists of energy management devices, distributed renewable energy sources, ESS, energy conversion devices, and variable loads. It can be treated as a controllable units of the energy Internet at the user terminal. Its flexible operation mode can reduce the energy consumption during transmission and realize the effective consumption of renewable energy sources.

The implementation of MEMG has brought various benefits to the energy system, for instance, to improve the accommodation capacity of DERs; to increase the energy efficiencies; to satisfy various types of demand in an economic approach; to provide customized intelligent services to customers; to offer emergency energy supply under severe circumstances; to support auxiliary services and black start to the grid. With the rapid development of MEMG worldwide, new challenges have been posed including technical issues related to MEMG planning, operation and management, various levels of legal and regulatory uncertainties, lack of internationally recognized standards and policies, as well as the inflexible utilities' pricing and incentive schemes. Therefore, scholars, practitioners as well as policy makers are eager to seek solutions in this particular field to enhance the capability in the planning, operation and management of MEMGs, to gain hands on experiences and real time data, to push the establishment of international standardization, and to constitute a social cognition that encourage active participation.

APEC economies comprises of the world's largest producers and consumers of energy, the major goal of APEC is to reduce energy intensity by at least 25% by 2030 and double the share of renewables in the APEC energy mix in 2030 via information and data exchanges, joint research and development, as well as open trade and investment.. The adoption of MEMG can certainly facilitate the progress, information and data sharing are key to bridge the knowledge gap between countries. With the support of APEC Energy Working Group, a cloud based sharing platform of MEMGs is established by Tianjin University to share the existing knowledge and techniques, to help fill the information gap and to inform how best to promote and accelerate MEMG adoption

in APEC economics by learning about how successful projects have been developed worldwide. In addition, drawing experiences and data from existing projects connected on the cloud based sharing platform throughout Japan, UK, Sweden, Middle East, China *etc*. help build a broader understanding of MEMG solutions and guide the industry about best practices for economic viability.

5.2 Prospects

In the near future, with the development of software and hardware technologies, maturity of power electronics and ESS, the MEMGs will no longer limited to lab and demonstration projects, widespread deployment with greater value in energy system will be expected.

From the equipment aspect, plug-and-play characteristics will be the key features to facilitate the integration of multiple types of energy resources, cost reduction will be the driver for smart equipment and emerging technologies. **From the systematic aspect**, the topology of the MEMGs will become complicated such as AC/DC hybrid architecture and MG clusters *etc*. A larger scale DER integration will be occurred at lower voltage level with coupling effects from various types of energy resources and demand, it will make the optimal operation, control and trading system become even difficult. On the other hand, MG clusters will play important role in auxiliary service market, peer-to-peer trading will become viable and promising. **From the user aspect**, MEMGs will further improve the end-use energy efficiency with customized energy supply on electricity, cooling/heating and gas. The improvement on energy marketing, regulation and bespoke incentives, the users will be encouraged to participate the energy market as prosumers with advanced DR techniques.

Therefore, the proposed cloud based sharing platform of MEMG will play important role for the future energy system. The knowledge, cases and data gathered from the platform will point out the strengths, weaknesses, opportunities and threats, will provide guidelines to the academia, industry and venders about best practices. Also, the platform will establish an effective approach to bridge the technical gap between countries/places remotely, and facilitate the nearby accommodation and high efficient utilization of clean and renewable energy even for people lack of experiences.

Reference

Chapter 1

[1] Ge S Y, Li J F, Liu H, *et al*. Research on operation–planning double-layer optimization design method for multi-energy microgrid considering reliability. Applied Sciences, 2018, 8(11): 2062.

[2] Gholizadeh N, Vahid-Pakdel M J, Mohammadi-ivatloo B, Enhancement of demand supply's security using power to gas technology in networked energy hubs. International Journal of Electrical Power & Energy Systems, 2019, 109: 83-94.

[3] Sun Y. Research on Integrated Multi-Energy System to Improve Energy Efficiency and Enhance Technological Progress of Renewable Energy in APEC Region. SOM Steering Committee on Economic and Technical Cooperation (SCE), October 2019.

[4] Hirsch A, Parag Y, Guerrero J. Microgrids: A review of technologies, key drivers, and outstanding issues. Renewable and Sustainable Energy Reviews, 2018, 90:402-411.

[5] Hatziargyriou N, Asano H, Iravani R, *et al*. Microgrids. IEEE Power and Energy Magazine, 2007, 5(4):78-94.

[6] Lasseter R, Akhil A, Marnay C, *et al.* The CERTS microgrid concept. White Paper Transmission Reliability Program, Office of Power Technologies, US Department of Energy, 2002, 2:30.

[7] Marnay C, Bailey O C. The CERTS microgrid and the future of the macrogrid. Lawrence Berkeley National Laboratory, 2004.

[8] Lasseter R H, Eto J H, Schenkman B, *et al*. CERTS microgrid laboratory test bed. IEEE Transaction on Power Delivery, 2011, 26:325–332.

[9] Alegria E, Brown T, Minear E, Lasseter R H. CERTS microgrid demonstration with large-scale energy storage and renewable generation. IEEE Transaction on Smart Grid, 2014, 5:937–943.

[10] Panora R, Gehret J, Furse M, Lasseter R H. Real-world Performance of a CERTS microgrid in Manhattan. IEEE Transaction on Sustainable Energy 2014, 5:1356–1360.

[11] Recovery Act: Renewable and Distributed Systems Integration Program. Available: https://www.smartgrid.gov/recovery_act/overview/renewable_and_distributed_systems_integration_program.html. [assessed 25.07.19].

[12] Marnay C, DeForest N, Lai J. A Green Prison: The Santa Rita Jail Campus Microgrid panel paper. IEEE PES general meeting. San Diego, CA. p. 24–25, July 2013.

[13] SPIDERS Joint Capability Technology Demonstration. Available: https://energy.gov/eere/femp/downloads/smart-power-infrastructure-demonstration-energyreliability-and-security-spiders. [assessed 25.07.19].

[14] Happold Consulting. Sandy Success Stories, June 2013. Available: https://issuu.com/burohappold/docs/sandysuccessstories. [assessed 25.07.19].

[15] The State of New York's Prize (NY Prize) program. Available: https://www.nyserda.ny.gov/All-Programs/Programs/NY-Prize/FeasibilityStudies. [assessed 25.07.19].

[16] The Distributed Utility Integration Test (DUIT). Available: http://www.dua1.com/DUIT. [assessed 25.07.19].

[17] Nakanishi H. Japan's approaches to smart community. Assessment Policy Division, Ministry of Economy, Trade and Industry, Japan, 2014.

[18] Tokyo Gas. Challenge for the future society: smart energy network. Available: http://www.tokyogas.co.jp/techno/challenge/002_e.html. [assessed 25.07.19].

[19] Ren H B, Wu Q, Qiu L L, *et al.* An analysis of configurations and operational status of Japan's distributed energy systems and what can be learned for China. Sino-Global Eenergy, 2015, 20(7):9-14. (in Chinese).

[20] National Energy Administration. Relevant Policies in China Regarding MEMGs. Available: http://www.nea.gov.cn/policy/tz.htm. [assessed 25.07.19].

[21] APEC Project Database (PDB) (2019) APEC. Available: https://aimp2.apec.org/sites/PDB/default.aspx. [assessed 25.07.19].

[22] Peng K, Zhang C, Xu B X, *et al.* Status and prospects of demonstration projects of multi-energy cooperative integrated energy system, Electric Power Automation Equipment, 2017, 37 (6): 3-10. (in Chinese).

[23] Energy U. DOE Microgrid Workshop Report. 2018.

[24] Lambert T，Gilman P，Lilienthal P. Micropower system modeling with HOMER, Integration of Alternative Sources of Energy, Farret FA, Simões MG, John Wiley &Sons, December 2005，ISBN 0471712329．
[25] Stadler M，Marnay C, Distributed energy resources (DER) web optimization service (WebOpt) version 2.2, Berkeley, CA, USA: Lawrence Berkeley National Laboratory．
[26] Xiao J, Bai L, Wang C *et al.* Method and software for planning and designing of Microgrid, Proceedings of the CSEE, 2012, 32(25):149-157(in Chinese)．
[27] Zhao B, Zhang X, Chen J. Integrated microgrid laboratory system, IEEE Transactions on Power Systems, 2012, 27(4):2175-2185.
[28] Khaitan S, McCalley J, Liu C, Cyber physical systems approach to smart electric power grid. Berlin Heidelberg: Springer, 2015:1-23.
[29] Simon R, Christian S, Matthias W, A modular approach for co-simulations of integrated multi-energy systems, IEEE Transactions on Smart Grid, 2015, 7(1):451-459.
[30] Zhang R, Hong T. Modeling of HVAC operational faults in building performance simulation, Applied Energy, 2017, 202:178-188.
[31] Ghaderi A, Sanandaji B M, Ghaderi F. Deep forecast: deep learning-based spatiotemporal forecasting. 2017, arXiv e-prints, arXiv:1707.0811.
[32] Amarasinghe K, Marino D, Manic M. Deep neural networks for energy load forecasting, 2017 IEEE 26th International Symposium in Industrial Electronics, 2017, 1483–1488.

Chapter 2

[1] Iov F, Hansena D, SØrensenp, *et al.* Wind turbine blockset in Matlab/Simulink, PhD thesis: Aalborg University, March, 2004.
[2] Permanent Magnet Synchronous Machine Device, EMTPWorks．
[3] Nicholas W, Willam W, *et al,* Dynamic modeling of GE 1.5 and 3.6 MW wind turbine-generators for stability simulations, IEEE Power Engineering Society General Meeting, July, 13-17, 2003:1977-1983.
[4] Darren M, Bagnall, Boreland M, Photovoltaic technologies, Energy Policy, 2008, 36:4390-4396.
[5] Gow J A, Manning C D, Development of a photovoltaic array model for use in power-electronics simulation studies, IEEE Proceedings-Electric Power Applications, 1999, 146(2):193-200.
[6] Molina M G, Mercado P E, Modeling and control of grid-connected photovoltaic energy conversion system used as a dispersed generator, Transmission and Distribution Conference and Exposition, Latin America, 2008:1-8.
[7] Louis N, George J, Fardanesh B, A governor turbine model for a twin-shaft combustion turbine, IEEE Transactions on Power Systems, 1995,10(1):133-140.
[8] Working group on prime mover and energy supply models for system dynamic performance studies, Dynamic models for combined cycle plants in power system studies, IEEE Transactions on Power Systems, 1994, 9(3):1698-1708.
[9] Wingelaar P J H, Duarte J L, Hendrix M A M, Dynamic characteristics of PEM fuel cells, IEEE Power Electronics Specialists Conference, June, 16, 2005:1635-1641.
[10] Kong X, Khambadkone A M, Thum S K, A hybrid model with combined steady-state and dynamic characteristics of PEMFC fuel Cell stack, 2005, 3(2-6):1618-1625.
[11] Zhu Y, Tomsovic K, Development of models for analyzing the load-following performance of micro turbines and fuel cells, Electric Power Systems Research, 2002, 62(1):1-11.
[12] Li Y, Choi S, Rajakaruna S, An analysis of the control and operation of a solid oxide fuel-cell power plant in an isolated system, IEEE Transactions on Energy Conversion, 2005, 20(2):381-387.
[13] Khan M J, Lqbal M T, Modeling and analysis of electro-chemical, thermal and reactant flow dynamics for a PEM fuel cell system, Fuel Cells, 2005, 5(4):463-475.
[14] Na W, Gou B, A thermal equivalent circuit for PEM fuel cell temperature control design, IEEE International Symposium on Circuits and Systems, May, 18-26, 2008:2825-2828.
[15] Wang C, Nehrir M H, A physically based dynamic model for solid oxide fuel cells, IEEE Transactions on Energy Conversion, 2007, 22(4):887-897.
[16] Chan H L, Sutanto D, A new battery model for use with battery energy storage systems and electric vehicles

power systems, Power Engineering Society Winter Meeting, 2000, 1:470-475.
[17] Giglioli R, Buonarota A, Menga P *et al*, Charge and discharge fourth order dynamic model of the lead-acid battery, Proceedings of the 10th International Electric Vehicle Symposium, 1990:371-382.
[18] Saiju R, Heier S, Performance analysis of lead acid battery model for hybrid power system, Transmission and Distribution Conference and Exposition, Kassel, April, 21-24, 2008:1-6.
[19] K. Kundert. Sparse 1.3 - A Sparse Linear Equation Solver [EB/OL]. http://www.netlib.org/sparse/, 1986. [accessed on 2019.09.18].
[20] Davis T A, Natarajan E P. Algorithm 907: KLU, A Direct Sparse Solver for Circuit Simulation Problems, ACM Transactions on Mathematical Software, 37(6):1-17.
[21] Ho C W, Ruehli A E, Brennan P A. The modified nodal approach to network analysis. IEEE Transactions on Circuits and Systems, 1975, 22(6): 504-509.
[22] J. Mahseredjian, S. Dennetière, L. Dubé, et al. On a new approach for the simulation of transients in power systems, Electric Power Systems Research, 77(11): 1514-1520, 2007.
[23] Verma S C, Odani H, Ogawa S, et al. Real time interface for interconnecting fully digital and analog simulators using short line or transformer. 2006 IEEE PES General Meeting, 2006, 1: 1–7.
[24] Moreira F, Marti J, Zanetta L, et al. Multirate simulations with simultaneous-solution using direct integration methods in a partitioned network environment. IEEE Transactions on Circuits and Systems-I: Regular Papers, 2006, 53(12): 2765-2778.
[25] Sakallah K A, Director S W. SAMSON2: An event driven VLSI circuit simulator. IEEE Transactions on Computer-Aided Design of Integrated Circuits and Systems, 1985, 4(4): 668–685.
[26] Maguire T, Giesbrecht J. Small time-step (< 2μ Sec) VSC model for the real-time digital simulator. International Conference on Power System Transients, Montreal, Canada: IPST, 2005, 1-6.
[27] Yu B, Optimal Planning of Microgird and Energy Storage System, PhD thesis: Tianjin University, 2012 (in Chinese).
[28] Wang J, Jing Y, Zhang C, Optimization of capacity and operation for CCHP system by genetic algorithm, Applied Energy, 2010, 87(4):1325-1335 .
[29] Wang C, Lv C, Li P, *et al.* Modeling and optimal operation of community integrated energy systems: A case study from China, Applied Energy, 2018, 230:1242-1254.
[30] IBM . IBM ILOG CPLEX Optimization Studio . Academic Initiative, Available: https://www.ibm.com/products/Ilog-cplex-optimization-studio [assessed 25.07.19].
[31] Ruan Y, Liu Q, Li Z, Wu J. Optimization and analysis of Building Combined Cooling, Heating and Power (BCHP) plants with chilled ice thermal storage system, Applied Energy, 2016, 179;738-754.
[32] Huang W, Zhang N. Yang J, *et al.* Optimal configuration planning of multi-energy systems considering distributed renewable energy, IEEE Transactions on Smart Grid, 2019, 10(2):1452-1464.

Chapter 3

[1] Alegria E, Brown T, Minear E, *et al.* CERTS Microgrid Demonstration With Large-Scale Energy Storage and Renewable Generation[J]. IEEE Transactions on Smart Grid, 2014, 5(2):937-943.
[2] Lai J, Marnay C, Deforest N. A Green Prison: The Santa Rita Jail Campus Microgrid, Office of Scientific & Technical Information Technical Reports, 2013:1-2.
[3] Chris Clarke. Alameda County Jail Builds Microgrid. Available: https://www.kcet.org/redefine/alameda-county-jail-builds-microgrid. [assessed 25.07.19].
[4] Hatziargyriou N, Asano H, Reza I, *et al.* Microgrids, IEEE Power & Energy Magazine, 2007, 5(4):78-94.
[5] Hirose K, Shimakage T, Irie H. The sendai microgrid operational experience in the aftermath of the tohuku earthquake: A case study, NNT Facilitates Inc., Case Study, 2013. Available: https://building-microgrid.lbl.gov/news/sendai-microgrid-operational-experience. [assessed 25.07.19].
[6] Marnay C, Zhou N, Qu M, *et al.* International Microgrid Assessment. Governance, INcentives, and Experience (IMAGINE). 2012.
[7] Smart Integrated Energy Microgrid in Customer Service Center of State Grid Corporation of China. Available: https://www.esci-ksp.org/archives/project/smart-integrated-energy-microgrid-in-customer-service-center-of-

state-grid-corporation-of-china. [assessed 25.07.19]
[8] Project information provided by State Grid Zhejiang Electric Power CO., LTD, China.
[9] Gusdorf J, Charron R, Winder K. Canada's EQuilibrium™ Housing Demonstration Initiative: Net-Zero Energy Houses in Cold Climates, ACEEE Summer Study on Energy Efficiency in Buildings. 2010: 88-102.
[10] Pan, W. and Li, K. Clusters and Exemplars of Buildings towards Zero Carbon. Building and Environment, 2016, 104: 92-101.
[11] CMHC (2007) EQuilibrium Healthy Housing for a Healthy Environment Project Profile: ÉcoTerra—Eastman, Quebec, CMHC, Ottawa.
[12] Noguchi M, Athienitis A, Delisle V, *et al*.Net Zero Energy Homes of the Future: A Case Study of the ÉcoTerraTM House in Canada. Renewable Energy Congress, Glasgow, Scotland, 2008.

Chapter 4

[1] Yu B, Optimal Planning of Microgird and Energy Storage System, PhD thesis: Tianjin University, 2012 (in Chinese).
[2] Wang D, Jia H J, Hou K, Wang X D. Optimal scheduling strategy of district integrated heat and power system with wind power and multiple energy stations considering thermal inertia of buildings, Applied Energy, 2019, 240: 341-358.
[3] Liu Z, Chen Y, Zhuo R, *et al.* Energy storage capacity optimization for autonomy microgrid considering CHP and EV scheduling. Applied Energy, 2018, 210: 1113-1125.
[4] Wang M, MU Y F, Jiang T, Load curve smoothing strategy based on unified state model of different demand side resources. Journal of Modern Power System and Clean Energy, 2018, 6: 540–554.
[5] Hou K, A Reliability Assessment Approach for Integrated Transportation and Electrical Power Systems Incorporating Electric Vehicles, IEEE Transactions on Smart Grid, 2018, 9(1): 88-100,
[6] Jin X, Jiang T, Mu Y, et al. Scheduling distributed energy resources and smart buildings of a microgrid via multi-time scale and model predictive control method. IET Renewable Power Generation, 2018, 13(6): 816-833.
[7] Hou K, Wang Y, Jia H J, Zhu L, Lei Y, Liu Y, Yu X D, Reliability modeling for integrated community energy system considering dynamic process of thermal loads. 2019, IET Energy Systems Integration, 1(3): 173-183.
[8] Lin W, Jin X L, Mu Y F *et al.* A two-stage multi-objective scheduling method for integrated community energy system, Applied Energy, 2018, 216:428-441.
[9] Zeng Y, Zhang R W, Mu Y F, Jia H J, A regional power grid operation and planning method considering renewable energy generation and load control. 2019, Applied Energy, 237, 304-313.
[10] Lin W, Jin X, Mu Y, *et al.* Game-theory based trading analysis between distribution network operator and multi-microgrids. Energy Procedia, 2019, 158: 3387-3392.
[11] Dong X H, Mu Y F, Xu X D, Jia H J, Wu J Z, A charging pricing strategy of electric vehicle fast charging stations for the voltage control of electricity distribution networks, Applied Energy, 2018, 225: 857-868.
[12] Gao S, Jia H J, Marnay C, Techno-economic evaluation of mixed AC and DC power distribution network for integrating large-scale photovoltaic power generation.2019, IEEE Access, 7 (1), 105019-105029